(23)

Fabrication and Characterization of Beta-Prototype MIT Manus: an Intelligent Machine for Upper-Limb Physical Therapy

by

Debo A. Adebiyi

B.S., Mechanical Engineering
Mississippi State University, 1995

SUBMITTED TO THE DEPARTMENT OF
MECHANICAL ENGINEERING
IN PARTIAL FULFILLMENT OF THE REQUIREMENTS
FOR THE DEGREE OF

MASTER OF SCIENCE IN MECHANICAL ENGINEERING

at the

MASSACHUSETTS INSTITUTE OF TECHNOLOGY

FEBRUARY 1998

©1998 Massachusetts Institute of Technology
All rights reserved

Signature of Author:_____
Department of Mechanical Engineering
January 30, 1998

Certified by:_____
Professor Neville Hogan
Professor of Mechanical Engineering
Thesis Supervisor

Accepted by:_____
Professor Ain A. Sonin
Chairman, Departmental Committee on Graduate Studies

APR 27 1998

Fabrication and Characterization of Beta-Prototype MIT Manus: an Intelligent Machine for Upper-Limp Physical Therapy

by

Debo Adebiyi

Submitted to the Department of Mechanical Engineering
on January 30, 1998 in Partial Fulfillment of the
Requirements for the Degree of Master of Science in
Mechanical Engineering

Abstract

MIT Manus is a robot designed to be used in the physical rehabilitation of stroke patients. The robot is designed to gently hold and guide a patient's hand. An alpha-prototype was built several years ago, and has been used in several clinical trials. Results have shown that MIT Manus enhances recovery of stroke patients.

The objective of this thesis is to build a beta-prototype of the 2-dof module of the MIT Manus and characterize the performance of the beta-prototype. The beta-prototype was fabricated, and the performance of the actuator packages was characterized. This thesis presents the results of the characterization.

Acknowledgments

It was indeed a great joy and privilege to have worked on this research project, and I am very thankful to several organizations and several people. I will like to begin by thanking Burke Rehabilitation Center for providing funding for this project and for providing half of the financial support for me. I will also like to thank GEM fellowship for providing the other half of the financial support for me.

I am thankful for the opportunity to work under the leadership of Dr. Neville Hogan, my advisor. I highly respect his intellectual ability and his keen insight into a lot of physical phenomena. His attention to details, his ability to discern the real issues, and his ability to ask the right question is quite outstanding. His quest for new knowledge inspires me to want the same.

I will like to extend a word of thanks to all of Neville's students. Hermano Igo Krebs was very helpful to me. His technical advice was very good and very helpful. He had a keen interest in the research project, and he offered several suggestions and instructions which were helpful throughout all stages of the research. At times when things were not going well and I am discouraged, Igo had a joke or a piece of advice which made things go a little better. Justin Won was also very helpful to me. I have great respect for his intellectual ability. He was very helpful in getting me started on my experiments, and he helped me tremendously in identifying and solving some of the problems with the actuator packages. He was always willing to give a helping hand and I greatly appreciate his help. Joe Doeringer was very helpful to me. His detail understanding of a lot of different subjects never ceases to amaze me. He was very helpful in identifying some of the problems, and he offered a lot of technical tools and instructions that helped me analyze my experimental results. Michel Lemey was also very helpful to me in diagnosis some of the electrical problems. Without the help of these guys, I will still be battling with my research. I will also like to thank Lori Humphrey for all her help; she is indeed a wonderful person.

Special thanks to Dr. Ian Hunter and his students for allowing me to use their equipment for fabricating parts of the robot. I will like to especially thank Peter Madden for taking the time to show me how to use the CNC machine and some of the other equipment in the lab.

Special thanks to Jerry Wentworth of the Laboratory for Manufacturing and Productivity. He showed me how to properly use end mills, and he offered several valuable advises on fabricating parts. I will like to thank the machinists in Pappalardo Laboratory for their many helpful advises. I will like to thank Norman Berube for his advice pertaining to the assembling of parts, and his suggestions on making some design changes.

Finally, I will like to thank my family and friends for their generous support. Without their encouraging words, I won't have made it through MIT. I especially want to thank my mom, dad, and older sister for their very encouraging words and for being there for me. A special word of thanks to my dad and older sister for proofreading my thesis.

Table of Contents

List of Figures

List of Tables

1. Introduction

1.1 Motivation

According to the American Heart Association [1993], stroke is the third largest cause of death and the leading cause of serious, long-term disability in the United States. Over half a million people suffer from stroke each year, and about 400,000 of them survive [American Heart Association, 1993]. Stroke is a cardiovascular disease which affects the arteries of the central nervous system and is caused by rupture or obstruction of a blood vessel that supplies oxygen and nutrients to the brain. The rupture or obstruction of the blood vessel deprives part of the brain of needed blood flow, causing nerve cells in the affected area of the brain to malfunction and die within minutes. The part of the body controlled by the nerve cells in the affected area of the brain also ceases to function. The devastating effects of stroke can be permanent because dead cells are irreplaceable.

The effects of stroke are highly dependent on the neural area affected. Brain damage from a stroke can affect the senses, speech and ability to understand speech, behavior patterns, thought patterns, memory, and eyesight. Brain damage from a stroke may also affect the neural area responsible for controlling movements, resulting in limited motion, abnormal posture, muscle weakness, hyperactive reflexes, and inability to co-activate muscles [Reinkensmeyer, 1997]. Medical treatment for stroke varies and often includes a combination of drug therapy, speech therapy, occupational therapy, and physical therapy. Therapy (rehabilitation therapy) for stroke patients is a restorative or learning process geared towards enhancing and maximizing their recovery by treating

resulting impairment, disabilities, and handicaps. It works on the principle that service or help is provided when needed and withdrawn when no longer needed [American Heart Association, 1993].

Conventional physical therapy often involves a one-to-one interaction between a patient and a therapist. For a limb impaired patient, a therapist may hold and gently guide the patient's limb through various positions in an effort to widen the passive range of motion or to reduce hyperactive reflexes of the limb. This is a very common technique that therapists use in the rehabilitation process. Success in therapy is partially dependent on the therapist being able to make good evaluation of the patient's response to the therapy. Evaluation is based on the therapist's visual observation and physical interaction with the patient, both of which are subjective. The therapist can use these evaluation results to determine which techniques benefit the patient the most and apply those techniques; in some cases, application of new techniques might be required.

However, there are two primary problems affecting the effectiveness of conventional physical therapy: (1) the required one-to-one interaction between a patient and a therapist often makes therapy expensive and also makes it difficult for the therapist to spend enough time with a patient, and (2) the subjective nature of the patient evaluation method makes it difficult to quantify how a patient recovers when improvements in a patient's condition from one therapy session to the next are barely noticeable. The subjective nature of the patient evaluation method makes it difficult to analyze the treatment methods and obtain scientific data that quantify and support the effectiveness of practices in therapy. Furthermore, the absence of adequate scientific data makes it

difficult to develop practice guidelines that can be used by therapists [American Heart Association, 1993].

In the quest to develop an objective method of evaluating patients in rehabilitation therapy and to increase the overall effectiveness of rehabilitation therapy, robots are being designed to interact with therapists and patients. These robots apply some of the physical therapy techniques on patients, and thereby, require fairly limited interaction of the therapists with their patients and the robots. Each therapist is then free to interact with more than one patient in a given therapy session. Another added benefit to using robots is that robots are capable of performing repetitive tasks consistently and effectively. Therefore, if desirable, patients can be given the same level of physical therapy treatment for each therapy session. Also, these robots may be equipped with sensors which can be used to sense the velocity, acceleration, and forces exerted by the patient. The resulting data may be useful in providing an objective method of evaluating a patient's response to therapy, and perhaps, useful in establishing practice guidelines for therapists.

1.2 Background

Only a few research groups are currently working on developing robots for therapeutic use. This is probably because designing a robot to dynamically interact with humans is quite challenging. The following is a brief survey of work that has been done in the area of robot design for therapeutic use:

Khalili and Zomlefer [1988] developed a continuous two-arms robot. Each arm of the robot has two planar degrees of freedom (dof) and is coupled across a human joint to provide continuous passive motion for rehabilitation.

Lum *et al.* [1994] developed "Bimanual Rehabilitators" for the rehabilitation of bimanual control in hemiplegic stroke patients (patients with impairment in only one side of their bodies). Bimanual control involves coordinating the two hands of a patient to accomplish a task. The Bimanual Rehabilitators rely on the patient's unimpaired hand, along with mechanical assisting devices, to train the impaired hand [Reinkensmeyer, 1997]. Lum *et al.*, also developed a "Mirror Image Movement Enhance" (MIME) robot which is used for manipulating a patient's limb. The MIME robot employs two arm supports and a 6-dof robot arm. Each arm support is constrained to horizontal movements. The arm supports hold the forearm against gravity while the 6-dof robot arm manipulates one of the arm supports; thereby, manipulating the patient's upper limb. MIME employs a position control law [Reinkensmeyer, 1997].

Hogan *et al.* [1995] developed "MIT-Manus" robot which is used in rehabilitation of stroke patients with upper limb and wrist impairment. MIT-Manus has two modules, a 2-dof module and a 3-dof module. The 2-dof module consists of a five bar linkage Selective Compliance Assembly Robot Arm (SCARA) mechanism[1] that provides two translational degrees of freedom along the horizontal plane. The 2-dof module gently

[1] Although this is a five bar linkage mechanism, this mechanism has only four links (or bars). This is the standard method employed in describing mechanisms. This standard has, for example, helped to unify equations and methods for calculating the dof of mechanisms. To calculate the dof of a mechanism, it is assumed that the mechanism has a fixed link (or ground link) while the other links are free to move. In cases where the mechanism does not have a ground link, an additional link (ground link) is assumed to exist in the mechanism; then, the equations used in calculating the dof can be applied to these cases. In our case, all four links move, therefore, an additional link (ground link) is assumed to exist in the mechanism.

holds and guides a patient's hand while recording the position, velocity, and forces exerted by the patient. The 3-dof module consists of a differential mechanism which provides three degrees of freedom of motion for the wrist. The MIT-Manus robot is computer controlled and employs impedance control [Hogan, 1985], a key feature distinguishing it from other mentioned robots. Impedance control was specifically designed to handle the dynamic interaction between machine and humans [Hogan, 1987].

MIT-Manus is still in the experimental stage. The 3-dof module has not been used in rehabilitation therapy or clinical trials, but the 2-dof module has been used in several clinical trials. A picture of MIT-Manus being used in a clinical trial is shown in Figure 1.1. Results from the clinical trials show that MIT-Manus enhances recovery of stroke patients. Although the results are promising, the high cost of manufacturing this research prototype may make it difficult for MIT-Manus to gain acceptance in rehabilitation therapy. However, it is believed that a characterization of the performance of MIT-Manus may indicate opportunities for reducing the cost of manufacturing the robot.

1.3 Objective

The objective of this thesis is to build a beta-prototype of the 2-dof module of the MIT-Manus and characterize the performance of the beta-prototype. The beta-prototype design will retain most of the design features of the alpha-prototype. Complex parts of the robot which are difficult and costly to manufacture may be redesigned, but these redesigns should not adversely affect the performance of the robot.

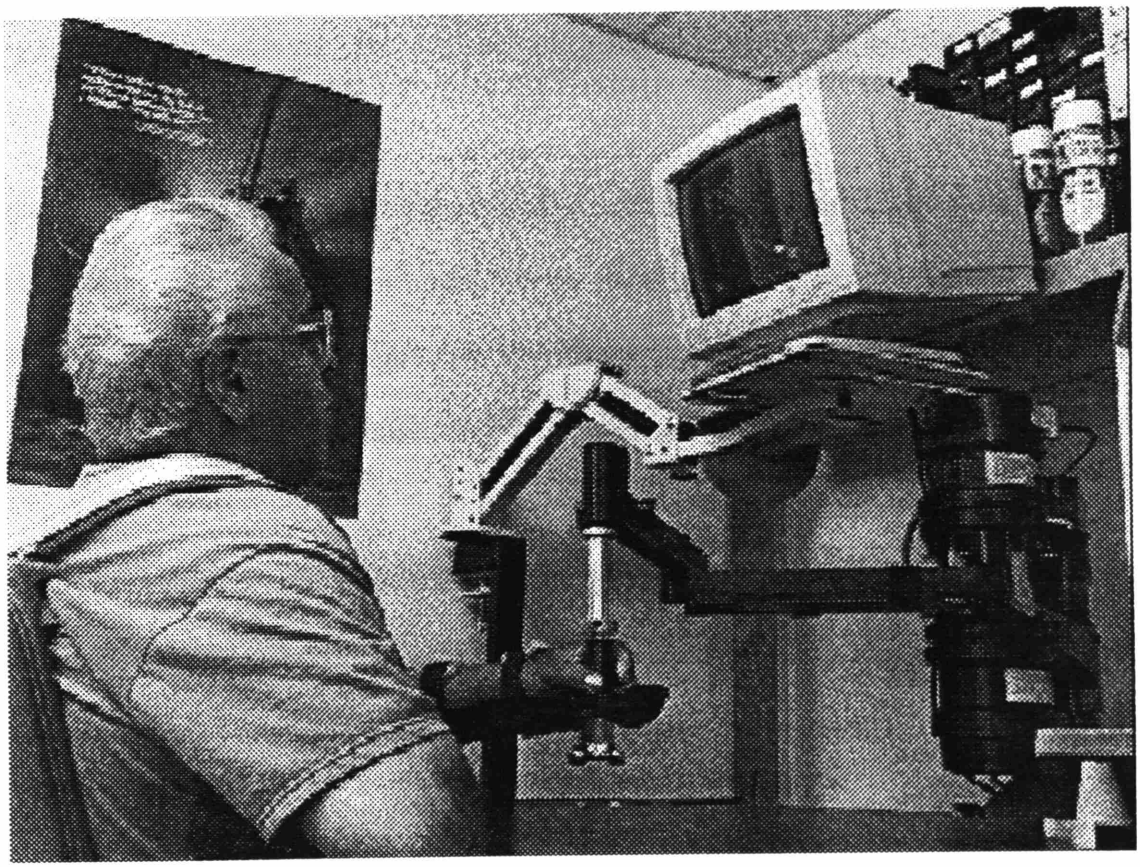

Figure 1.1: Picture of MIT-Manus Used in Therapy [Hogan, 1995]

2. Overview of the Alpha-Prototype of the MIT Manus

This chapter briefly describes the alpha-prototype of the MIT Manus robot since this is necessary for understanding some of the design modifications made in the beta-prototype of the robot. A detailed explanation of the design considerations, the reason for the design choices, and a full description of the design of the alpha-prototype are presented in Charnnarong's masters thesis [1991].

The alpha-prototype of MIT-Manus is comprised of an arm assembly, an actuator package assembly, and a support assembly. The arm assembly consists of links, joints, and end-point joint. The actuator package assembly consists of two identical actuator packages which house the actuators and sensors. The support assembly consists of an upper mounting plate, a lower column holder, a lower motor holder, two mounting straps, a mounting column, and a mounting base.

2.1 Arm Design

The links and the joints of the arm assembly are identified in Figure 2.1, which shows the top view of the arm. There are four links and four sets of joints in the arm assembly. The arrangement of the links and joints form a parallelogram with link 1 parallel to link 3 and link 2 parallel to link 4, and the axes of the joints are parallel to the vertical axis. This type of arrangement is based on the Selective Compliance Assembly Robot Arm (SCARA). The SCARA design is commonly used in assembly robots and is noted for

having high stiffness in the vertical planes and being compliant in the horizontal plane [Charnnarong, 1991].

There are four sets of joints. Each set of joints consists of a male and a female joint, and each joint is fabricated from 6061-T6 aluminum. Each joint's name as specified in Figure 2.1 identifies the links which the joint connects and the type of joint it is. For example, joint 14 male means that the joint is a male type joint and is one of two joints that connect link 1 to link 4. The main features of a male joint are its pilot core, which is inserted into a mating link, and its round extension, which is inserted into a mating female joint's hollow interior. Figure 2.2 identifies these main features in joint 14 male. The main features of a female joint are its pilot core, which is also inserted into a mating link, and its hollow interior, which connects to a mating male joint's round extension. Figure 2.2 also identifies these main features in joint 14 female. There are some slight differences between the design features on some of the male joints and between the design features on some of the female joints, but the function of the design features in each type of joint still remains the same. Figure 2.3 shows a drawing of all the male and female joints.

Figure 2.4 illustrates the arrangement of a joint set by using joint 14 set. The joints are connected together using two internal retaining rings, two radial bearings, and a retainer. The two retaining rings are inserted into the slots located inside the hollow interior of the female joint. The bottom lip of the first bearing's inner ring sits on the shoulder of the male joint, while the top lip of the outer ring banks against one of the two internal retaining rings.

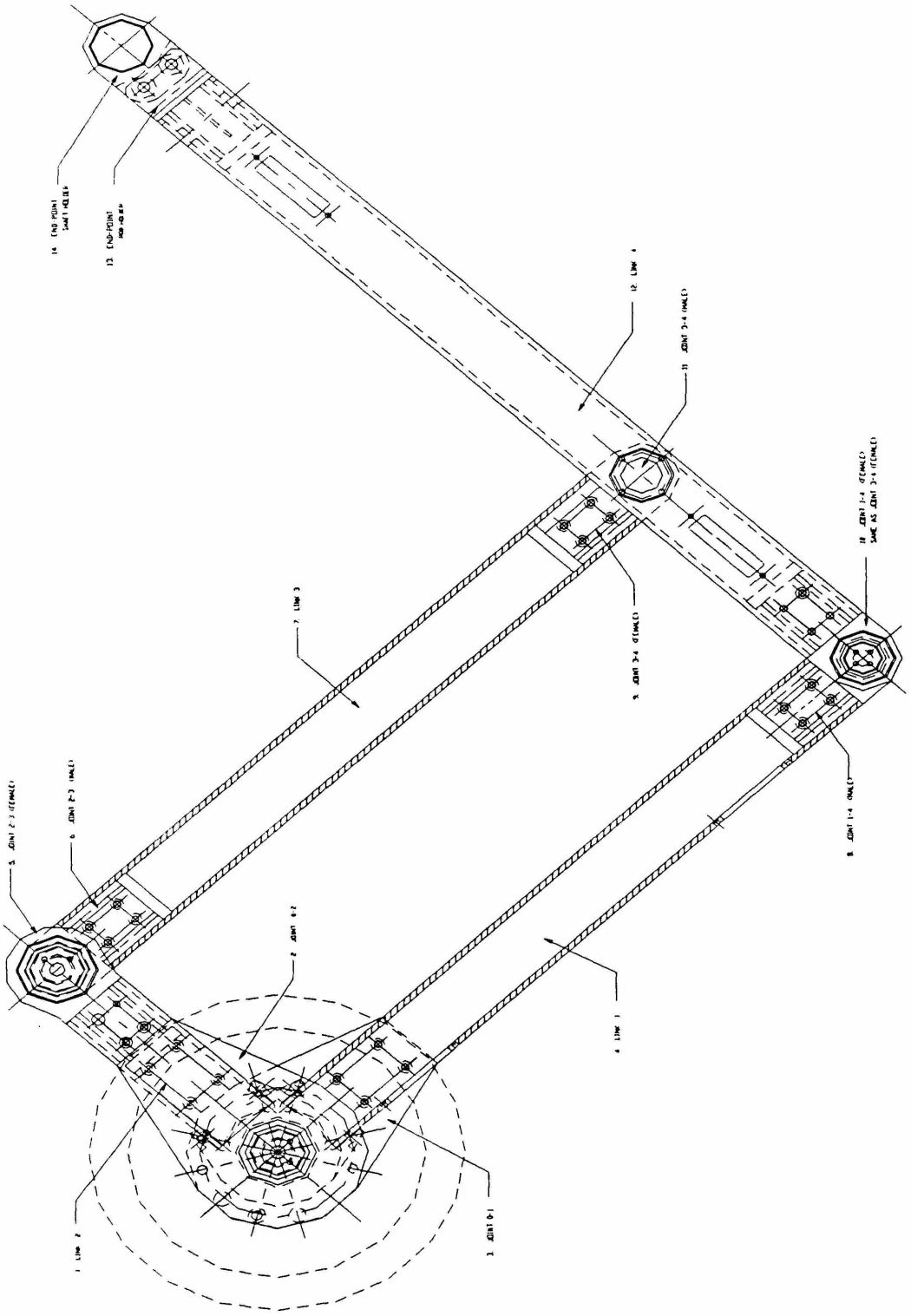

Figure 2.1: Top View of Arm [Charnnarong, 1991]

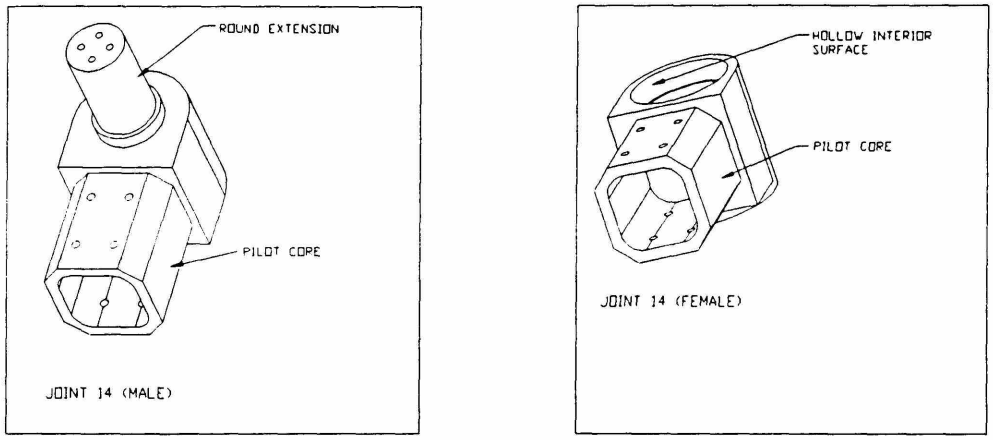

Figure 2.2: Joint 14 Male and Joint 14 Female

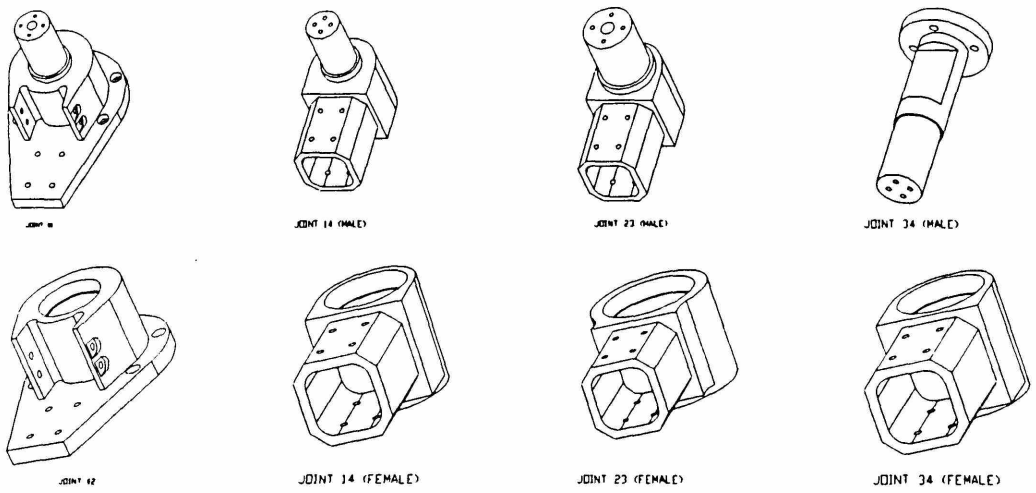

Figure 2.3: Male and Female Joints

The bottom lip of the second bearing's outer ring sits on the second internal retaining ring, while the inner ring's surface lies along the surface of the round extension of the male joint. The second bearing and the joints are held in place with a retainer, and then, covered with a joint cap.

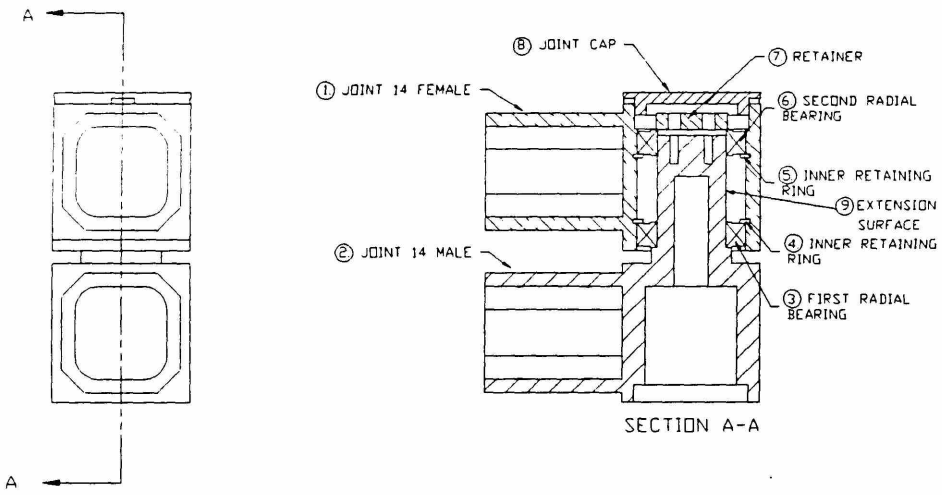

Figure 2.4: Joint 14 Arrangement

There are four links. Each link is fabricated from a standard 1.5" square 6061-T6 aluminum tube with wall thickness of .120". The main design feature present in all the links is the pilot holes, which receive the pilot cores of their mating joints. Figure 2.5 shows the pilot hole of link 1; the hole extends 1.75" into the link (the overall length of link 1 is 14.375"). The pilot core of joint 14 male is inserted into this pilot hole. The figure shows four trapezoidal slots on the side of link 1, the slots are wire connector slots used for holding D-subminiature connectors. The connectors are used in transferring power and signals to and from electrical components attached to the end-effector. Also in the figure is an external mating surface; this design feature allows link 1 to be connected to joint 01 -- joint 01 has a special pilot core design (see Figure 2.3). There are slight differences in design features between each of the links, but most of the general design features of each link are exemplified in the drawing of link 1.

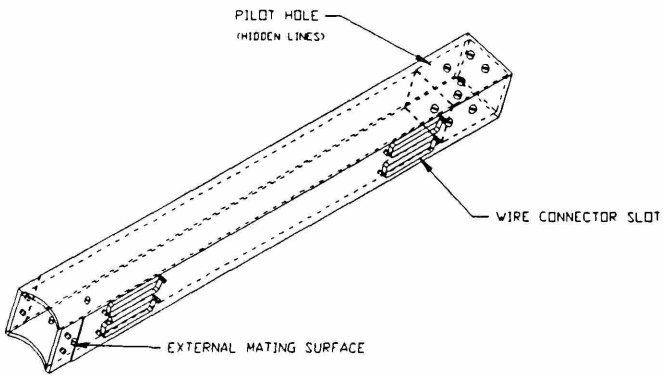

Figure 2.5: Link 1

The end-point joint is different from the other joints; it is designed to hold the end-effector. The joint is designed in a C-shape frame (see Figure 2.6), and has a pilot core which fits into the pilot hole of link 4. The pilot core is held in place inside link 4 by a pin, which fits through the hole on the side of the pilot core, and two knobs, which are screwed onto the two ends of the pin. The frame has two circular rods (not shown) held along the C section. Connected to the rods is an end-point shaft holder. The connection has compression springs and a linear bearing which holds the end-point shaft holder in place. The springs are designed to compress all the way when the end-point load exceeds maximum allowable load.

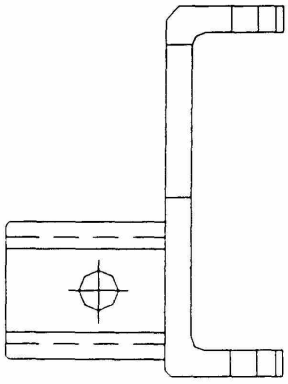

Figure 2.6: End-Point Joint [Charnnarong, 1991]

2.2 Actuator Package Design

The actuator package assembly consists of two identical actuator packages: an upper and a lower actuator package. Both employ a direct-drive transmission and are connected to the arm through two output shaft flange connectors. The upper actuator package connects to joint 02 and controls the movement of link 2, while the lower actuator package connects to joint 01 and controls the movement of link 1. Each actuator package houses a frameless brushless dc motor, a resolver (position sensor), a tachometer (velocity sensor), and a torque sensor. The actuators and the sensors are aligned along a single axis. A cross-section view of the design is shown in Figure 2.7.

As shown in Figure 2.7, each actuator package consists of a front housing, a middle housing, a rear housing, a cover plate, a motor shaft, and an output flange connector. One main thing to note about the actuator package is the construction of the motor shaft. The motor shaft is cylindrical and has a blind hole through its center. It supports the resolver's rotor, the middle bearing's inner ring, the motor's rotor, the rear bearing's inner ring, and the tachometer's rotor. Attach to the front end of the motor shaft is the reaction torque sensor. The torque sensor is held to the motor shaft by four screws inserted through the blind hole of motor shaft from the tachometer side. The other end of the torque sensor is attached to the output shaft flange connector, and is also held to the output shaft flange connector by four screws. Mechanical power is transmitted to the arm through the output shaft flange connector.

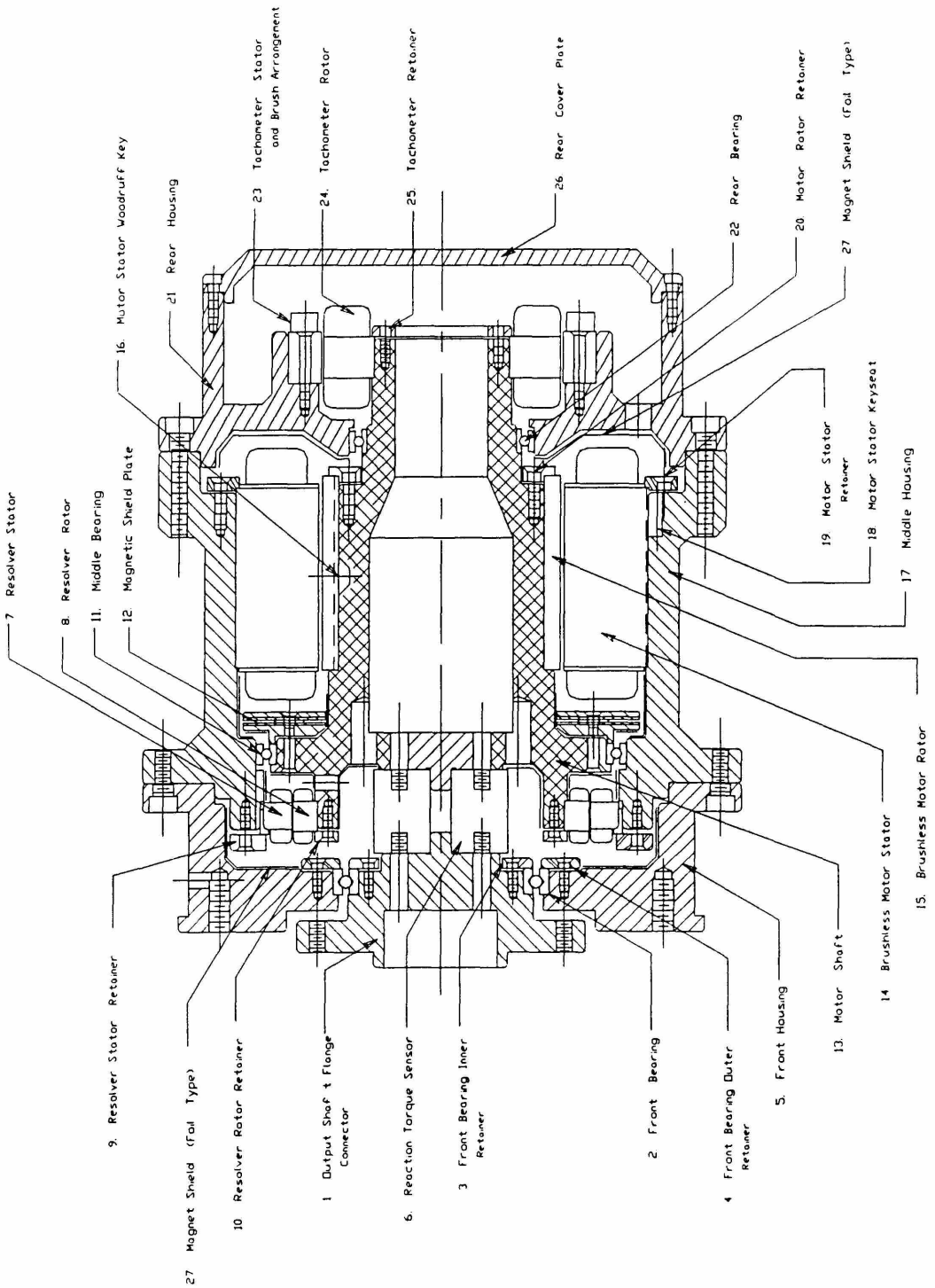

Figure 2.7: Cross-section of Actuator Package [Charnnarong, 1991]

2.3 Support Assembly

The support assembly is designed to support the actuator packages and the arm. The assembly is comprised of an upper mounting plate, a lower column holder, a lower motor holder, two mounting straps, a mounting column, and a mounting base. As shown in Figure 2.8, the mounting base supports the entire structure. The mounting base has holes along its edges. These holes provide a means through which the mounting base is bolted to a sturdy mounting surface. The mounting base has four flanges; these provide extra support for the entire structure.

The mounting column sits inside the mounting base. Inside the mounting base, the mounting column is prevented from turning or rotating by two set screws, located at the rear of the base, and also by a tight fit with the base.

The upper mounting plate, along with one of the mounting straps, holds the upper actuator package. The actuator package is located to the upper mounting plate with a dowel pin, and is held in place by a mounting strap. Through holes are drilled on top of the upper mounting plate to help reduce weight and to allow wires from electronic components in the actuator packages to pass through them. The upper mounting plate is slit at the back and this allows it to be clamped, using three screws, to the mounting column.

The lower motor holder, along with the second mounting strap, holds the lower actuator package. The actuator package is also located to the lower motor holder by a dowel pin. The lower motor holder is held to the mounting column by the lower column holder.

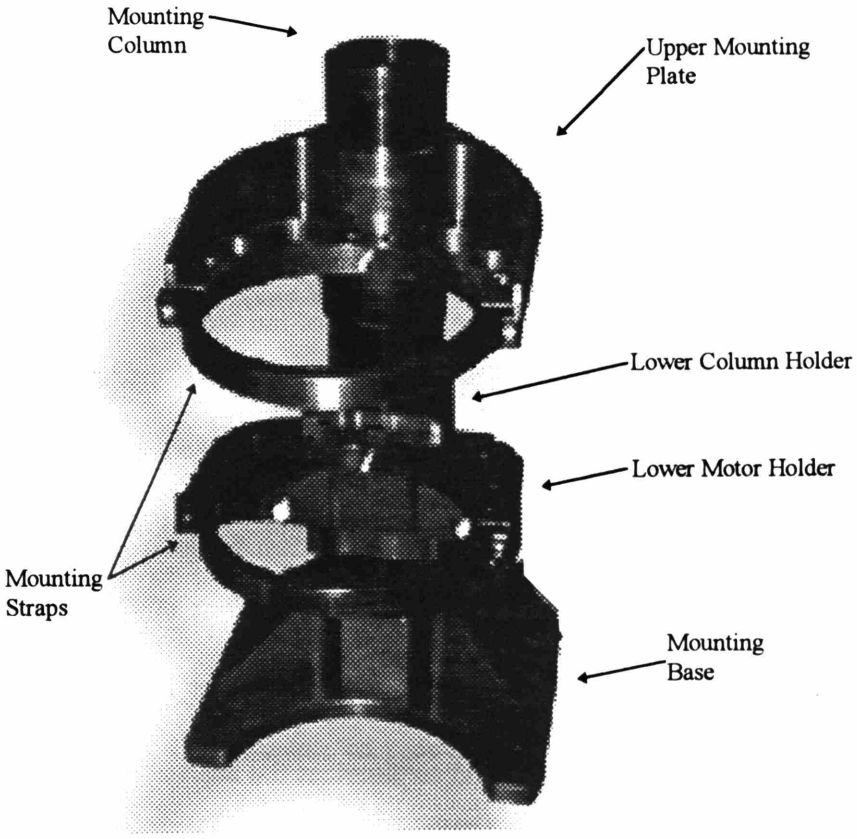

Figure 2.8: Support Assembly [Hogan, 1995]

3. Beta-Prototype of MIT Manus: *Design Modifications*

Part of the goals of this thesis was to simplify complex parts of the robot which were going to be difficult and costly to manufacture. There were two main design modifications and a few minor design modifications made to the robot. The first main design modifications were to the mounting base, and the second were to the actuator packages. Minor design modifications were made to the female joints, joint 01, joint 02, joint 34 male, and the end-point joint.

The objective of this chapter is to elaborate on the main design modifications. Section 3.1 focuses on the design modifications made to the mounting base. The section discusses the motivation for making the design modifications, describes the new design, presents a detail analysis of the new design, and summarizes the analysis results. Section 3.2 focuses on the design modifications made to the actuator package. The section discusses the motivation for the design modifications, describes the new design, and makes recommendations for future improvements to the actuator packages.

3.1 Modifications to the Mounting Base Design

Classification of design features and parts as being complex to manufacture is somewhat subjective. The way one perceives fabrication complexity sometimes depends on the tools and machines one has available and the level of understanding of how to properly use that equipment. A part might not be considered complex because it is based

on a standard design. That is, "everybody in the industry makes it like this", and therefore, there are readily available tools to fabricate the part. This complicates the classification process, perhaps a better way to capturing the idea of "complex parts" is to examine the costs involved in producing the part.

The primary costs of producing parts come mainly from design and manufacturing costs, and these costs should be taken into account when trying to reduce production cost. In both design and manufacturing, the critical parameter is usually time. For example, it's possible to optimize a design for manufacturing, but that usually involves some additional design time which can be accounted for in dollars. Also, typically, costs of manufacturing a part come mainly from the machinist (or machining) time. Typically, the machining time accounts for 90% of the total costs of manufacturing[1], and the remaining 10% is the cost of material. So, if one wants to reduce manufacturing cost, one must target reducing machining time, which often means that one should simplify designs such that the designs are easy to fabricate. A comprise must be reached between how much design time is required and how much machining time is required. Another parameter which often comes into the equation is the quantity of the parts to be produced. The larger the quantities, the more significant the cost of manufacturing and the less significant the cost of spending the extra time to redesign. So, production cost can be qualified as being a function of at least three parameters: design time, manufacturing time, and quantity of parts to be produced.

How does this relate to the beta-prototype? If all the parts of the robot are examined from a cost perspective or, more specifically, a manufacturing perspective, then

[1] Joe Co-owner of Eastern Tool Corporation, a Machine Shop

it will be observed that the support structure and the actuator packages have the greatest potential for resulting in cost reduction. This is primarily because some of these parts require a lot of machining time. Simplifying some of these designs may result in significant reduction in production costs. Even with all these explanations, the basic question still comes up: how to identify "complex parts" or how to identify parts that require significant machining time. The answer is that one needs to be able to visualize the machining process and see if there is room for reducing machining time. Consideration for the machining process should include accounting for available tools and machines, and the skill level required to use the equipment. One also might consider questions like:

1) Is special tooling required and how much does the tool cost? Does it require more than basic machining experience to properly use the tool?
2) Is the material stock or workpiece of the part too large or too small to be held in a standard vice?
3) Are special clamping tools such as v-blocks or C clamps required to hold the workpiece?
4) Is machining time very long due to workpiece mounting setup time or tooling setup time?

These questions are still ill-defined at this stage, but would soon become more meaningful when illustrated by an example. Considering the design time and the questions listed above, the main parts of the robot were examined, and it was decided that the mounting base of the support assembly was complex and it was selected to be simplified.

Although there are other parts which qualify as complex parts, only one major design change was made to simplify a complex part and that was to the mounting base. Some of the other complex parts are the upper mounting plate, the lower mounting column, the lower motor holder, and the actuator packages houses. These other parts were not redesigned partly because the required design time was expected to far exceed the potential manufacturing savings. When larger quantities of these parts are being produced, it would be very important to consider doing some redesigning. The alpha-prototype design of the mounting base is shown in Figure 3.1. Table 3.1 summarizes the responses to the questions listed above when applied to the alpha-prototype mounting base. Note, considerations for tools were based on readily available tools and machines in a typical school machine shop. The basic assumption was that if parts are easy to manufacture in a typical school machine shop, then it would probably be even easier to fabricate in a professional machine shop.

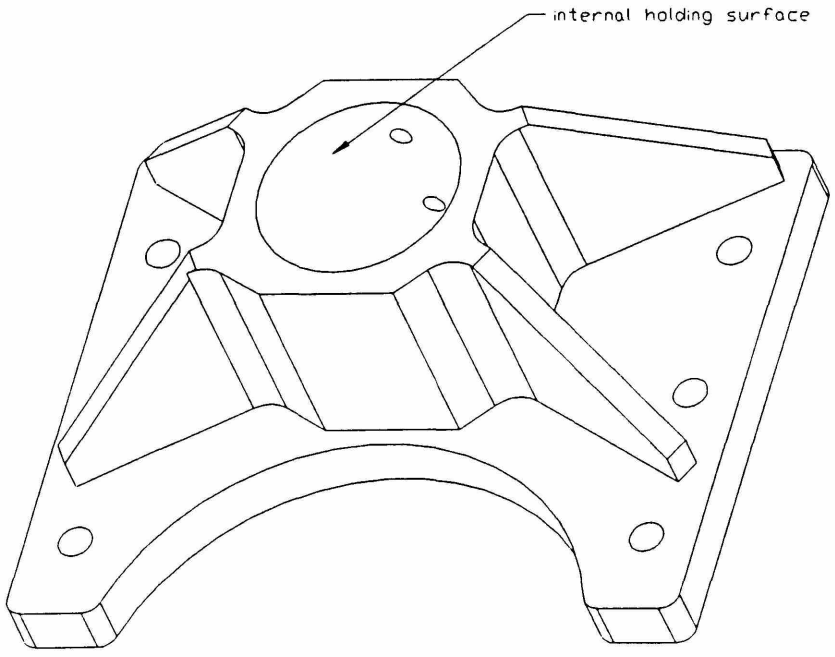

Figure 3.1: Alpha-Prototype's Mounting Base

Table 3.1: Responses to the Questions used in Classifying the Mounting Base as a Complex Part

Questions	Responses
Is special tooling required?	Some drills, regular end mills, and extra long end mills are needed. 5/8" end mill with under head length of 2 ¾" is needed. 1" end mill with under head length of 5" is needed.
How much does the special tooling cost?	5/8", extra long is $30 (regular is $20) 1", extra long is $65 (regular is $32)
What level of experience is required to properly use the tool?	Proper use of the extra long end mills requires appropriate reduction of feed rates, spindle speeds, and depths of cuts to avoid or minimize tool vibration and achieve good surface finishes
Is the material stock too large to be held on a standard vice?	The mounting base is fabricated from a 4" x 8" x 10" aluminum stock. This workpiece is too large to fit into the standard available vice. An additional support plate needs to be fabricated and mounted on the available vice.
Are special clamping tools required.	C clamps are needed to properly secure and hold the workpiece and the additional support plate in place.
Machining time.	Estimated machining time using MasterCAM is 15 hours.

As shown in Table 3.1, the machining time for the part is 15 hours. One reason for such a lengthy machining time is that a lot of material has to be removed from the workpiece, requiring several hours of machine time. The labor rate for fabricating the part is estimated at $40 per hour and the cost of fabrication material is estimated at $250. This gives a total fabrication cost of $800. Figure 3.2 shows a new, simplified design of the mounting base. This new design is manufactured in two pieces instead of the one-piece design of the alpha-prototype. For the new design, the estimated machining time using

MasterCAM[2] is 4 hours. This is a substantial reduction from the 15 hours machining time for the mounting base of the alpha-prototype. The estimated cost of fabricating the new design is $260, a savings of $540 over the mounting base of the alpha-prototype. This includes the cost of fabrication material, which was $100, and the assumed labor rate for fabricating the part is still $40 per hour. It should be noted that the cost of setting up the workpiece is not included in the fabrication cost. However, it is assumed that the setup time for both the mounting bases is roughly the same.

In addition to redesigning the mounting base of the robot, the actuator packages were also redesigned. However, the modifications to the actuator packages were made mainly to accommodate some new sensors. Subsequent parts of this section contain the description of the new design, a detail analysis of the new design, and a summary of the analysis results.

[2] MasterCAM is a software used for generating machining programs for Computer Numerical Control (CNC) machines.

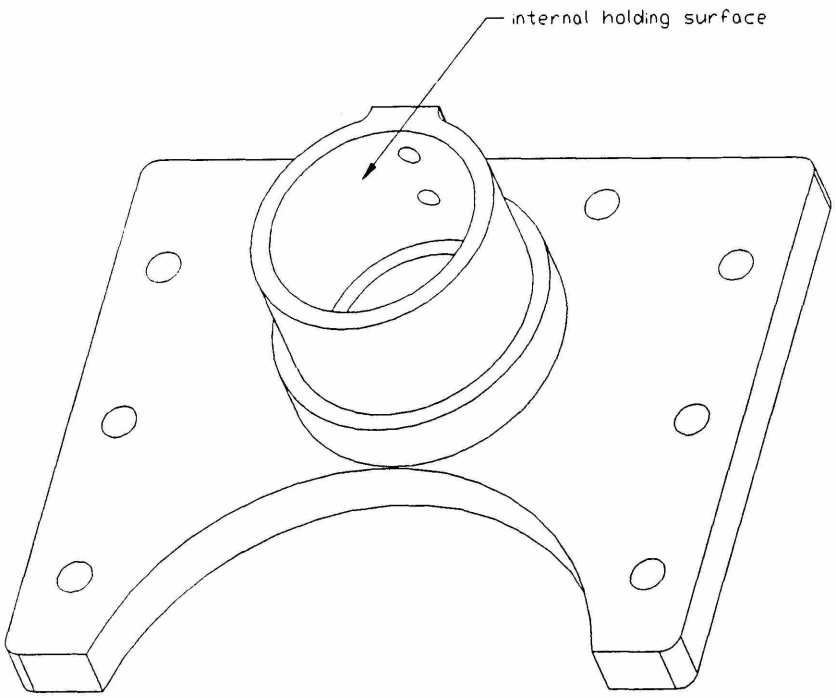

Figure 3.2 : Beta-Prototype's Mounting Base

3.1.1 Description of the New Design

The new mounting base design shown in Figure 3.2 includes two separate parts: a mounting column holder and a mounting base. The mounting column holder is received in a hole in the mounting base. Figure 3.3 shows how the two parts are assembled together. The root of the mounting column holder is inserted into the hole of the base plate; there is a diametrical clearance fit of .005" between the outer surface of the root and the inner surface of the hole in the base plate. Glue is applied between the two surfaces, providing a strong bond between the surfaces. The bottom side of the flange sits on top of the base plate, and two stainless steel dowel pins are inserted between the two parts. The dowel pins aid in ensuring proper alignment between the column holder and the base plate and in transferring shear forces and torsion to the base plate.

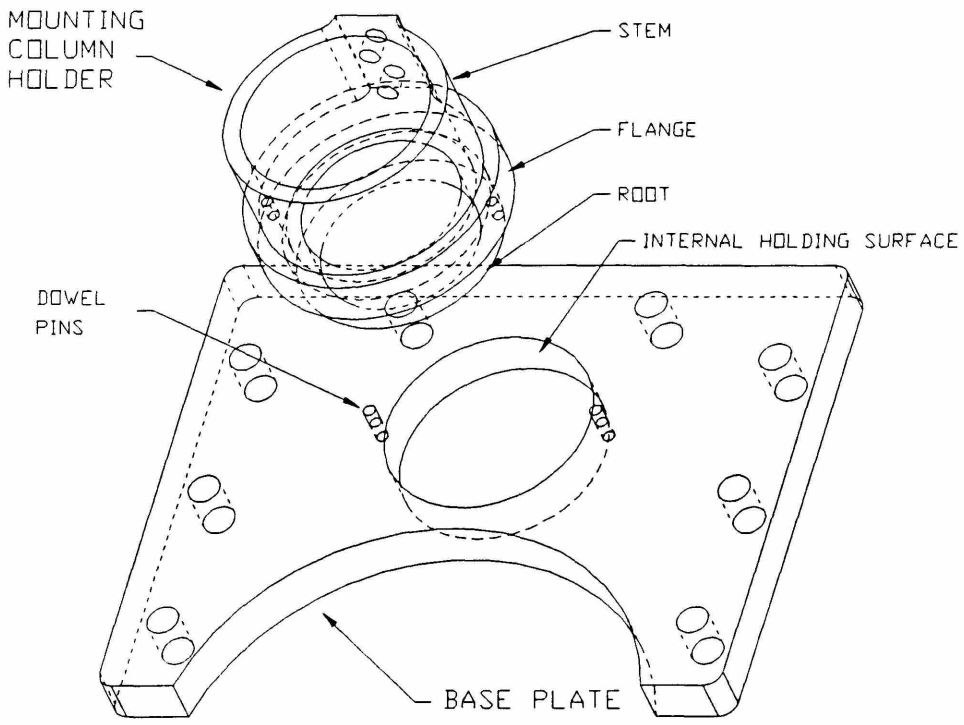

Figure 3.3: Mounting Column Holder and Mounting Base Plate

3.1.2 Detail Analysis of the New Design

In designing the new mounting base, it was necessary to consider the worst case scenario where the base will be subjected to maximum forces and moments. This included considerations for static and dynamic loading under normal operating conditions, and static and dynamic loading under abnormal operating conditions. Abnormal operating condition, for example, might be when the end-effector of the robot hits a wall. The next two subsections show the analysis of the new mounting base design for: (1) normal

operating conditions with worst case loading, and (2) abnormal operating conditions with plausible extreme case loading.

1) Analysis for Normal Condition with Worst Case Loading

For normal operating condition, the first question is whether a static analysis is sufficient or dynamic analysis is needed to correctly analyze maximum stresses on the mounting base. Dynamic analysis requires good knowledge of the arm positions with highest accelerations, the corresponding dynamic forces and moments, the distribution of masses, the center of gravity of the masses, and static forces and moments. On the other hand, static analysis requires some of the same thing required in dynamic analysis, but one can neglect dynamic forces and moments, and the knowledge of the distribution of masses is less critical. Naturally, static analysis is preferable over dynamic analysis because it's much simpler and less time consuming. However, static analysis can only be justified if acceleration of the robot's arm is sufficiently low and if worst case loading occurs under static conditions.

Can dynamic forces be neglected? Within the workspace and under normal operating conditions, yes, acceleration of the arm is low, and this will be illustrated with the arm in the fully extended position. Since the robot is designed to gently guide and move a patient's hand, the actuators are constrained by the controller to effect fairly low accelerations. Typically, the arm operates or oscillates at fairly low frequencies -- less than 2 Hz. However, it is possible to induce relatively high accelerations if, for example, a patient moves the end-effector very quickly. An extreme case may occur if the robot

interacts with a patient who suffers from pathological traumas. Some patients with pathological traumas may vibrate their hands around 8 Hz with an amplitude varying between 1 in and 4 in. Assuming worst case, the robot's end-effector is oscillated at 8 Hz with amplitude of 4 in. For sake of simplicity, the movement is approximated as a one dimensional translational motion. The amplitude of the acceleration is

$$a = w^2 A = (2\pi 8 / \sec)^2 (4.0\,\text{in}) (1\text{ft} / 12\text{in}) = 842.2\ \text{ft} / \sec^2$$

The effective mass of the mechanism and actuators reflected to the end-point should be between 1.5 lbm and 3 lbm [Charnnarong, 1991]. Therefore, the corresponding dynamic force at the end-point is between 39 lbf and 78 lbf. This result shows that dynamic forces can be quite high, therefore, this must be taken into account during the design analysis. These dynamic forces will be transferred to the mounting base, and will be treated as fluctuating loads on the mounting base. Note, however, that moments (or torsion) due to these dynamic forces will not be transferred to the base since torsion is transferred to the base by the reaction torque generated by the stators of the motors.

Next step is to determine worst case loading conditions. The manipulator has both an active and a passive mode. In the active mode, the manipulator gently guides the hand of the user, and in the passive mode, the manipulator allows the user to move its end-effector while absorbing energy generated by the user. In the active mode, the maximum end-point interaction force is limited to 10 lbf by the controller [Charnnarong, 1991]. In the passive mode, the manipulator is designed to exert minimal end-point resistance to the user's motion. However, sometimes in the passive mode, the manipulator is made to simulate a "wall". The "wall" is a controller program that defines an imaginary boundary

in space within which the end-effector must lie; this specifies a workspace. When the user moves the end-effector to the boundary, the manipulator exerts a force which prevents movement past the boundary or penetration into the "wall". Under this static operating condition, the user can apply very high forces. The maximum stresses in the mounting base should occur under this static loading condition.

Another question is what arm configuration yields maximum forces and moments. This corresponds to a configuration when the arm is fully extended. When forces are applied at the end-point, maximum moments occur when the distance from the end-point to the point of support is greatest.

Maximum Forces and Moments on Mounting Base

The free-body diagram of the manipulator under static loading condition is shown in Figure 3.4. The parameters in the figure are defined as follows:

I. R_1 represents the distance from the center of mass of mounting column to the combined center of mass of the upper mounting plate, lower column holder, lower motor holder, the two actuator packages, and the arm. Although, the center of mass of each of the components specified was not calculated, their combined center of mass should be very close to the center of mass of the actuator packages. This is because the actuator packages weigh much more than the other parts, and their center of mass lies along their central axis. The two actuator packages together weigh about 58 lbf, the arm weighs about 8 lbf, and the upper mounting plate, lower column holder and lower motor holder together weigh about 19 lbf. Based on the weights and some

rough estimates of the distribution of the masses, it was determined that the combined center of mass must lie within 2 inches of the actuator packages' center of mass. The center of mass of the actuator packages is located 6 inches from the center of the mounting column. Later in this section, the location of the combined center of mass is varied between 4 inches and 8 inches to see the effects on moments and forces. This would show how critical it is to know the actual location of the center of mass. R_1 is 6 in.

II. R_2 represents the distance from the center of mounting column to the end-point. R_2 is 36 in, which corresponds to the fully extended position of the arm.

III. L_1 is the distance from bottom of mounting column to the vertical location of the arm. L_1 is 15 inches.

IV. L_2 is the distance from the vertical location of the arm to the location of the placement of a user's hand. L_2 is 10 inches.

V. F_{3x} is the horizontal force in the x-direction applied by the user. The maximum horizontal force (push force) that can be applied by a weak man is 31 lbf, and for a weak woman is 22 lbf [Diffrient, 1981]. For design purposes, F_{3x} was chosen to be 31 lbf, which corresponds to the maximum force that can be applied by a weak man.

VI. F_{3z} is the horizontal force in the z-direction (into the page) applied by the user. The maximum force that can be resisted by the actuators is 34 lbf; this corresponds to each of the motors applying its maximum torque of 51.2 ft-lbf. F_{3z} is 34 lbf. The resultant of F_{3x} and F_{3z} is 46 lbf, which exceeds the maximum force that can be applied by a

weak man or woman, but is slightly less than the maximum force that can be applied by a strong man [Diffrient, 1981].

VII. F_{3y} is the combination of vertical force applied by the user and the weight of the user's hand in seated posture. The maximum downward force that can be applied by a weak man is about 20 lbf, and by a weak woman is about 12 lbf [Diffrient, 1981]. This does not include the rest weight of the hands. Based on my literature search, I found no published data specifying an average rest weight for people's hands in seated posture. Therefore, to compensate for the rest weight, a factor of safety of 2 is assumed. Using the maximum downward press force of a weak man and the assumed factor of safety, F_{3y} is 40 lbf.

VIII. F_1 is the weight of the mounting column. F_1 is 4 lbf.

IX. F_2 is the combined weight of the upper mounting plate, lower mounting column, lower motor holder, the two actuator packages, and arm. F_2 is 85 lbf.

X. F_{rx}, F_{rz}, F_{ry}, M_{rx}, M_{rz}, and M_{ry} is horizontal reaction force in the x-direction, horizontal reaction force in the z-direction, vertical reaction force in the y-direction, reaction moment around the x axis, reaction moment around the z axis, and reaction moment around the y-axis at the mounting base, respectively.

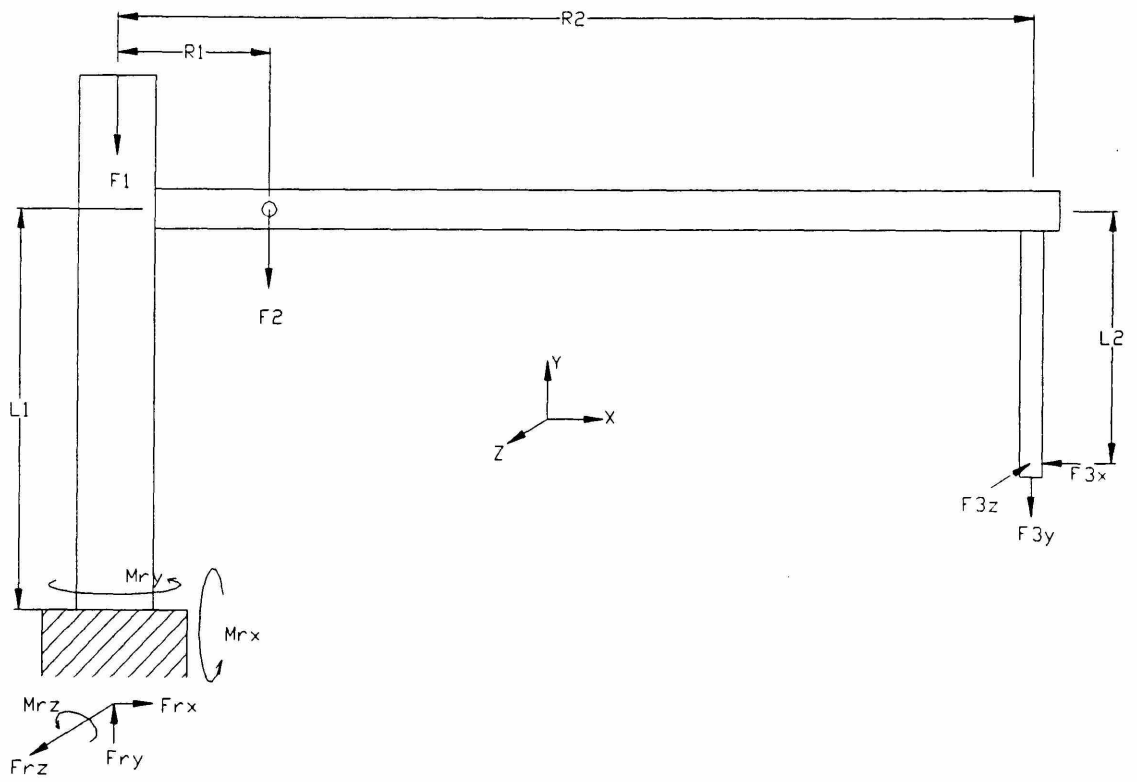

Figure 3.4: Free Body Diagram

The reaction forces, moments, and torques are obtained by solving static equilibrium equations. The results of the calculation are as follows:

$F_{rx} = 31$ lbf

$F_{ry} = 129$ lbf

$F_{rz} = 34$ lbf

$M_{rx} = 170$ lbf

$M_{ry} = -1224.0$ in-lbf

$M_{rz} = 1285.0$ in-lbf + (85.2 lbf) * (R_w)

The reaction moment or bending moment is specified as a function of R_w because it is desirable to know the consequence of not precisely calculating the center of mass of F_2.

The result is plotted below in Figure 3.5; R_w is allowed to vary between 4 in and 8 in. Expected value for R_w is about 6 inches (R_1); an increase in R_w of 2 inches results in about 9% increase in bending moment. As will become evident later in this section, 9% increase is still acceptable because of the applied or realized factors of safety. Therefore, it is not necessary to precisely know the center of mass. The bending moment, M_{rz}, used in subsequent analysis is equal to 1796 lbf-in.

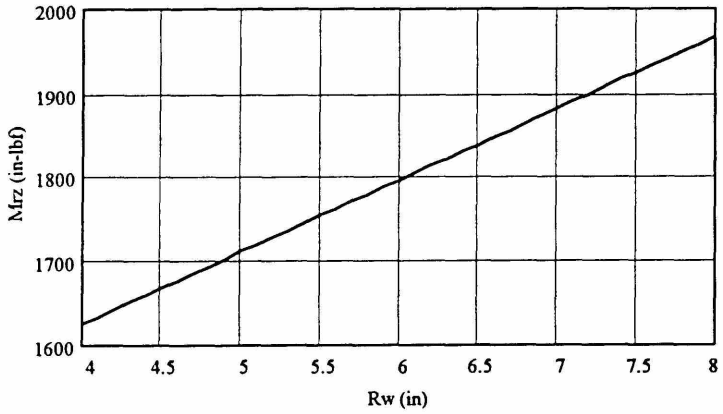

Figure 3.5: M_{rz} versus R_w

Stress Analysis on the Mounting Column Holder

The mounting column holder can be divided into three sections: the stem, the flange, and the root. These sections were identified in Figure 3.3.

For the stem, maximum stresses occur along the outer surface of the stem, at points a and b, as shown in Figure 3.6. At point a, the stress is due to bending moment M_{rz}, torsion M_{ry}, and shear force F_{rz}. At point b, the stress is due to bending moment M_{rx},

torsion M_{ry}, and shear force F_{rx}; Figure 3.7 shows a detail drawing of mounting column holder. The normal and shear stresses at point a are calculated as follows:

$$\sigma_{\max} = \frac{M_{rz}(d_o/2)}{I} + \frac{F_{rz}}{A} = \frac{(1796\,lbf*in)(1.75in)}{3.603in^4} + \frac{34\,lbf}{2.740in^2} = 884.7\,psi$$

$$\tau_{\max} = \frac{M_{ry}(d_o/2)}{J} = \frac{(-1224\,lbf*in)(1.75in)}{7.206in^4} = -297.3\,psi$$

where I is the second moment of inertia, J is the polar moment of inertia, A is the cross-sectional area, and d_o is the outside diameter of the stem. Using von Mises equation for combined bending and torsional loading, the resulting stress is calculated as follows [Shigley 1989]:

$$\sigma' = (\sigma_{\max}^2 + 3*\tau_{\max}^2)^{\frac{1}{2}} = 1023.6\,psi$$

The factor of safety is calculated using maximum shear stress theory. The maximum shear stress theory states that an element begins to yield when its shear stress exceeds the shear stress in test specimens. By considering the principal stresses, it is possible to show that the yield strength in shear is equal to half of the yield strength of the material [Shigley 1989]. The factor of safety is

$$n = \frac{0.5S_y}{\sigma'} = \frac{0.5(35kpsi)}{1023.6\,kpsi} = 17.1$$

where S_y is the yield strength of 6061-T6 aluminum.

Let's consider what happens under the dynamic loading condition presented earlier. The dynamic force is a fluctuating force and replaces F_{rz}; all the other forces and moments stay the same except for M_{ry}. M_{ry} is zero since the actuators are not resisting the

motion of the user; consequently, the shear stress is zero. The normal stress can be replaced by two other stresses. The first is the mean stress, which denotes the average stress on a stressed member, and the second is the alternating stress, which denotes the fluctuating stress on that stressed member. The mean stress in this case is the same as above (884.7 psi), and the alternating normal stress is zero. The resulting average stress using the von Mises equation is simply the mean stress, and the corresponding factor of safety is 19.8. This analysis shows that dynamic forces in the horizontal plane generated by a user has no significant effect on the supports. If this high dynamic force is generated by the actuators, then the effects on the support would be quite significant. However, as stated earlier, the actuators oscillate at fairly low frequencies and consequently, generate fairly low accelerations to the arm. This analysis shows that dynamic forces can be neglected, and therefore, dynamic forces will not be considered in further analysis.

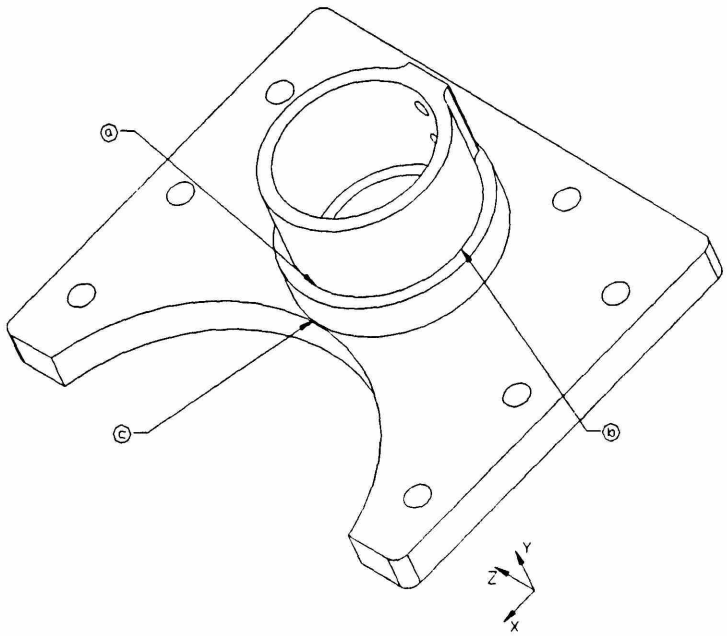

Figure 3.6: Critical Stress Points on Mounting Column Holder

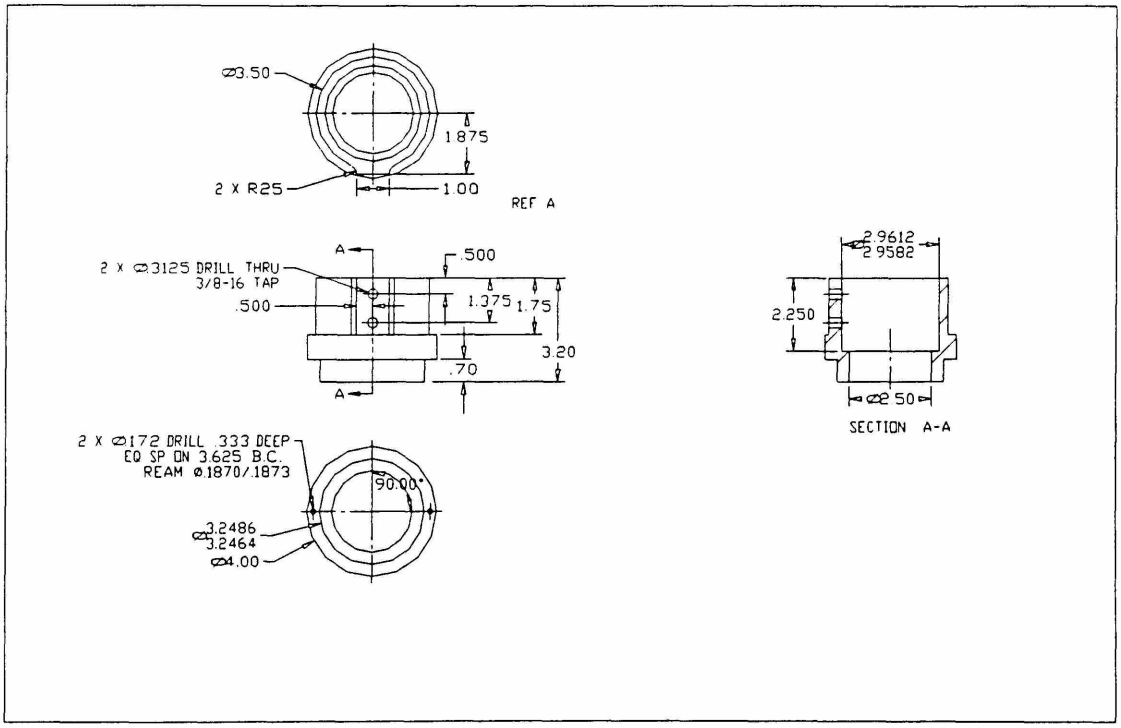

Figure 3.7: Detail Drawing of Mounting Column Holder

The stresses at point b are calculated as follows:

$$\sigma_{\max} = \frac{M_{rx}(d_o/2)}{I} = \frac{(170\,lbf*in)(1.75in)}{3.603in^4} = 82.6\,lbf$$

$$\tau_{\max} = \frac{-M_{ry}(d_o/2)}{J} + \frac{F_{rx}Q}{It} = \frac{(1224\,lbf*in)(1.75in)}{(7.206in^4)} + \frac{(31lbf)(1.414in^3)}{(3.603in^4)(0.541in)} = 319.7\,psi$$

where I is second moment of inertia, J is polar moment of inertia, Q is first moment of inertia, and t is the thickness of the stressed cross-section of the mounting column. Using von Mises equation, the combined stress is

$$\sigma' = (\sigma_{\max}{}^2 + 3\tau_{\max}{}^2)^{\frac{1}{2}} = 559.9\,psi$$

The corresponding factor of safety is 31.2.

The factors of safety at point a and point b are 17.1 and 31.2. Point a is the most stressed area, and clearly, has a high factor of safety. Consideration was given to the deflection of the stem under these loading conditions. Approximating the stem as a cantilever beam, the deflection of the stem was determined to be 2.22×10^{-6} in. Assuming the mounting column is very rigid, this translates to 4.43×10^{-5} in deflection at the tip of the mounting column. These are very small deflections and quite desirable. However, these results do suggest that there is opportunity for reducing the stem's dimensions.

Maximum stresses in the flange occur at the location of the left dowel pin (see Figure 3.3), and at point c (see Figure 3.6). The stress at the dowel pin is the combination of shear stress due to torsion M_{ry} and shear force F_{rx}, and normal stress due to bending moment M_{rx} and normal force F_{ry}. At point c, the stress is normal stress due to bending moment M_{rz}. The stresses at the location of the left dowel pin are calculated as follows:

$$\sigma = \frac{F_{ry}}{A_f} + \frac{M_{rx}(BC/2)}{I_1} = \frac{(129\,lbf)}{4.286\,in^2} + \frac{(170\,lbf*in)(1.813\,in)}{10.649\,in^4} = 59.0\,psi$$

$$\tau = \frac{-M_{ry}(BC/2)}{J} + \frac{F_{rx}Q}{I_2 t} = \frac{(1224\,lbf*in)(1.813\,in)}{13.117\,in^4} + \frac{(31\,lbf)(2.667\,in^3)}{(6.559\,in^4)(1.125\,in)} = 180.4\,psi$$

where A is surface area of the flange touching the base plate, I_1 is second moment of inertia of the flange, BC is the bolt circle (or the placement diameter) of the dowel pin, J is polar moment of inertia, Q is first moment of inertia, I_2 is second moment of inertia of the stressed area of the flange, and t is thickness of the stressed area. Using maximum shear stress theory, the corresponding factor of safety is 55.0.

The stress at point c is calculated as follows:

$$\sigma = \frac{M_{rz}(d_o/2)}{I_1} = \frac{(1796\,lbf*in)(2\,in)}{5.324\,in^4} = 674.7\,psi$$

Using maximum shear stress theory, the corresponding factor of safety is 25.9.

Again, the factors of safety for the critical areas in the flange are high. Point c is the most stressed area, and has a factor of safety of 25.9. This is quite high and does suggest that some of the dimensions can be reduced.

The stresses in the dowel pins can also be calculated in the same way. Out of the two pins, the left pin is subjected to the most stress. Stress in the left pin is shear stress due to shear force F_{rx} and moment M_{ry}. The shear stress is calculated as follows:

$$\tau = \left[\frac{-M_{ry}}{BC} + \frac{F_{rx}}{2}\right]\frac{Q}{It} = \left[\frac{(1224\,lbf*in)}{3.625\,in} + \frac{31\,lbf}{2}\right]\frac{5.493\,x\,10^{-4}\,in^3}{(6.067\,x\,10^{-5}\,in^4)(.188\,in)} = 1.70\,x\,10^4\,psi$$

where BC is bolt circle of the dowel pins, I is moment of inertia, and t is thickness (or diameter) of dowel pin. The corresponding factor of safety is

$$n_3 = \frac{0.5S_y}{\tau} = 3.4$$

where S_y (115 kpsi) is the yield strength of 416 stainless steel. This factor of safety is quite reasonable.

The stresses on the root of the mounting column holder can also be calculated. The maximum stresses occur at point d (see Figure 3.8). The stresses are normal stress due to bending moment M_{rz} and normal force F_{ry}, and shear stress due to shear force F_{rz}. The normal stress is calculated as follows:

$$\sigma = \frac{M_{rz}(d_o/2)}{I} + \frac{F_{ry}}{\frac{\pi}{4}(d_o^2 - d_i^2)} = \frac{(1796\,lbf\,in)(1.623\,in)}{3.539\,in^4} + \frac{129\,lbf}{3.372\,in^2} = 861.9\,psi \qquad (3.1)$$

The shear stress is calculated as follows:

$$\tau = \frac{F_{rz}\, Q}{I\, t} = \frac{(34 lbf)(1.551 in^3)}{(3.539 in^4)(0.747 in)} = 19.9\ psi \qquad (3.2)$$

The corresponding factor of safety is 20.3. Again, this seems high and does suggest that some of the dimensions can be reduced.

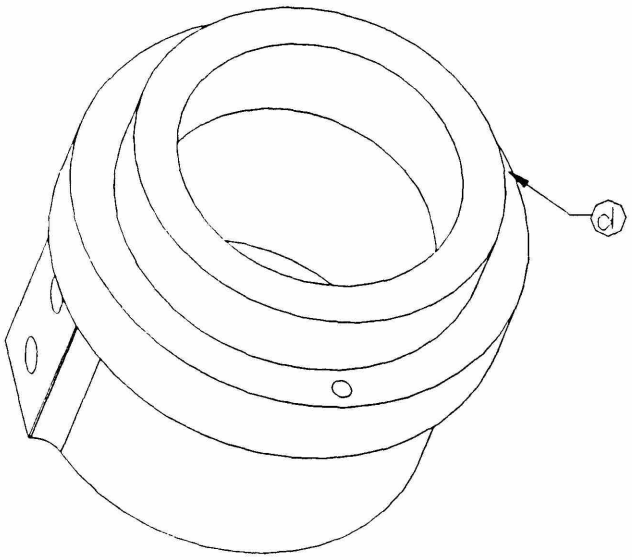

Figure 3.8: Stress Points at Mounting Column's Root

Stress Analysis of Base Plate

Figure 3.9 shows the top view of the base plate and Figure 3.10 shows the detail drawing. Assuming stresses acting on the base plate are localized around the mating surface of the base plate with the mounting column holder, maximum stress would occur at point e. The stresses are normal stress due to moment M_{rz} and force F_{ry}, and shear stress due to force F_{rx}. The stresses are calculated as follows:

$$\sigma = \frac{M_{rz}\, c}{I} + \frac{F_{ry}}{A} = \frac{(1796\, lbf * in)(2\, in)}{7.11 in^4} + \frac{129\, lbf}{4.286 in^2} = 535.3\, psi$$

$$\tau = \frac{F_{rx}\, Q}{I\, t} = \frac{(31 lbf)(4.961 in^3)}{(7.11 in^4)(0.753 in)} = 28.7\, psi$$

where I is moment of inertia of the section in dashed lines, A is cross-sectional area of the section, Q is first moment of inertia of the section, and t is the thickness of the stressed section. Using maximum shear stress theory, the corresponding factor of safety is 32.6. This suggests that some of the dimensions, such as thickness of the base plate, can be reduced.

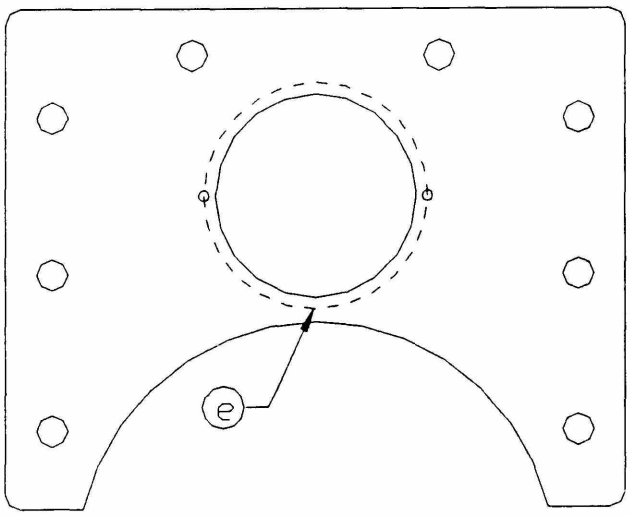

Figure 3.9: Stress Points on Base Plate

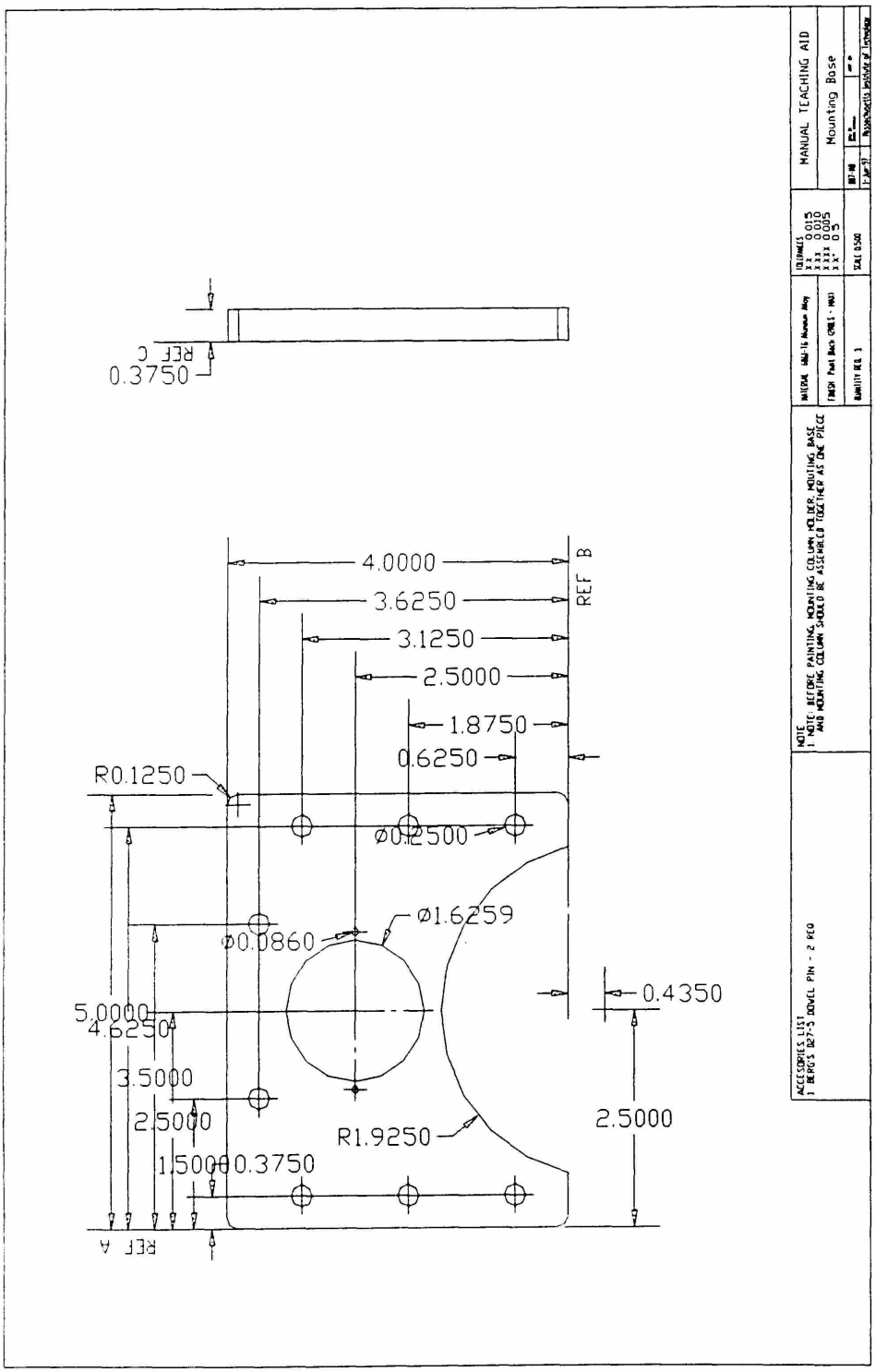

Figure 3.10: Detail Drawing of Base Plate

Analysis for Abnormal Conditions with Plausible Extreme Case Loading

Abnormal operating conditions are conditions that happen as a result of an accident. For example, it is not impossible to imagine the arm of the robot flinging and hitting a wall. The arm bounces back and forth because of the high impact force exerted by the wall and the torques exerted by the actuators. It is assumed that the displacement amplitude during this back and forth bounce is very small, and torque supplied by the actuators is fairly constant. Large accelerations can develop in the robot arm and the resulting dynamic forces can be quite significant. The impact of such an accident will be illustrated below.

Suppose the arm is moving at a constant angular speed of 2 rad/sec, and the end-effector hits a concrete wall. The modulus of elasticity of the wall is assumed to be 3.6×10^6 psi. To model the wall, the wall is assumed to be a cantilever beam, and the end-effector hits the unsupported end of this beam. The cross-sectional area of the beam (rectangular beam) is assumed to be 6 in wide, 12 in high, and 12 in long. The resulting impact force on the arm during the collision is approximately 6,000 lbf. This impact force is transferred to the base, and must be supported by the root of the mounting column holder (F_{rz} becomes 6,000 lbf). Note that only the shear force is transferred to the base and not the resulting moment or torsion since torsion is transferred to the base only through the reaction torque of the stator, which is dictated by the applied current to the actuators. The normal stress is still the same 861.5 psi (Equation 3.1), but the resulting shear stress is 3520.1 psi (Equation 3.2). The corresponding factor of safety is 2.8. If the

arm is moving at much higher speeds (4 rad/sec or more), the impact force could be quite detrimental and the root might start to yield.

Another effect that should be considered is the effects of high accelerations on the mounting base. If the robot arm's frequency of oscillation matches the natural frequency of the support structure, very high stresses will result in the support structure and the support is very likely to fail. As stated previously, the maximum end-point interaction force in the active mode is limited to 10 lbf. If during the back and forth bounce the actuators maintain end-point force of 10 lbf, when the end-effector leaves the wall the actuators decelerate the arm to zero and the end-effector stops, and then, starts heading towards the wall again. Based on the end-point force of 10 lbf, the end-point effective mass of 3.0 lbm, and Newton's second law, the deceleration rate is approximately 107.3 ft/sec^2. Assuming the collision with the wall is a perfectly elastic one, then the velocity immediately after collision is same as the velocity immediately before the collision. Using kinematics equation for constant acceleration, the resulting end-effector frequency of oscillation is approximately 9 Hz and the corresponding end-point displacement is approximately 2.0 in. Based on the performance of the alpha-prototype, the natural frequency of the support structure, although not determined, is much higher than 9 Hz. It is assumed that the beta-prototype support structure design is quite comparable to the alpha-prototype support structure design, and therefore, structural resonance should not occur.

3.1.3 Summary of the Analysis Results

Under normal conditions with worst case loading, analysis shows that the mounting column holder and the base plate would hold up. For both parts, the calculated factors of safety suggest that the dimensions of the parts can be reduced.

Under abnormal conditions with plausible extreme case loading, the root of the mounting column holder is a critically stressed area. The realized factor of safety is significantly lower than that obtain under normal conditions with worst case loading. This suggest that modifications to the mounting column holder, such as dimension reductions, should be made cautiously. This is because the lower the factor of safety, the more stringent the requiremnent that the forces or loadings be well known.

3.2 Modifications to the Actuator Package

The actuator package had to be modified to accommodate the new components. The actuator packages consist of the following actuators and sensors: 1) Kollmorgen Inland Motor's RBE-03013 brushless dc motor, 2) Gurley Precision's hollow shaft incremental encoder, 3) Transducer Technique's TRT-500 reaction torque transducer, and 4) Kollmorgen's TG-2936-B tachometer. The tachometer and the torque transducer have not been mounted yet, but space has been provided for mounting them in the future. Later paragraphs present reasons for selecting each of the new components.

The type of actuators used in both the alpha-prototype and the beta-prototype are brushless dc motors. Brushless dc motors are particularly noted for their simple current

torque characteristics. They are best described as having an ac synchronous motor's construction with a dc motor's current torque characteristics. In the beta-prototype, the RBE-03013 brushless dc motor was picked instead of the RBE-03003 brushless dc motor used in the alpha-prototype. This was mainly because the RBE-03003 model was no longer manufactured, and therefore, a new model had to be selected. One of the performance requirement for the motors was they had to be able to supply approximately 6.75 ft-lbf of continuous torque [Charnnarong, 1991]. The smallest model that satisfies the continuous torque requirement is the RBE-03013, and this is the model that comes closest to matching other performance parameters of the RBE-03003. The new model weighs less than the old model, but has more rotor inertia than the old model; the table below shows a short comparison of the two models.

Table 3.2: Some RBE Motor Parameters

Motor Parameters	RBE-03003	RBE-03013
Rotor Inertia (lb-ft-sec^2)	5.61e-4	6.67e-04
Weight (lbf)	7.36	3.9
Max. Cogging Torque, Peak to Peak (lb-ft)	0.19	0.21
Continuous Stall Torque (lbf-ft)	5.80	7.19
Peak Torque (lbf-ft)	16.2	51.2

One observation from the Table 3.2 is that the rated continuous torque for the RBE-03003 is less than the design requirement. It should be noted that this model has

performed well in the alpha-prototype. This suggests that by experimentation, it should be possible to determine the actual continuous torque required of each actuator. This might lead to a conclusion that a smaller brushless dc model would suffice.

Position sensors are used as feedback devices to the controller and the servo amplifiers. In the alpha-prototype design, pancake resolvers (Clifton precision's SSJH-44-B-2) were used as the position sensors. Resolvers are similar to three-phase wound-rotor motors, but have single winding on the rotor and two windings spaced 90° apart on the stator. When rotor is excited with an ac reference signal, the stator generates sine and cosine voltage outputs corresponding to the rotor's position. In essence, resolvers are absolute position sensors. Before deciding to use resolvers, considerations were given to other types of position sensors such as absolute optical encoders, incremental optical encoders, and synchros. Resolvers were shown to work better in hostile environments, provide good immunity from electrical interference [Charnnarong, 1991], and be very compact.

In the beta-prototype design, however, incremental encoders were used. The resolvers were not used mainly because the controller required a 16 bit position sensor and the best delivery time for a 16 bit resolver was 20 weeks. Each resolver (along with amplifier) cost about $3,000. Each incremental encoder (along with interpolators), on the other hand, cost just about $1500 each, and delivery time was less than 4 weeks. For our very low speed application, to correctly control the interaction force between a human and a machine using impedance control, at least 16 bits of position resolution is required [Charnnarong, 1991]. Also, it is desirable to differentiate position signals to obtain

velocity, and for the range of speeds of interest (0 to 8 rad/sec), especially at low speeds, at least 16 bits of resolution is desirable.

An incremental optical encoder contains disc with multiple tracks of slots, light sources, and light detectors. In the simplest case, only one light source and one light detector are used. The light source and light detector directly face each other and are positioned on opposite sides of the disc. The slotted disc is mounted on a rotating shaft, and as the shaft rotates, the transparent and the opaque areas of the disc cross the path of the light from the light source to the light detector. To the light detector, the light interruption appears as a series of light pulses. By counting the number of interruptions or the number of light pulses, the change in the shaft position is determined. Incremental encoders are, however, not absolute position sensors, and therefore, at each startup, require a reference position. Attempts have been made to make the encoders behave more like absolute position sensors by the inclusion of indexing markers. An indexing marker is a unique arrangement of an index slot on the disc which gives a light pulse once per revolution. But, once again during startup, the shaft must be rotated until this indexing pulse is received before knowing the shaft's absolute position. There are absolute encoders, but these are not suitable to use since there are no readily available servo amplifiers that support the output format from these encoders. Ideally, an absolute encoder would have been better since absolute encoders know the position of the shaft at startup. Absolute encoders differ from incremental encoder in that the multiple tracks of slots are now arranged to give out a binary output called Gray Code. In Gray Code, the

binary output changes a single bit at a time, and is no longer in form of series of pulses which can be counted.

A hollow shaft incremental encoder with an indexing marker was used in the beta-prototype. The encoder is placed on the motor shaft and then clamped onto the shaft with an adapter ring. The outputs from the encoder are two channels of sine and cosine waves and one channel of indexing signal; these are sent to an interpolator. The interpolator takes in sinusoidal waves and generates quadrature waves. The interpolator has two sets of outputs, the first set has a 13 bit resolution and goes to the servo amplifier, and the second has a 17 bit resolution and goes to the controller. The servo amplifier requires resolution that is less than or equivalent to 16 bits.

The reaction torque transducer, TRT-500, has a torque measuring range between 0 and 500 in-lbf. A model TRT-200 was used in the alpha-prototype. The measuring range of the TRT-200 is between 0 and 200 in-lbf. The sizes of both models are the same. The TRT-500 provides a higher sensing range and a higher overload protection, which had been a limitation with the TRT-200 model.

3.2.1 Description of the New Design

Below in Figure 3.11 is the cross-sectional view of the new design of the actuator package and shown the layout is how the components are mounted. The actuator package is comprised of four housings: front housing, middle front housing, middle rear housing,

and rear housing. Figure 2.7 shows the cross-sectional view of the alpha-prototype actuator package.

Notice that the alpha-prototype design is more compact (about 1.5" shorter) than the beta-prototype design, this is due to the larger encoder in the beta-prototype design. The beta-prototype has an extra house which had to be included to enclose the encoder.

Another difference between the two designs is in the number of components that make up the drive. In the alpha-prototype, the drive consists of the output shaft flange connector, the reaction torque sensor, and the motor shaft. In the beta-prototype, the drive consists of the output shaft flange connector, the reaction torque sensor, the torque sensor connector, the rotor clamp, and the motor clamp. Clearly, the beta-prototype design has more parts on its drive than the alpha-prototype design. The reason for having the extra parts was to ease the disassembly and assembly of the torque sensor, and to reduce some of the manufacturing costs. In retrospect, this was a poor decision because by introducing more parts to a moving mechanism, one increases the possibility of misalignments between parts.

3.2.2 Recommendations for Future Improvements

There were some problems with aligning the beta-prototype's drive. The quest to solve these problems lead to several discussions on some of the desirable properties of an actuator package. Some of the future improvements that can be made to the actuator package are included here.

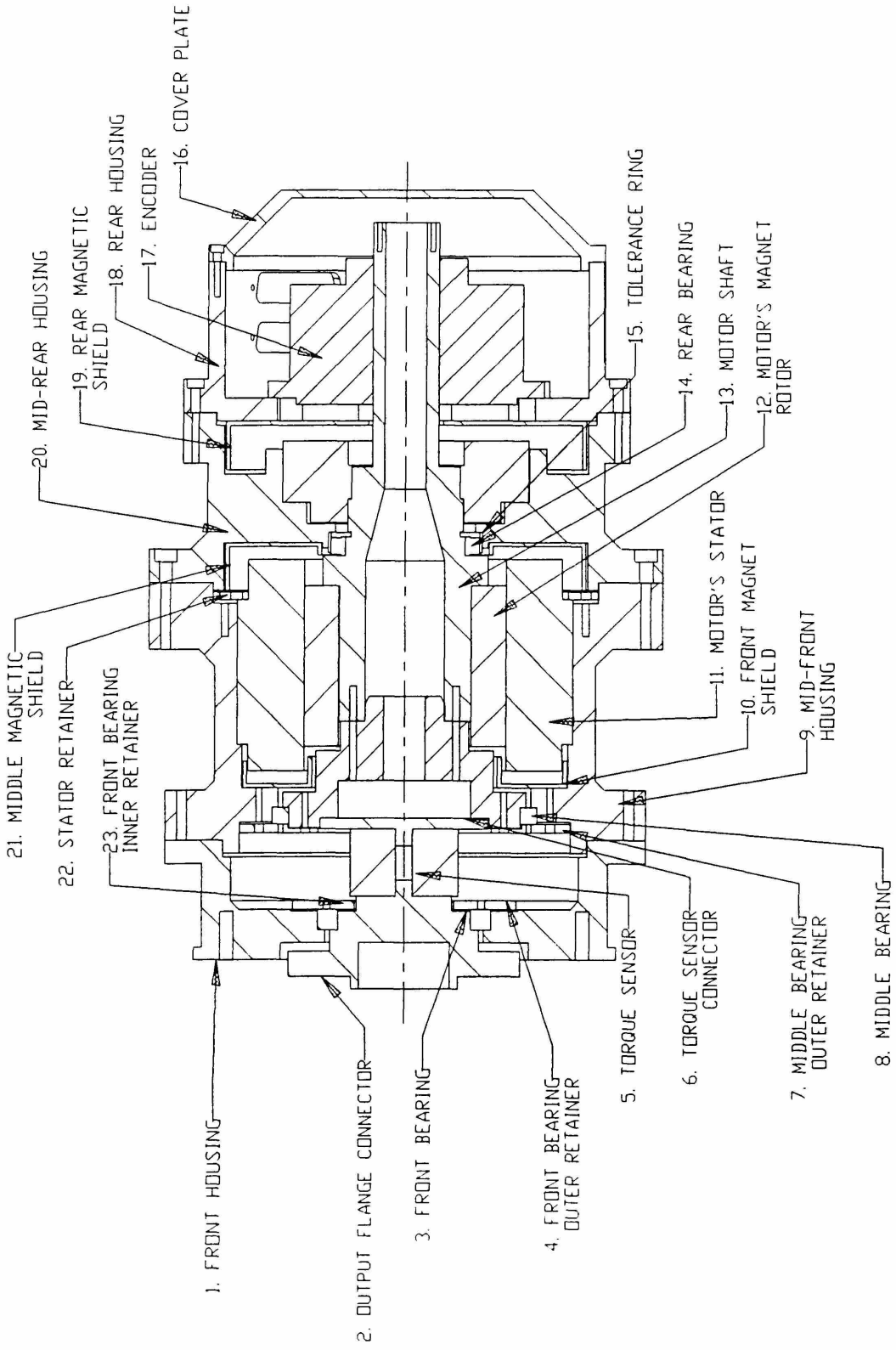

Figure 3.11: Cross-Sectional View of Actuator Package (Beta-Prototype)

4. Characterization of Beta-Prototype of MIT Manus

In most robotic systems, the performance of the actual system is usually short of the expected performance predicted by theoretical models. Therefore, it is important to characterize a robot's performance and compare it to the expected performance. Characterization of the beta-prototype will be useful in determining how to optimize the robot for its intended application and how to improve on future designs. Unfortunately, there are no standard guidelines on how to evaluate robot performances. Some of these difficulties stem from the fact that many robots are unique in their design and various control laws can be applied to these machines.

However, there are some works, such as by Hayward and Ashley [1995] for haptic devices, focused on developing a set of performance metrics which can be used to characterizing the performance of robots. Morrell and Salisbury [1996] established a set of performance metrics which can be used in quantify a robot's performance. They suggested that selection and categorization of performance metrics and experiments should be based on performance measurements which are independent of choice of control law, and those which are dependent on the choice of control law. These two categories of performance metrics can be further classified as performance metrics based on static experiments and dynamic experiments. Static experiments involve experiments where the actuator is stationary or close to being stationary (quasi-static), while dynamic experiments involve experiments where the actuator rotates. Examples of performance metrics independent of control law and based on static experiments are position

measurement resolution, force measurement resolution, peak torque, and continuous stall torque. Performance metrics independent of control law and based on dynamic experiments include device impedance and maximum acceleration at zero velocity. Performance metrics dependent on control law and based on static experiments include force and position precision[1], and force dynamic range[2]. Performance metrics dependent on control law and based on dynamic experiments include position bandwidth, force bandwidth, impedance and force fidelity.

The objective of this chapter is to present three types of experiments that were conducted in characterizing the beta-prototype of MIT-Manus. The structure and organization of the experiments are based on performance metrics suggested by Morrell and Salisbury [1996]; however, the actual experiments have been adapted to conform to our specific application. The experiments mainly focused on the performance of each of the actuator packages. Particularly, the experiments were geared towards understanding the relationship between torque and current, finding out if this relationship is a function of position and/or direction, and measuring other parameters which might give a better understanding of the performance of the actuators. All the experiments were conducted without any control law. Table 4.1 shows the listing of the experiments conducted, and the goal of each experiment.

[1] Steady state force and position error.
[2] Force dynamic range is the ratio of maximum controllable force to minimum controllable force.

Table 4.1: List of Experiments

CATEGORY #	EXPERIMENT	CATEGORY NAME	PURPOSE OF EXPERIMENT
1	**Sliding Friction Measurement**	Actuators: Changing Positions, No Control Law	1) measure sliding friction
2	**Constant Current Command versus Output Torque**	Actuators: Fixed Position, No Control Law	1) obtain actual torque constant 2) observe if torque constant varies with angle 3) observe if torque constant varies over the range of operation
3	**Sinusoidal Current Command versus Output Torque**	Actuators: Fixed Position, No Control Law	1) obtain torque bandwidth

4.1 Actuator Units, Sensor Units and Controller Description

Brief specifications of the actuators and sensors used in the actuator packages are presented in Chapter 3. This section provides additional relevant information about the actuators and sensors which is helpful in understanding the experiments.

4.1.1 Brushless DC Motor

The two actuator packages use the same brushless dc motor, RBE-03013-C, supplied by Kollmorgen Inland Motors. It is a 12 pole motor with permanent magnets on the rotor and a three phase wound stator. Theoretically, the motor has a torque constant of 4.002 N-m, +/- 10%.

4.1.2 Servo Amplifier

Each of the actuator packages is powered and controlled by a separate but identical servo amplifier. The servo amplifier is Kollmorgen Inland Motor's SE06 servo amplifier. It operates on 160 Vdc; it is designed to supply 6 amps RMS/phase of continuous current and 12 amps RMS/phase of peak current to the motor. Internally, the servo amplifier is digitally controlled by a 40 MHz micro processor which implements sinewave (or sinusoidal) commutation for the brushless dc motor, and uses pulse width modulation (PWM) at 16kHz to control the current output to the motor.

When the servo amplifier is turned on, the servo amplifier knows the absolute position of the motor to within 60 electrical degrees, which corresponds to 10 mechanical degrees. The servo amplifier knows the position because it uses the signals from three Hall-effect sensors mounted in the stator of the motor to determine the absolute position of the shaft. During initialization or as the shaft is rotated, the position resolution improves to 10 electrical degrees, which corresponds to 1.7 mechanical degrees, or better. However, to achieve smooth output torque using sinusoidal commutation, the servo amplifier requires another position sensor which gives better resolution than that given by the Hall-effect sensors. There are two common types of position sensors often used to provide better position resolution to the servo amplifier: resolvers and incremental encoders. For the beta-prototype, an incremental encoder was used. The incremental encoder provides a resolution of 13 bits, which corresponds to 0.044 mechanical degrees, to the servo amplifier.

During initialization, the servo amplifier uses both the signals from the Hall-effect sensors and from the incremental encoder to determine the position of the shaft. After initialization, the servo amplifier resorts to using only the signals from the incremental encoders.

Externally, the servo amplifier can be controlled in one of four possible modes: 1) serial velocity mode, 2) serial torque mode, 3) analog velocity mode, and 4) analog torque mode. In serial velocity mode, the servo amplifier is configured as a velocity controller and a velocity command is specified through its serial port. The velocity controller is internal to the servo amplifier, and its parameters can be tuned or optimized for each application. In serial torque mode, the servo amplifier is configured as a torque controller. In analog velocity mode, the servo amplifier is configured as a velocity controller, and velocity command is specified through its analog input channel. In analog torque mode, the servo amplifier is configured as a torque controller, and current command is specified through its analog input channel.

For all the experiments, analog torque mode was used. The analog input is supplied in differential form and ranges between +/- 10 V. The servo amplifier samples the analog channel at 4000 Hz, and uses a 12 bit analog to digital (A/D) converter to process the analog input. One of the 12 bit A/D line is a sign bit.

4.1.3 Incremental Encoder

Each of the actuator packages has an incremental encoder, and each encoder has a matching interpolator. The encoder is a hollow shaft encoder supplied by Gurley

Precision. It has 8192 lines and outputs two buffered sinusoidal waves to an interpolator. The interpolator takes the buffered sinusoids and generates two sets of output quadrature square waves. The first set of output square waves from the interpolator is not interpolated, and when counted, is equivalent to 13 bits of position information. This output is sent to the servo amplifier and is used for implementing sinusoidal commutation. The second set of output square waves is interpolated, and when counted is equivalent to 17 bits of position information. This 17 bit position information is sent to a 16 bit counter, and the counter is read by the digital input/output (DIO) card of the computer. The 16 bit counter is used for the 17 bits encoder output because the range of motion within the workspace during normal operation (not during experimentation) is less than 180°, which corresponds to 16 bits, for each actuator package. The advantage of using a 16 bit counter as opposed to a 17 bit counter is because a 32 channel DIO card (16 channels for each counter) can be used as opposed to the next size up DIO card (48 channel DIO card) which costs more.

4.1.4 Torque Sensor

The torque sensor used in the experimentation is not part of the actuator package nor part of the robot assembly: the torque sensor was used only for experimentation. The torque sensor is Barry Wright Corporation's 6 axis force/torque sensor, FS6-120A.

The range of torque that could be measured with the torque sensor is approximately between 0 and 5 N-m in the clockwise direction and between 0 and 4.8 N-

m in the counterclockwise direction. The resolution is about 0.002 N-m, and the estimated instrument error is +/- 0.107 N-m (see calibration results in the appendix).

4.1.5 Computer

A 100 MHz PC was used as the controller. The computer was equipped with a D/A card, an A/D card, and a DIO card. Through the D/A card, the computer sends out a current command to the servo amplifier, and through the DIO card, the computer receives 17-bits of position information from each set of encoders. The A/D channels are used to read torque data from the torque sensor.

4.2 Actuator Experiment #1: Sliding Friction Experiment

The objective of this experiment was to measure the sliding friction in the actuator packages. This result should establish the minimum torque that the actuator must apply to overcome sliding friction.

In this experiment, the torque sensor was connected to the output shaft flange (output shaft) of the actuator package with three dowel pins. The torque sensor was then held and supported at its bottom, and then, rotated very slowly, moving along with it the output shaft. The measured torque is equivalent to the sliding friction.

4.2.1 Experimental Results for Upper Actuator Package

Figure 4.1 shows a plot of sliding friction measurement versus position and time for clockwise shaft rotation (relative to the output shaft end). The plot shows fluctuations in torque measurements around a mean. These fluctuations are apparently due to the cogging torque of the actuator. Figure 4.2 is the same as Figure 4.1, except the time scale is now between 0 and 5 seconds. This gives a better view of the fluctuations. The experiment was repeated twice in the same direction and Figure 4.3 and Figure 4.4 show the plot of the experimental results. Table 4.2 summarizes the measured sliding friction for all the three experiments. Three sets of experiments were also conducted with the torque sensor rotating in the counterclockwise direction. Figure 4.5 shows a plot of one of the experimental results, and Table 4.2, also, summarizes the results for the counterclockwise rotation.

From the results, it is noted that there is a slight difference between sliding friction in the clockwise direction and in the counterclockwise direction. This difference may be due to differences in the way the bearings are loaded. The average sliding friction for clockwise rotation is 0.274 N-m, and for counterclockwise rotation is 0.286 N-m. This gives an idea of the minimum torque that must be commanded during movements. When the arm is connected to the actuators, it is expected that friction will increase due to the friction of the additional bearings in the arm.

4.2.2 Experimental Results for Lower Actuator Package

Figure 4.6 shows one of three experimental data for the sliding friction measurement versus position and time, for clockwise shaft rotation. Figure 4.7 shows one

of three measured experimental data for sliding friction versus position and time for counterclockwise shaft rotation.

Table 4.2: Summary of Sliding Friction Measurements (Upper Actuator)

Experiment #	Direction of Rotation	Sliding Friction (N-m)
1	clockwise	0.275
2	clockwise	0.271
3	clockwise	0.276
4	counterclockwise	0.289
5	counterclockwise	0.285
6	counterclockwise	0.284

A summary of all the results is presented in Table 4.3. The average sliding friction for clockwise rotation is 0.259 N-m, and for counterclockwise rotation is 0.291 N-m.

In fully extended robot arm position with both actuators connected, the minimum reflected sliding friction to the end-point is between 0.596 N and 0.618 N. (This assumes a radial arm of 0.914 m or 36 in.) This gives an idea of the smallest force a patient must apply to move the robot.

Table 4.3: Summary of Sliding Friction Measurements (Lower Actuator)

Experiment #	Direction of Rotation	Sliding Friction (N-m)
1	clockwise	0.265
2	clockwise	0.258
3	clockwise	0.253
4	counterclockwise	0.294
5	counterclockwise	0.288
6	counterclockwise	0.292

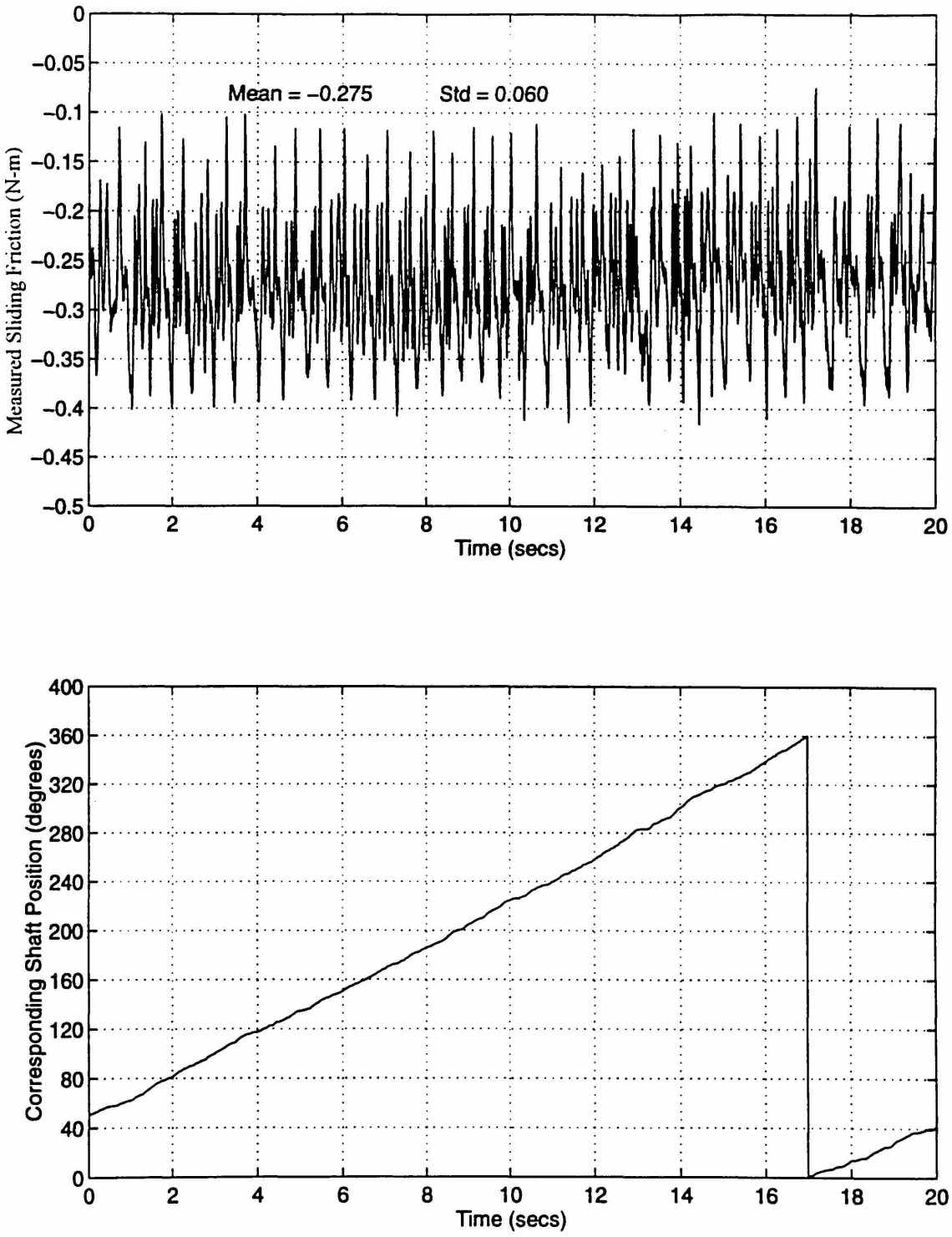

Figure 4.1: Upper Actuator: Sliding Friction Measurement (CW Rotation - #1)

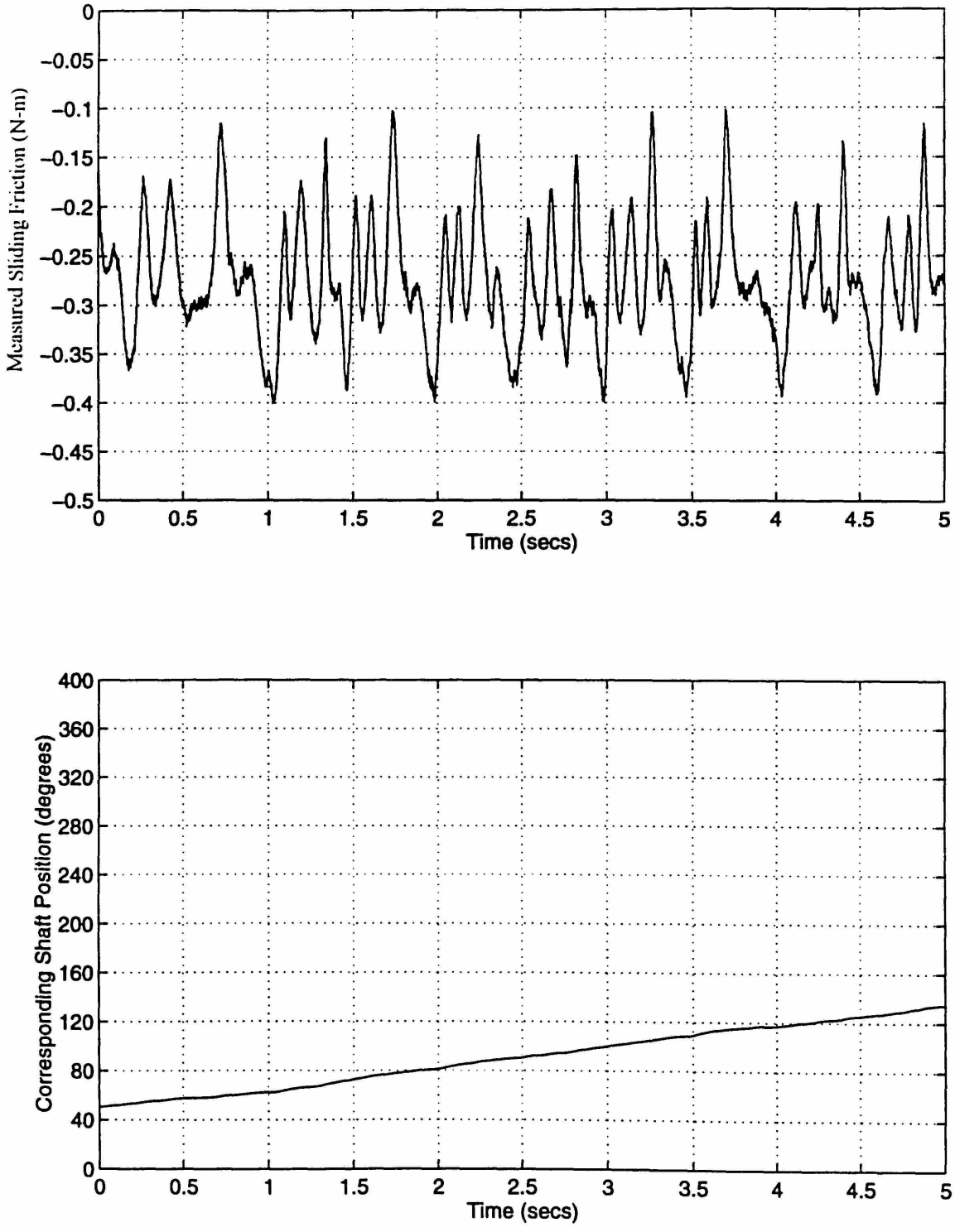

Figure 4.2: Scaled Copy of Figure 4.1

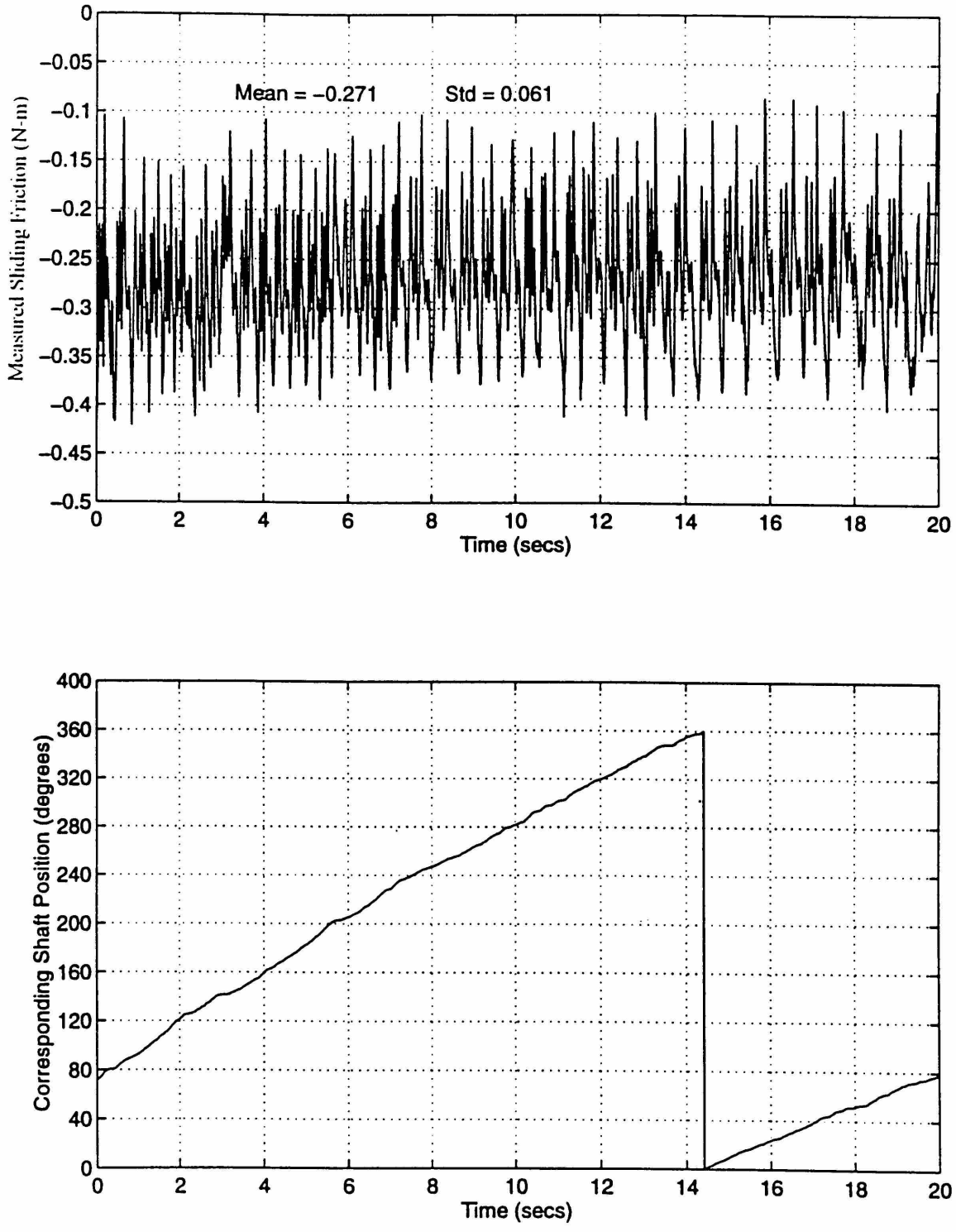

Figure 4.3: Upper Actuator: Sliding Friction Measurement (CW Rotation #2)

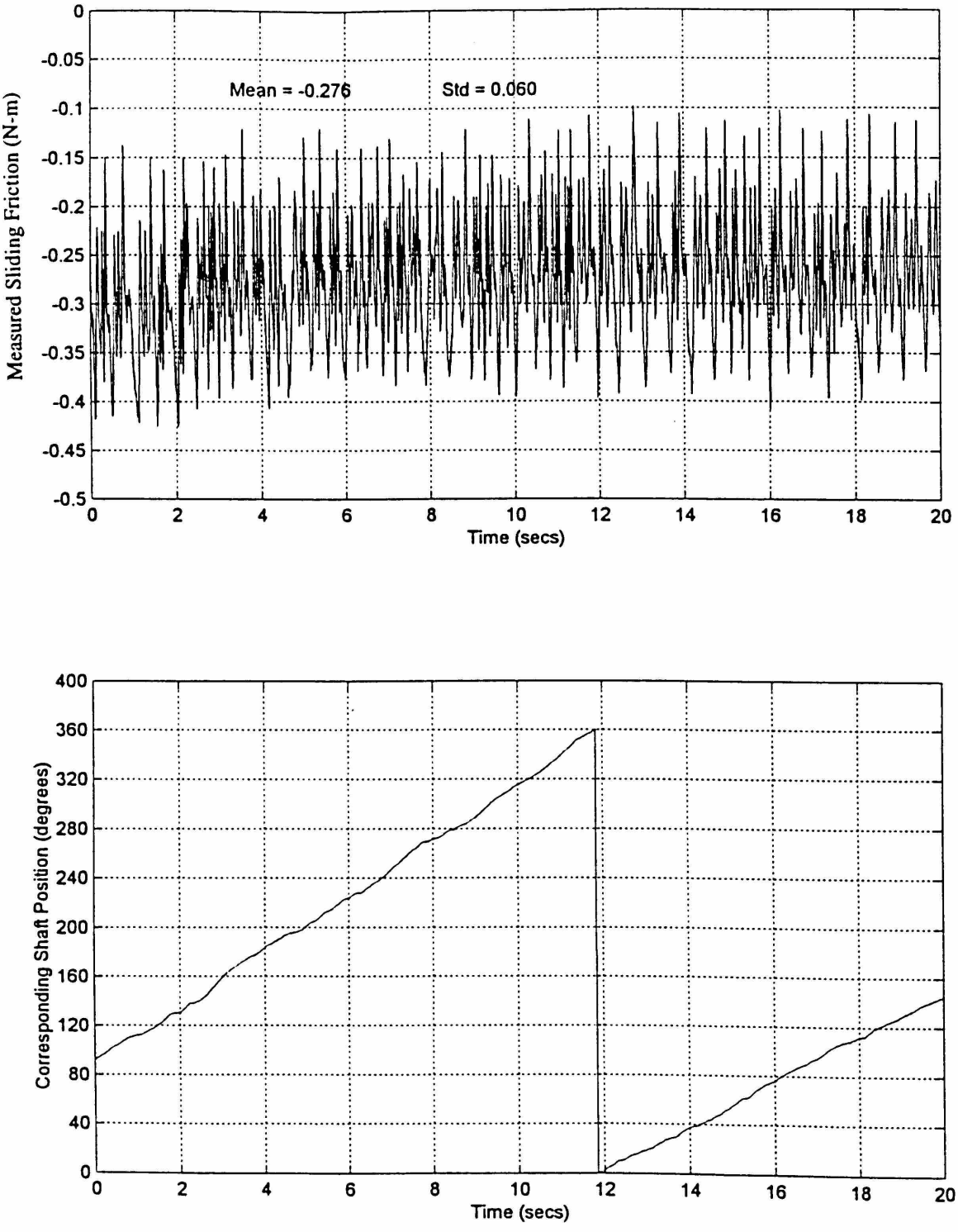

Figure 4.4: Upper Actuator: Sliding Friction Measurement (CW Rotation - #3)

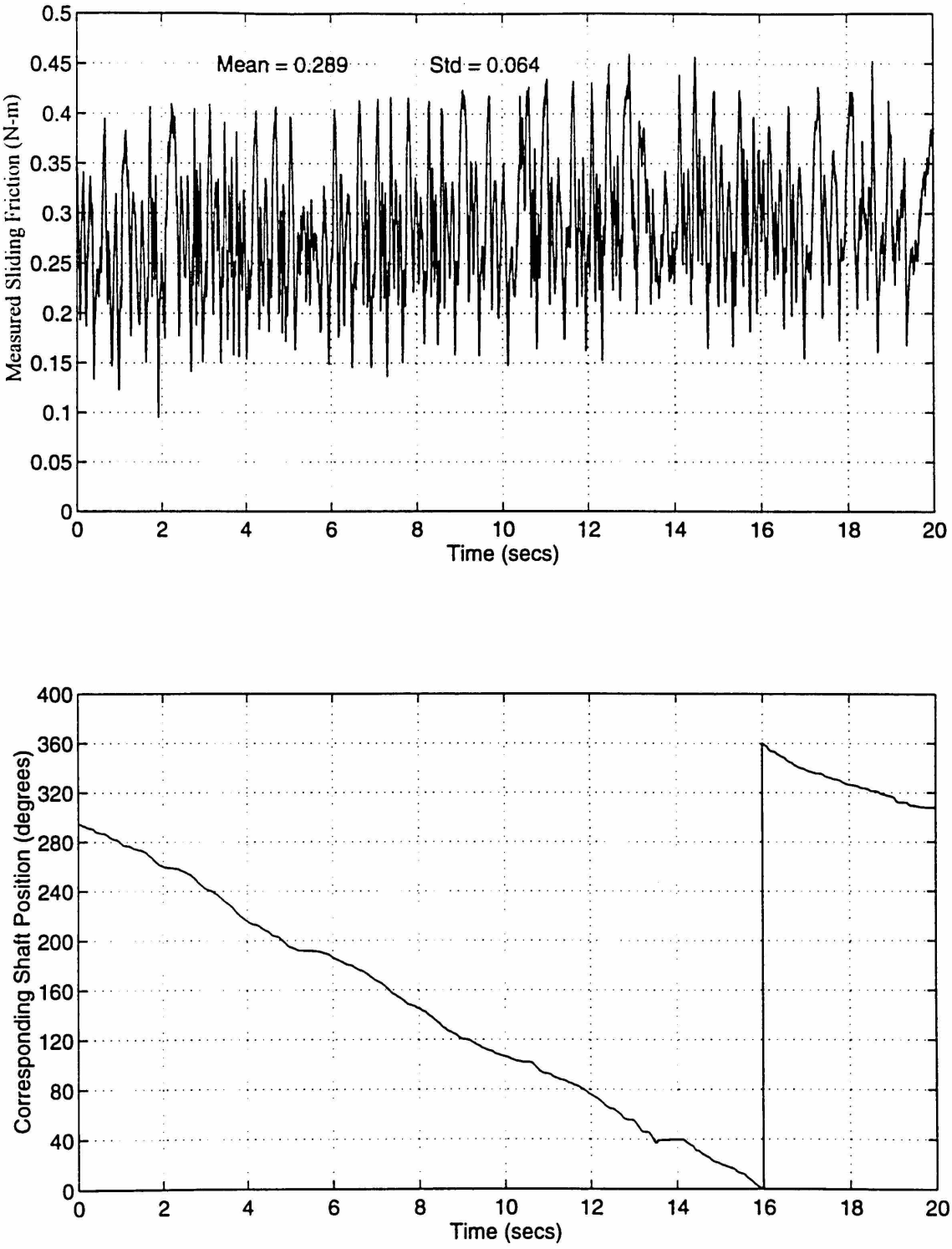

Figure 4.5: Upper Actuator: Sliding Friction Measurement (CCW Rotation - #1)

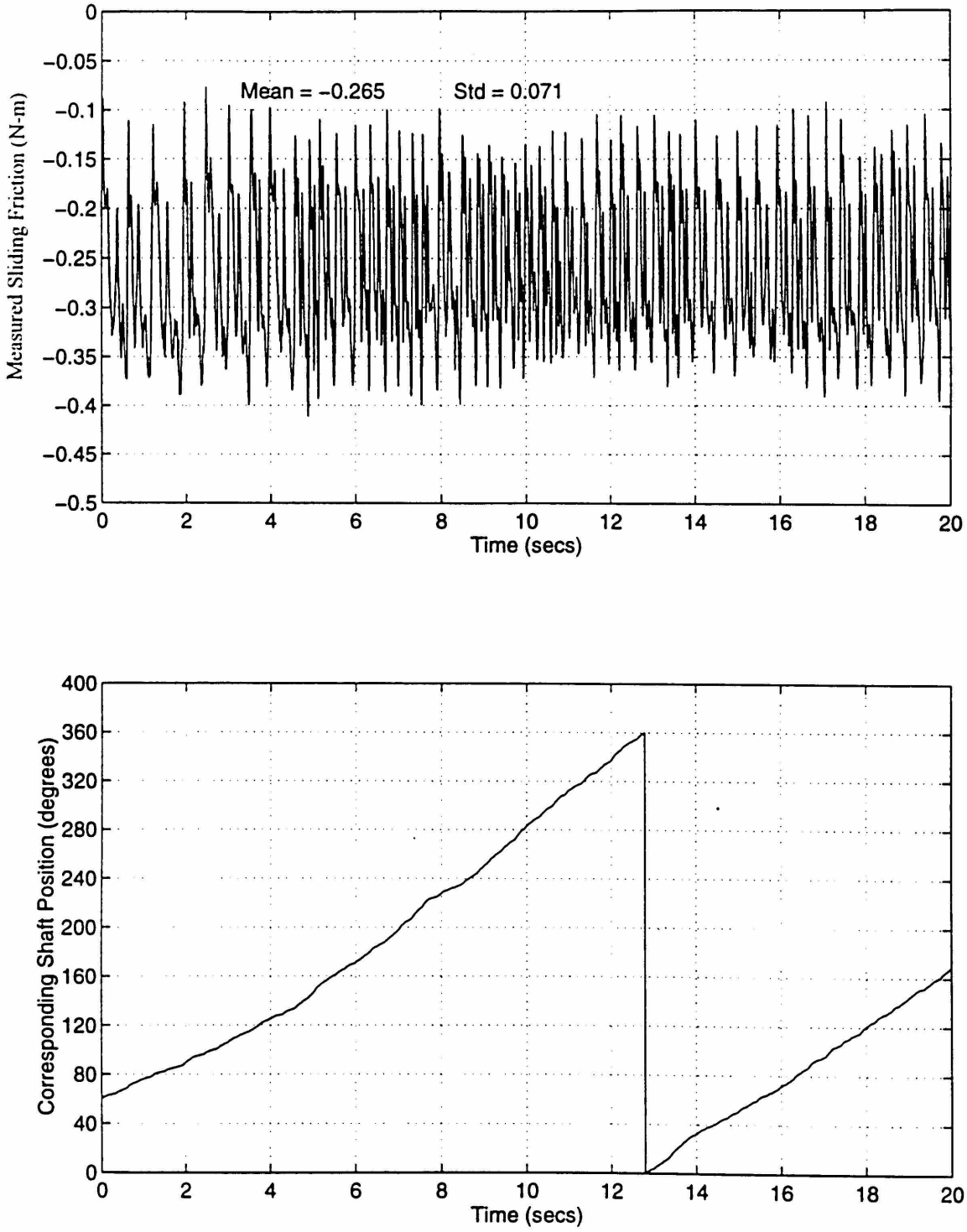

Figure 4.6: Lower Actuator: Sliding Friction Measurement (CW Rotation - #1)

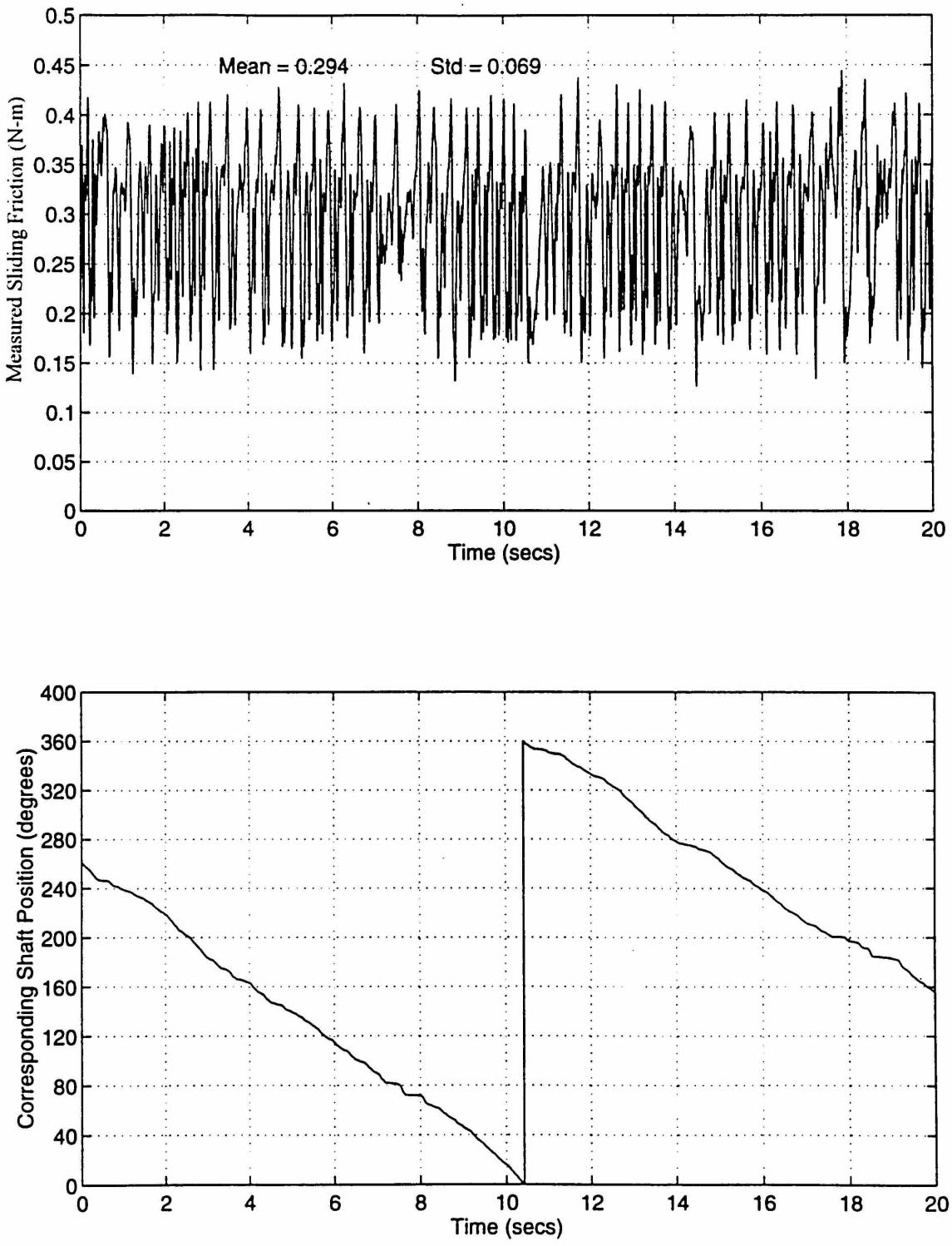

Figure 4.7: Lower Actuator: Sliding Friction Measurement (CCW Rotation - #1)

4.3 Actuator Experiment #2: Constant Current Command versus Torque Output

The objective of this experiment was to determine the torque constant of each of the actuator packages. For a brushless dc motor, theoretically, the torque constant should be constant, and according to the manufacturer, torque constant should be 4.002 N-m/amp with a tolerance of +/- 10%. In reality, torque constants are not that "constant", and it is therefore desirable to know the range of variability and how it can be compensated for by the controller.

The experimental setup is shown in Figure 4.8. The controller issues a constant current command to the servo amplifier, and reads the corresponding output torque from the torque sensor. An arbitrary mark is placed on the output flange of the actuator, and this establishes the 0° position of the shaft. The experiment was conducted on both actuator packages and was conducted at 0°, 60°, 120°, 180°, 240°, and 300° shaft positions. At each of these positions, a range of constant current was commanded, first in the clockwise direction (from output flange end), and then, in the counterclockwise direction. In the clockwise direction, constant current commands ranged between 0.120 amps and 1.440 amps in increments of 0.060 amps. In the counterclockwise direction, the range was between 0.120 amps and 1.080 amps in increments of 0.060 amps. The reason for the differences between the maximum currents commanded in both directions was due to torque sensor limitations. As stated earlier in this chapter, the torque sensor has a higher measuring range in the clockwise direction than in the counterclockwise direction. The actuator is capable of exerting higher torques. The available sensing range

corresponds to approximately half of the continuous torque requirement of 9.20 N-m for each of the actuators [Charnnarong, 1991].

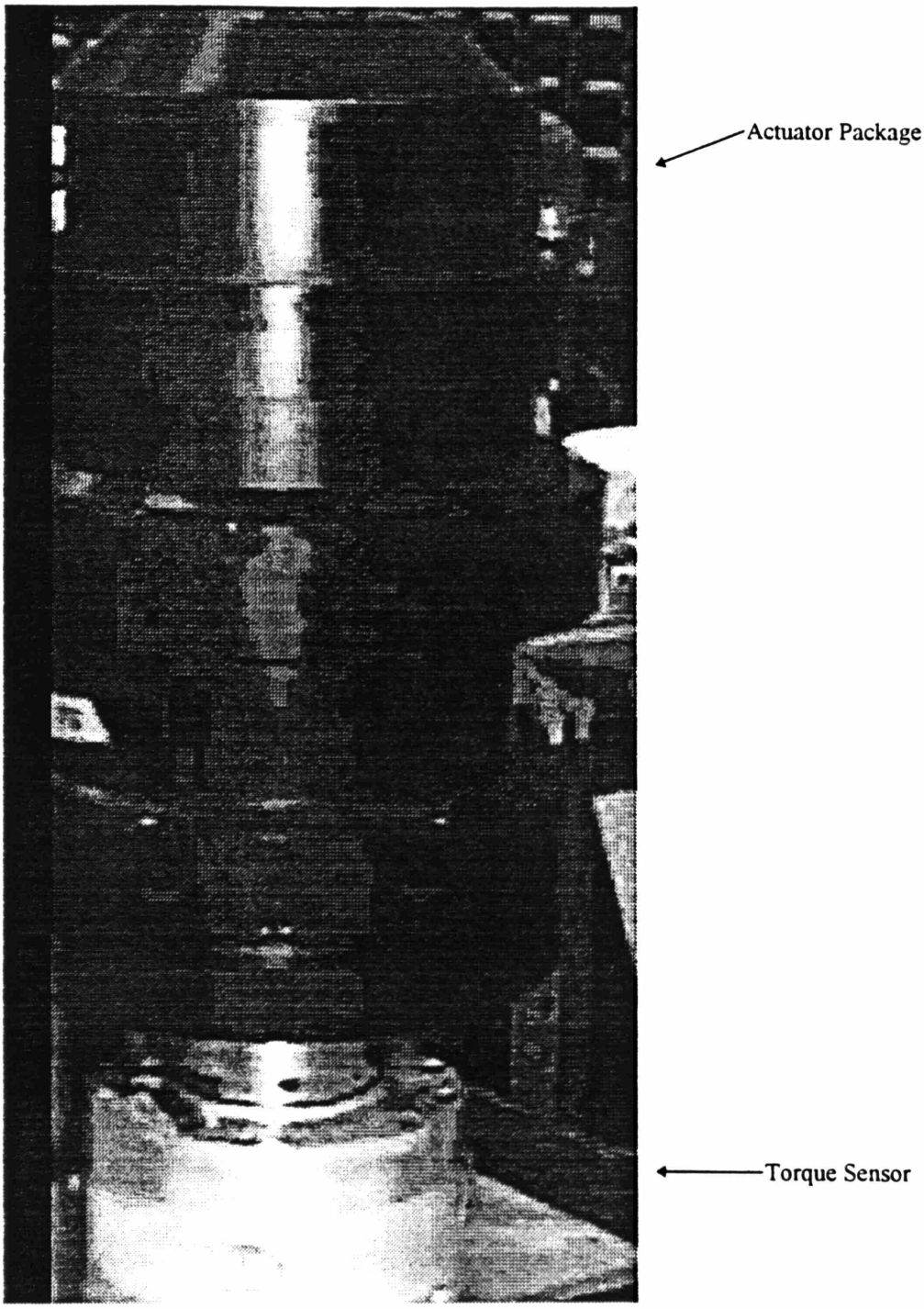

Figure 4.8: Experiment #2 Setup

4.3.1 Experimental Results for the Upper Actuator Package

Figure 4.9 through Figure 4.11 show plots of measured torque versus commanded current for the upper actuator package at the various shaft positions. Torque is defined positive when applied in the clockwise direction, and negative in the counterclockwise direction. On each of the plots are equations representing the relationship between measured torque and commanded current based on a least square approximation to the data. T_cw (shown in the plots) is based on a least square fit to all the data points in the clockwise direction, and so, valid for only positive currents I. T_ccw is based on a least square fit to all data points in the counterclockwise direction, and so, valid only for negative currents I. T is obtained based on least square fit to the entire data points, and so, valid for any current I.

Starting with Figure 4.9, the following general observations are made: 1) torque is directly proportional to current but with a slight offset (the intercept), and 2) the torque current relation depends on the direction of applied torque. Although, technically, the slope of the torque current equations cannot be called the torque constant because of the slight offset, for further discussion in this paper, it will be referred to as such. The slight offset might be due to insufficient data points in the very low torque range, but this offset should be retained in the equation.

Observe that the torque constant is higher in the clockwise direction than in the counterclockwise direction, and the same trend is observed from data at other positions. From the torque sensor calibration data (see Appendix), the torque sensor is not likely to be the source of this difference -- direction bias. Rather, the difference is probably due to

winding non-linearities or differences between the three winding coils. The windings of the motors are separately wound, so it is not unreasonable to suspect that slight differences between winding characteristics will exist. If one isolates each of the windings, one might be able to come up with individual torque constants for each winding. Furthermore, the possibility of winding differences is not contradicted by data collected at other shaft positions; the same trend is observed in all of them. Granted that this is a three phase motor, which means six electrical cycles per mechanical revolution, the same set of phase currents should be commanded by the servo amplifier every 60 degree change in shaft position, and the same trend should be observed.

The torque constants measured at various positions are different; torque constant is also a function of shaft position. Figure 4.12 shows a plot of the variation in torque versus shaft position given a 0.6 amps constant current command. The values plotted are based on using least square fit approximation to the experimental data. At least two things can be observed from the plot: 1) looking at shaft position, the torque calculated based on least square fit of all data points closely matches the torque calculated by least square fit of data points in each of the two directions, and 2) there is a pattern to the torque variation, that seems to repeat every 120°. The reason for this torque pattern is not clear.

The next meaningful step would be to see how these experimental results can be used to better control the actuator. Clearly, output torque of the actuator is a function of current, direction, and position. One possible approach is to make all but one of the parameters (i.e., current, direction, and position) constant and observe the output torque.

From Figure 4.12 and the discussion in the previous paragraphs, direction dependency might be assumed negligible if it can be shown that using least square fit of all data points is very comparable to the least square fits torque in both the clockwise and counterclockwise directions. That is, T is a good approximation of T_cw and T_ccw, and thereby, we can neglect T_cw and T_ccw and focus on using T. A similar argument can be made for position dependency. If a least square fit approximation can be used to account for variation in the torque as a function of position, then a single simple equation relating torque and current can be obtained.

This idea can be achieved by finding the least square fit to all the data points. That is, least square fit to all data points from all the positions. The data points obtained from each of the shaft positions was combined and the least square fit approximation was calculated. Figure 4.13 shows a plot of the combined data points. The least square fit equation is

$T = 3.917\, I + (0.025),\ Nm$

The error (or standard error of estimate, SEE) of the approximation is +/- 0.010 N-m. According to Coleman and Steele [1991], for a 95% level of confidence in approximation, the estimated error should be +/- 2(SEE). So for a 95% confidence level, the error in the approximation is +/- 0.020 N-m. The combined total error, accounting for estimated instrument error (see torque sensor calibration results in Appendix), for 95% confidence level, the error is 0.107 N-m using root sum square (RSS). Figure 4.13 shows the plot of the error band; more than 95% of the data points lie within the error band.

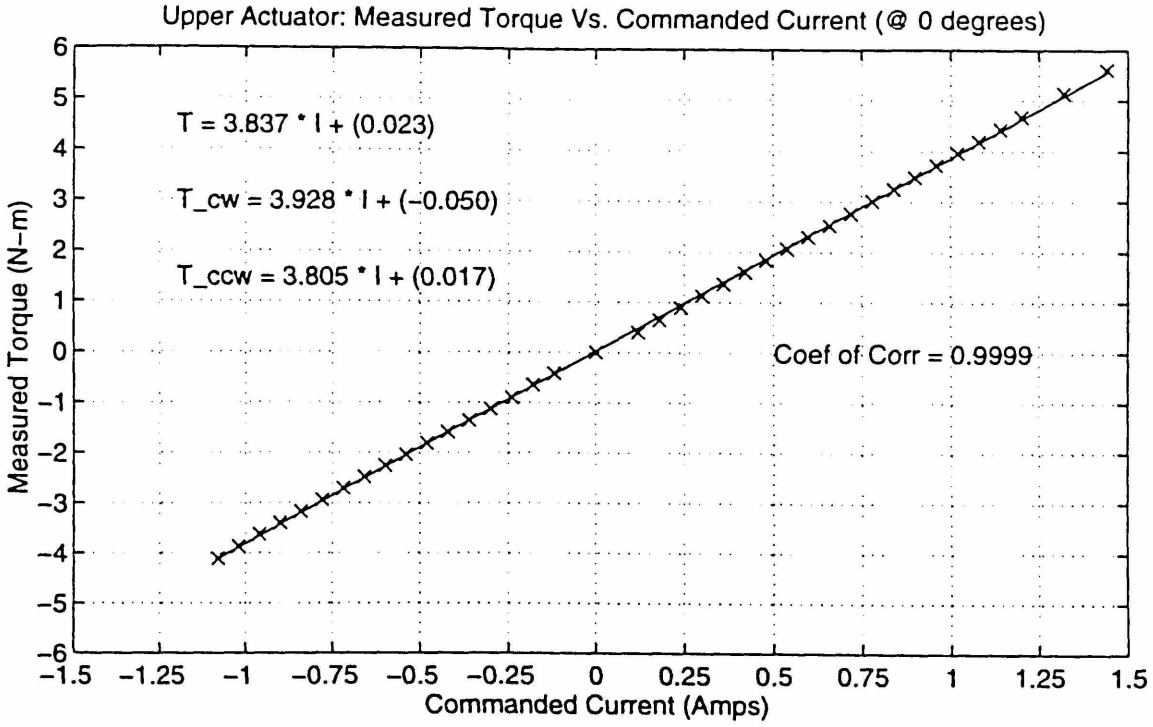

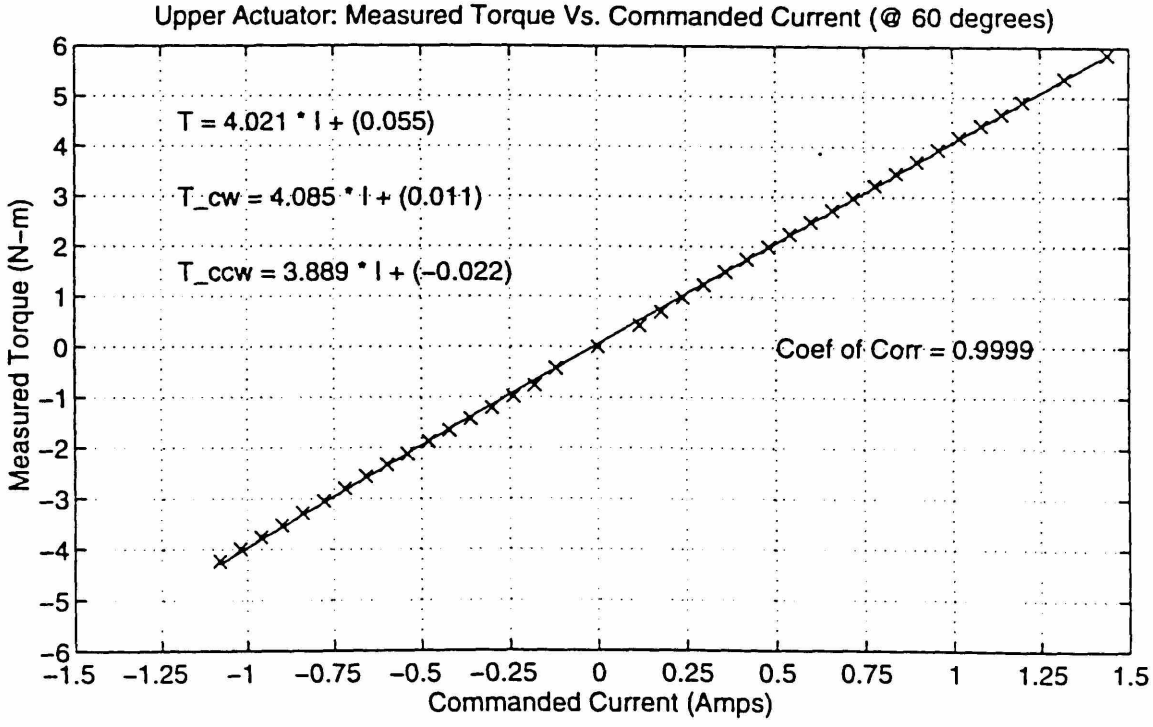

Figure 4.9: Upper Actuator: Measured Torque Vs. Commanded Current (@ 0 and 60 degrees)

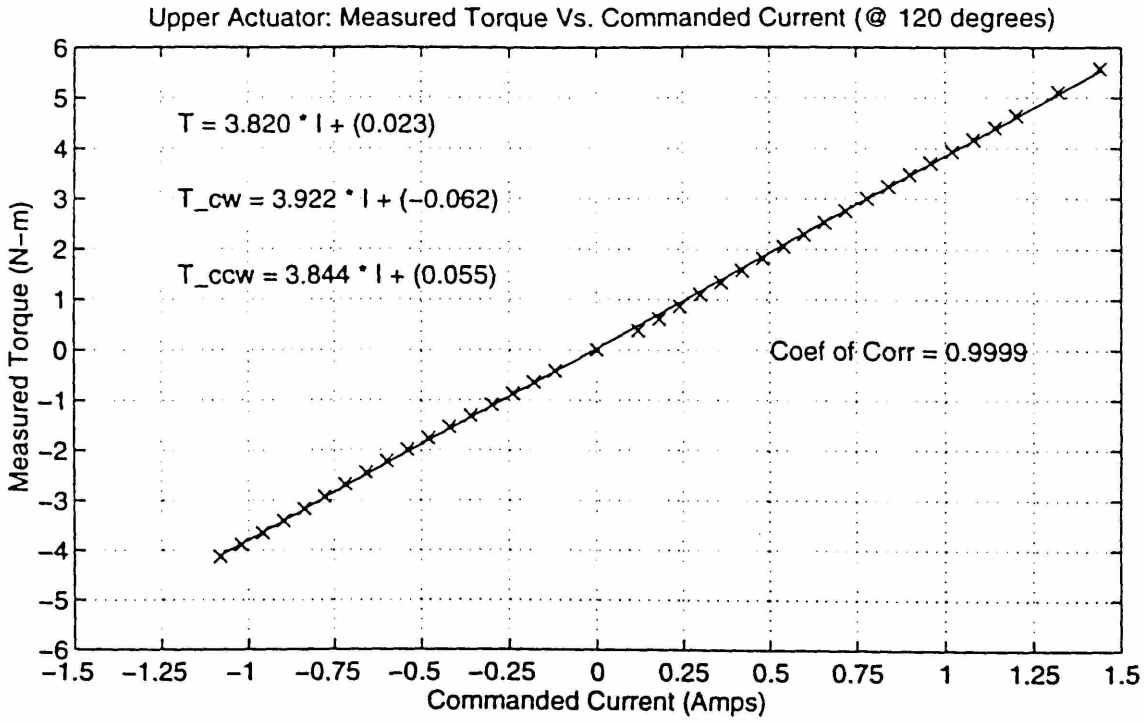

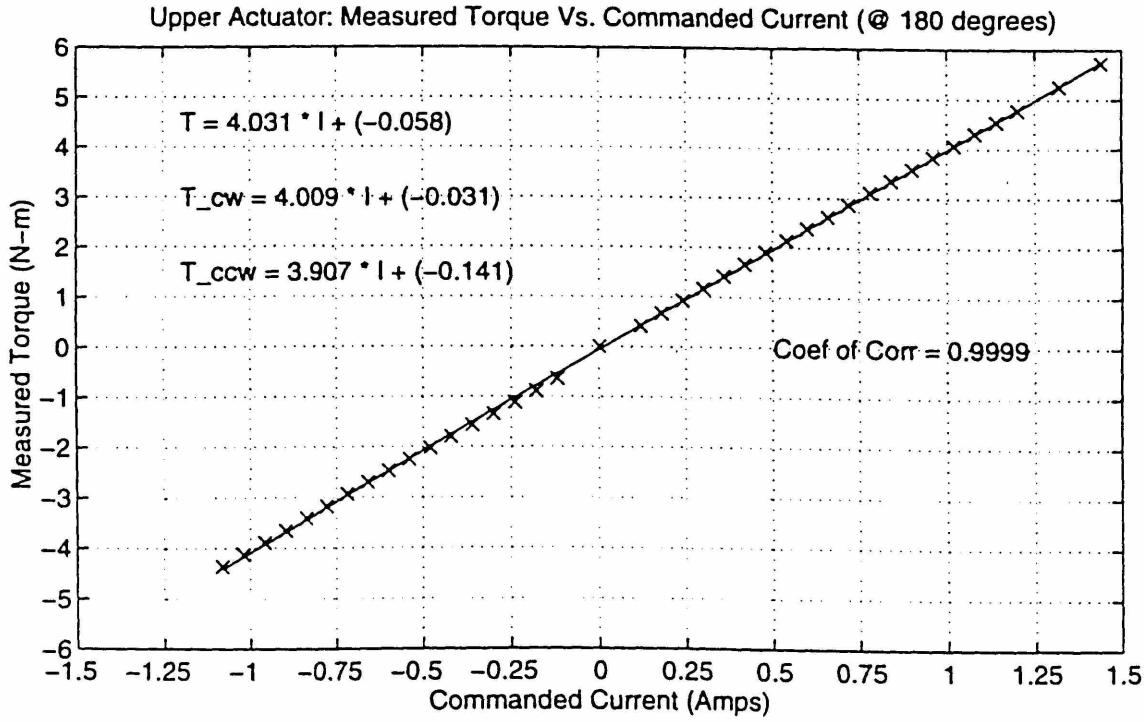

Figure 4.10: Upper Actuator: Measured Torque Vs. Commanded Current (@ 120 and 180 degrees)

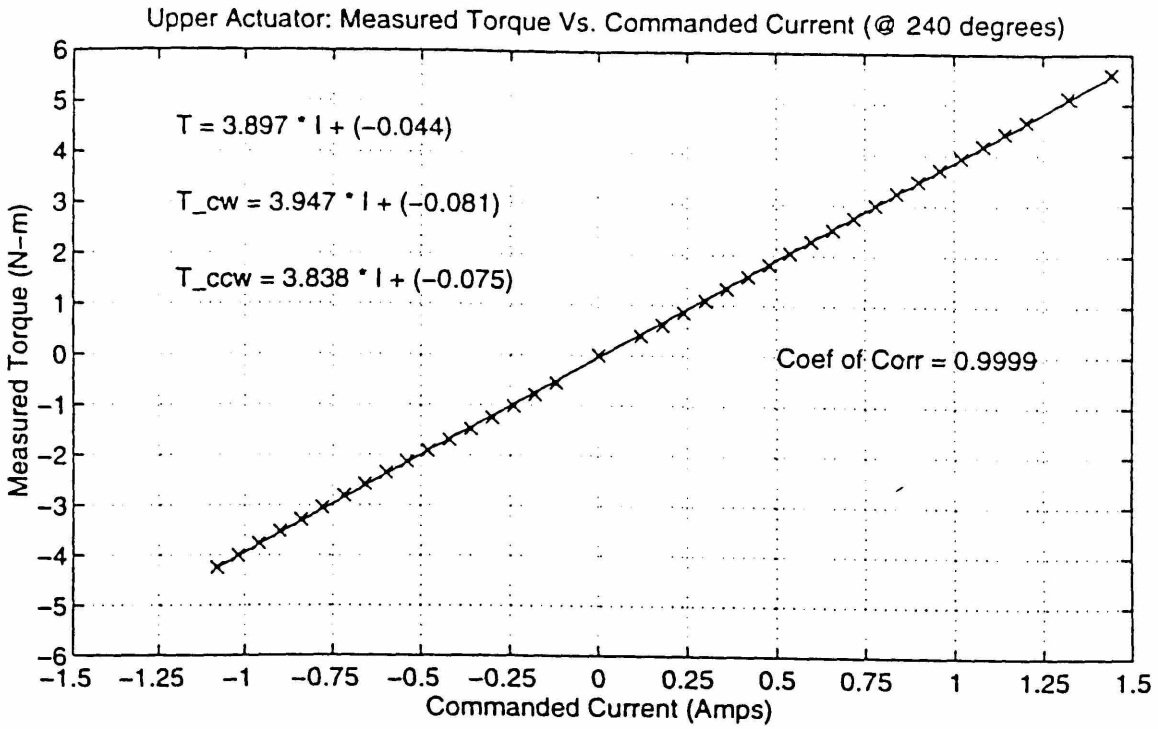

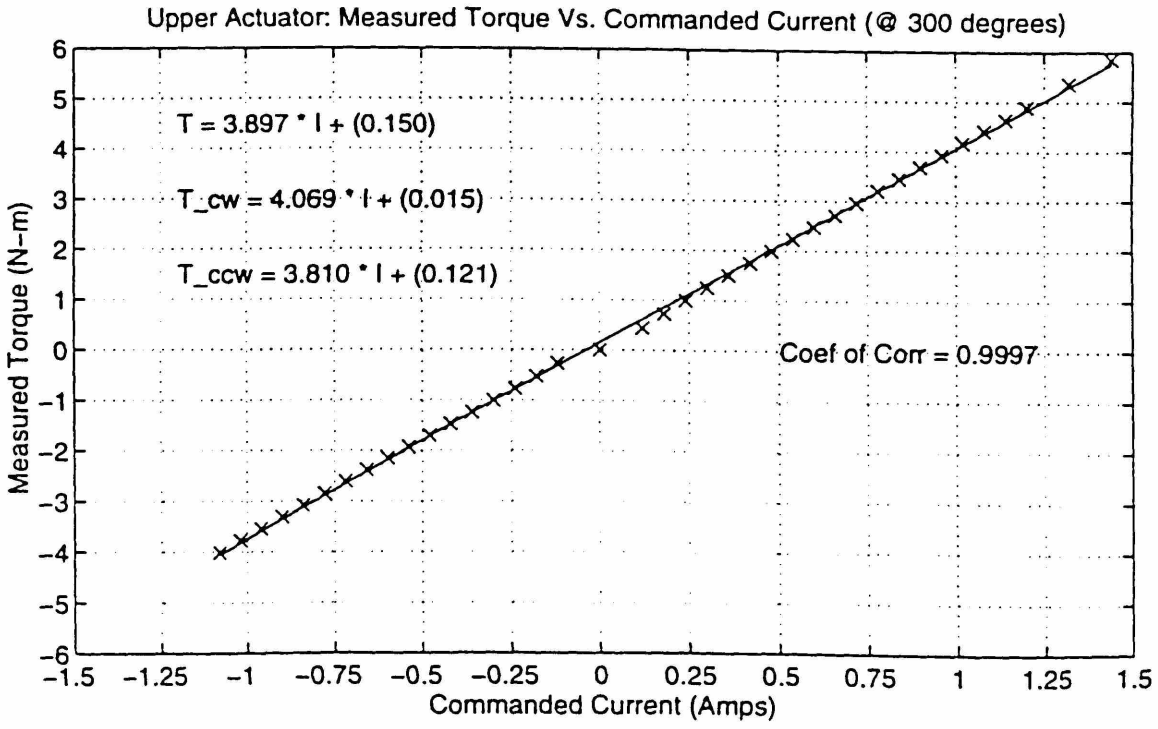

Figure 4.11: Upper Actuator: Measured Torque Vs. Commanded Current (@ 240 and 300 degrees)

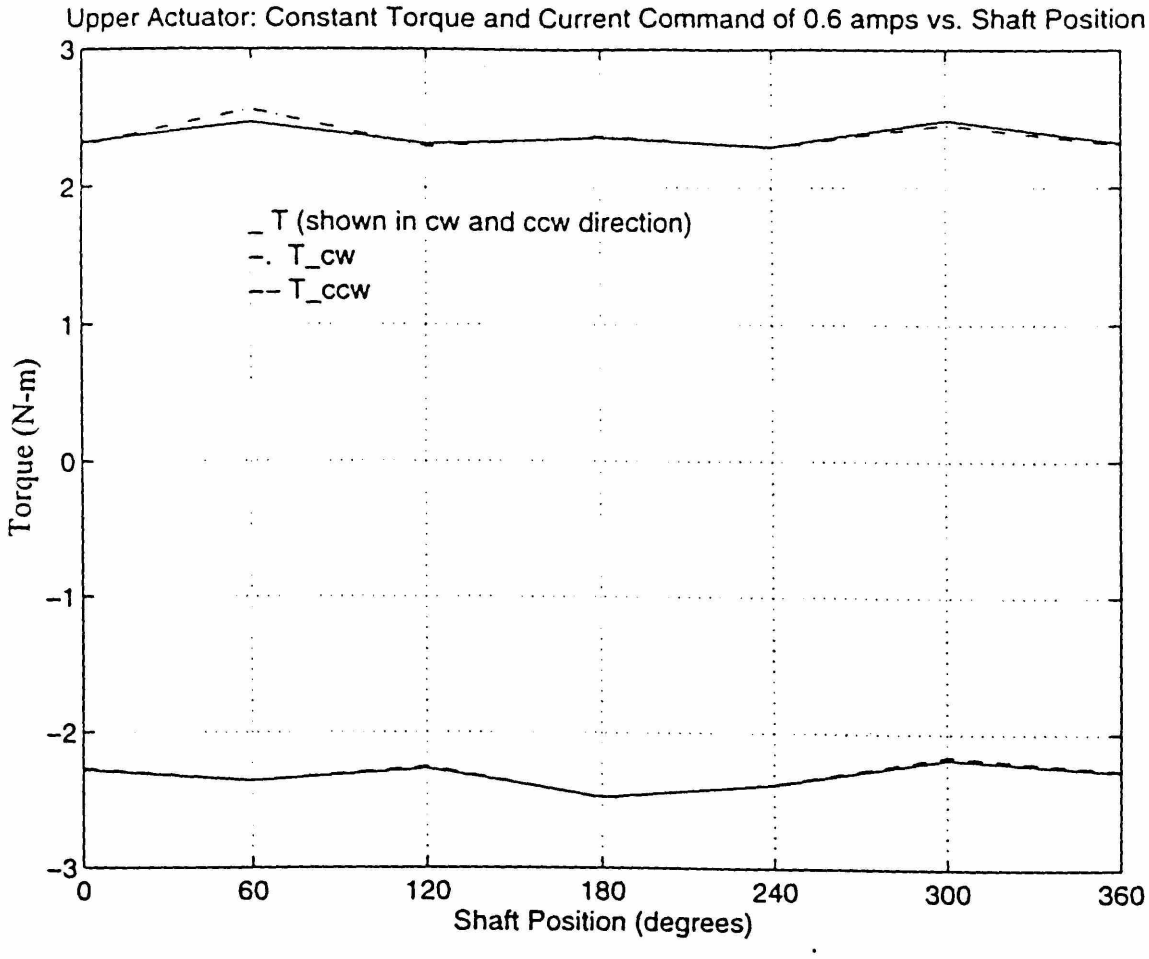

Figure 4.12: Upper Actuator: Constant Torque and Current Command of 0.6 amps Vs. Shaft Position

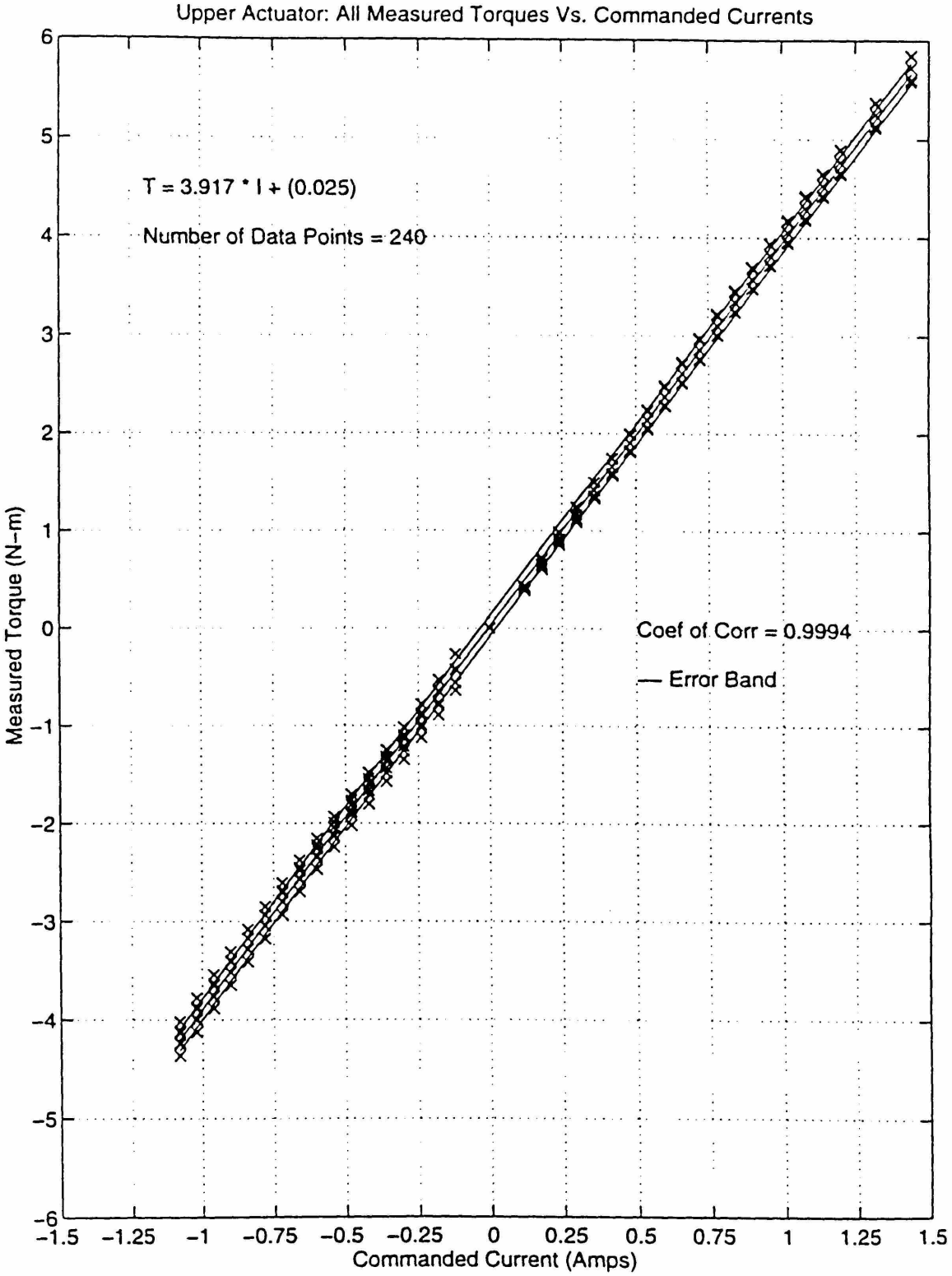

Figure 4.13: Upper Actuator: Combination of Measured Torque Vs. Commanded Current at All Shaft Positions

4.3.2 Experimental Results for Lower Actuator Package

Figure 4.14 through Figure 4.16 show the plots of measured torque versus commanded current for the lower actuator package at the various shaft positions. The same observations made from the upper actuator package experimental results are also observed here. Figure 4.17 shows a plot of the variation in torque versus shaft position given a 0.6 amps constant current command.

Again, the data points obtained from each of the shaft positions is combined and the least square fit is applied. Figure 4.18 shows a plot of the combined data points. The least square fit equation is

$T = 3.944\ I + (0.068),\ Nm$

The error (or standard error of estimate, SEE) of the approximation is +/- 0.0046 N-m. For 95% level of confidence in the approximation, the estimated error should be +/- 2(SEE). So, the error is +/- 0.0092 N-m. Combining this with the instrument error (see torque sensor calibration results in Appendix) yields a total error is 0.107 N-m using root sum square (RSS). Figure 4.18 shows the error band; more than 95% of the data points lie within the error band.

A total error of +/- 0.107 N-m in commanded torque translates to +/- 0.117 N at end-point of the robot (assuming fully extended arm position -- 36 in radial arm). If the applied torque is 4.1 N-m, which corresponds to half of the continuous torque requirement of each actuator, the corresponding end-point force is 4.5 N. The total estimated error is 5.2% of 4.5 N. This assumes that only the lower actuator package is

supplying the torque. At higher end-point forces, it is expected that the percentage of total error will be less than 5.2%. To put the magnitude of this error into a bit of perspective, according to Dr. Jones [1992], humans can perceive 6% to 8% change in force. This implies that the total estimated error at half of the continuos torque requirement of each actuator is slightly lower than the change in force that humans can perceive. This suggest that using the approximate torque constant equations will be a good first step in estimating applied actuator torques and in controlling these torques.

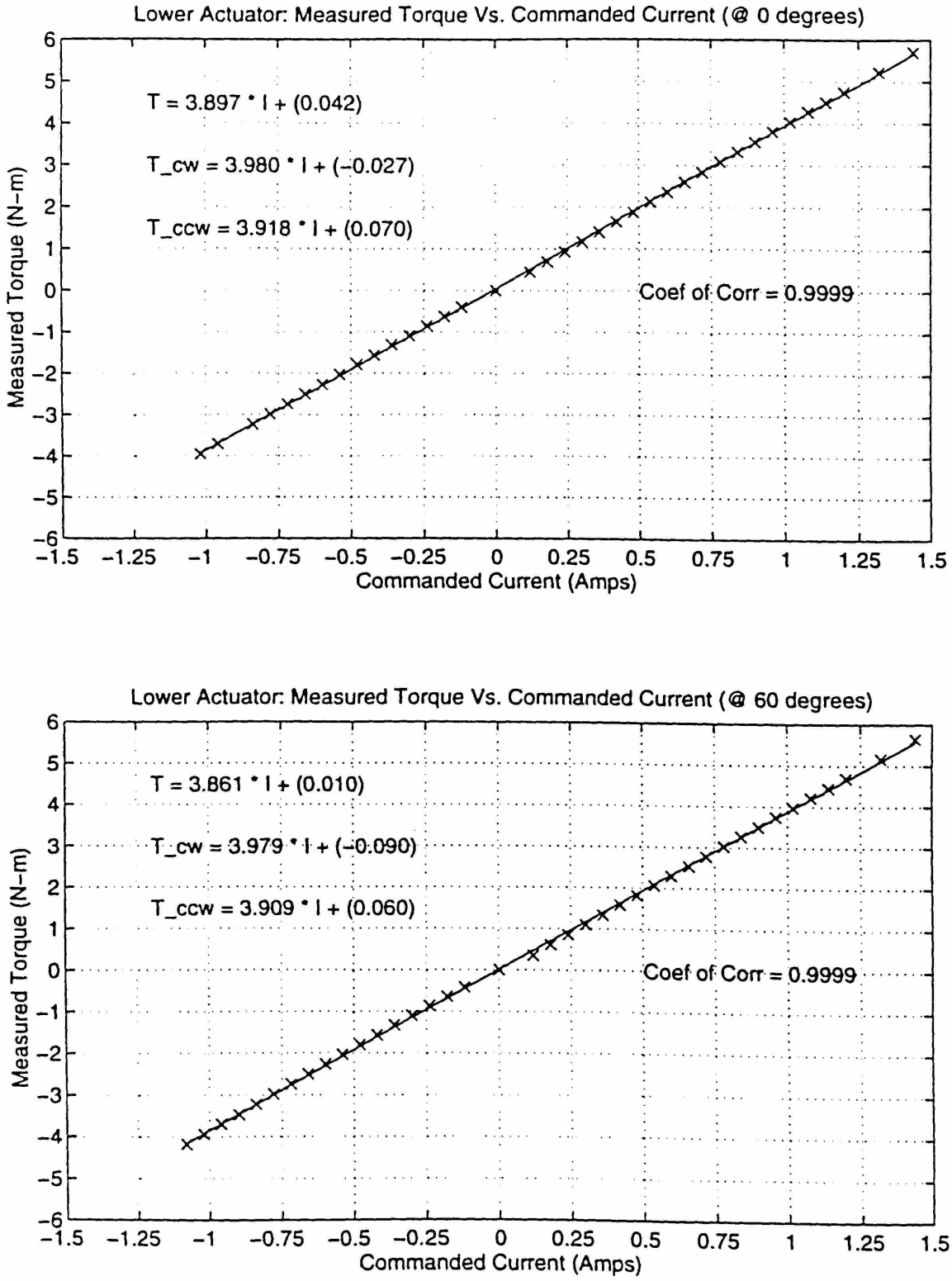

Figure 4.14: Lower Actuator: Measured Torque Vs. Commanded Current (@ 0 and 60 degrees)

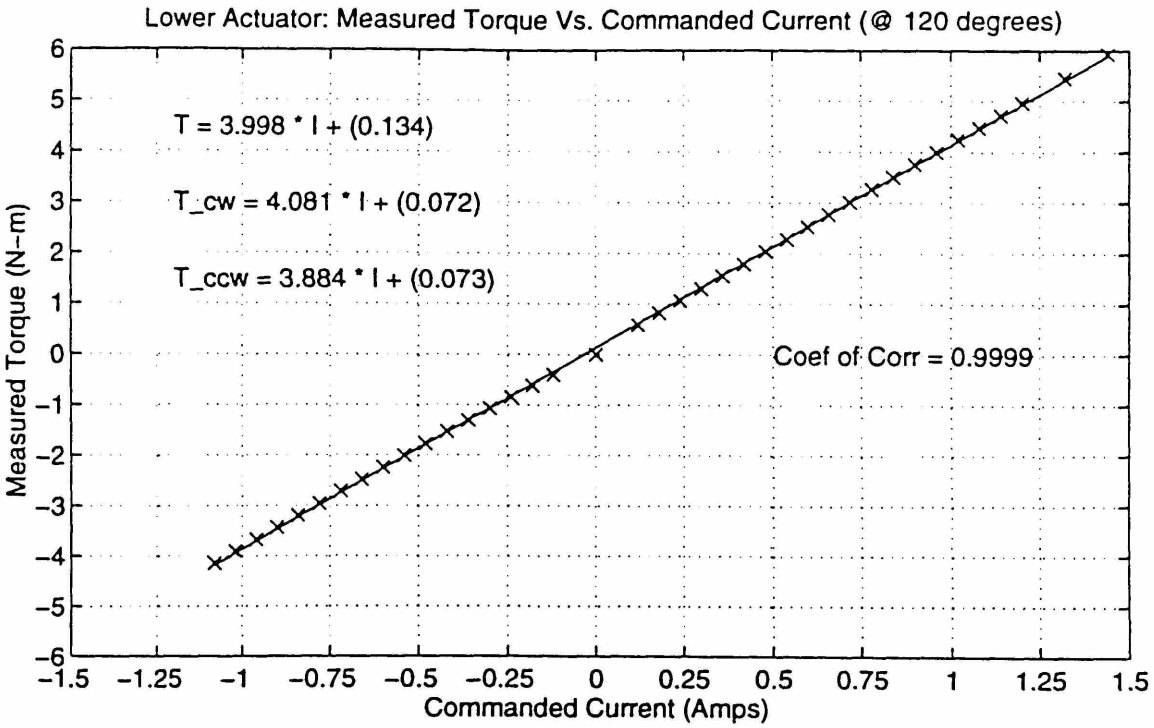

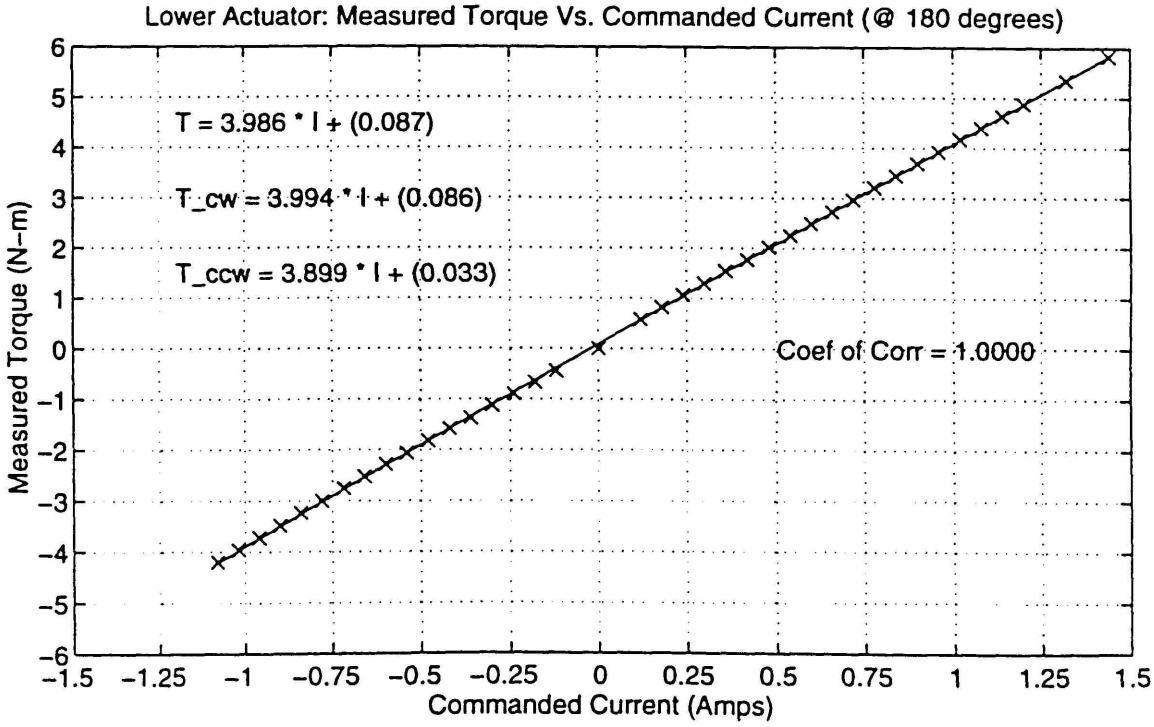

Figure 4.15: Lower Actuator: Measured Torque Vs. Commanded Current (@120 and 180 degrees)

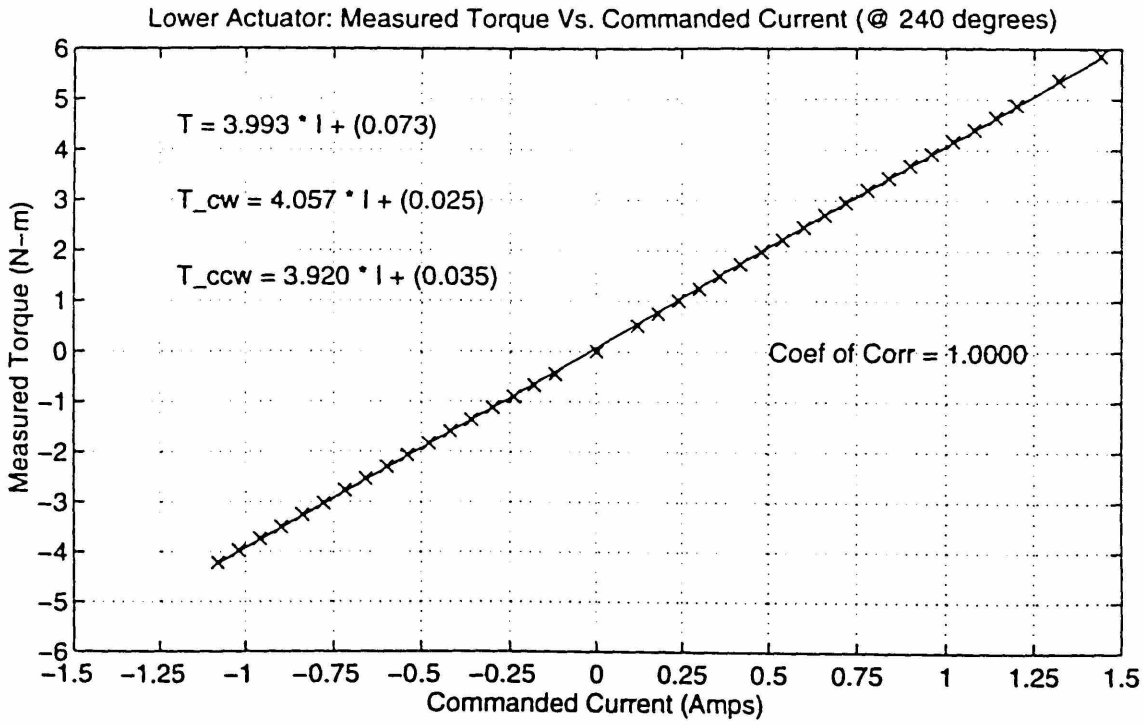

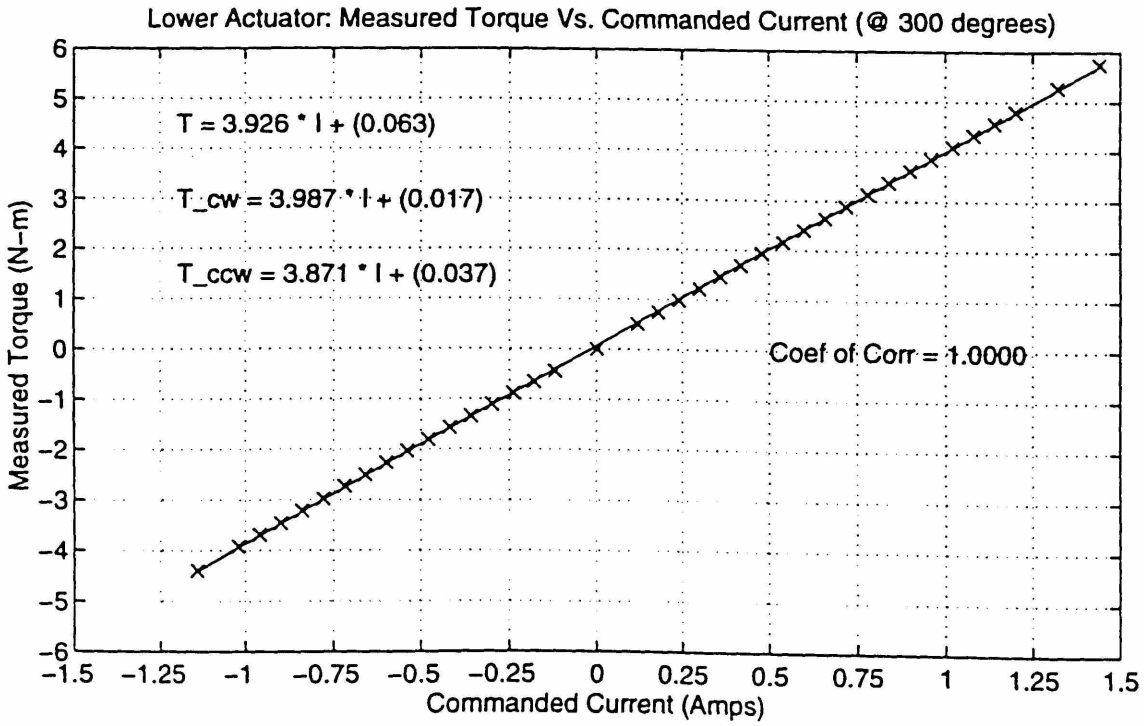

Figure 4.16: Lower Actuator: Measured Torque Vs. Commanded Current (@ 240 and 300 degrees)

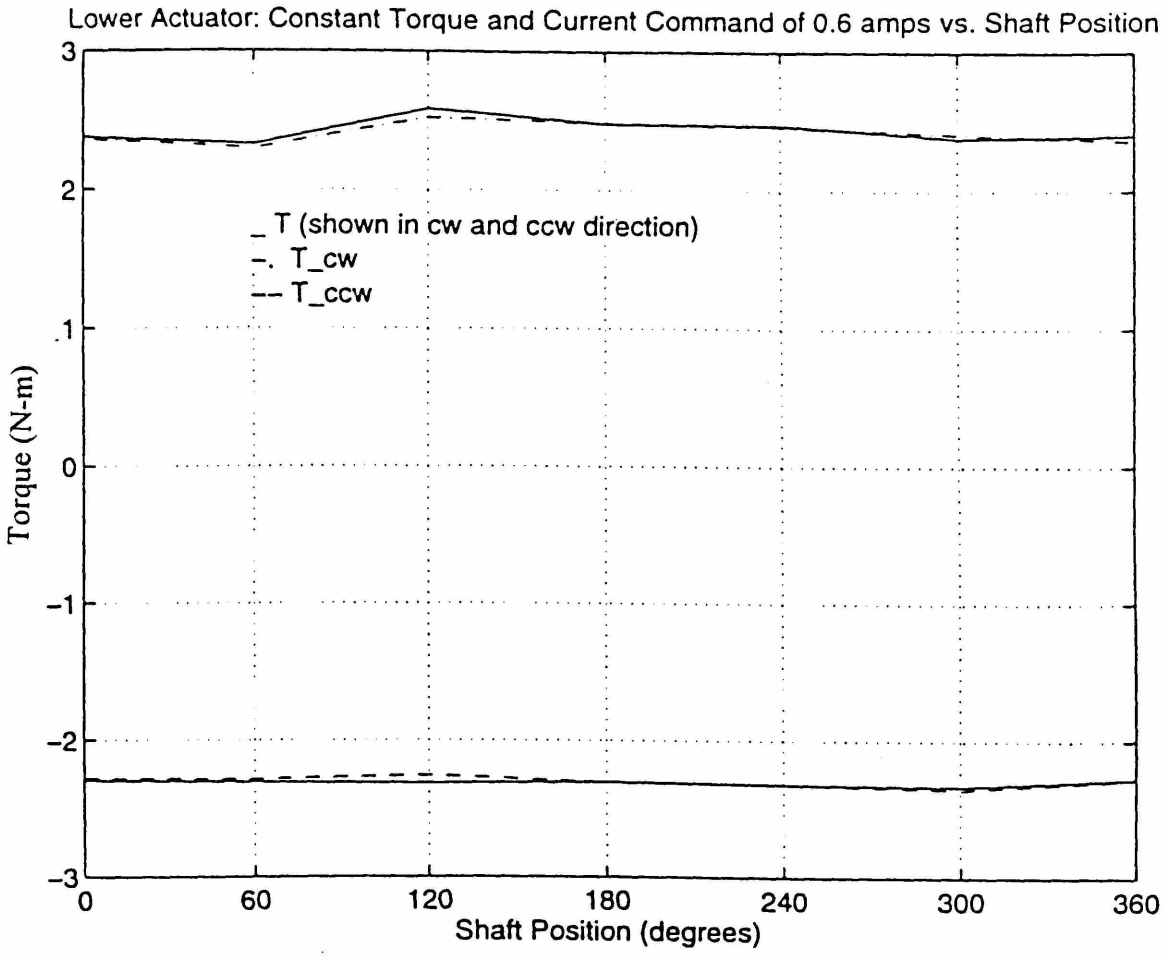

Figure 4.17: Lower Actuator: Constant Torque and Current Command of 0.6 Amps Vs. Shaft Position

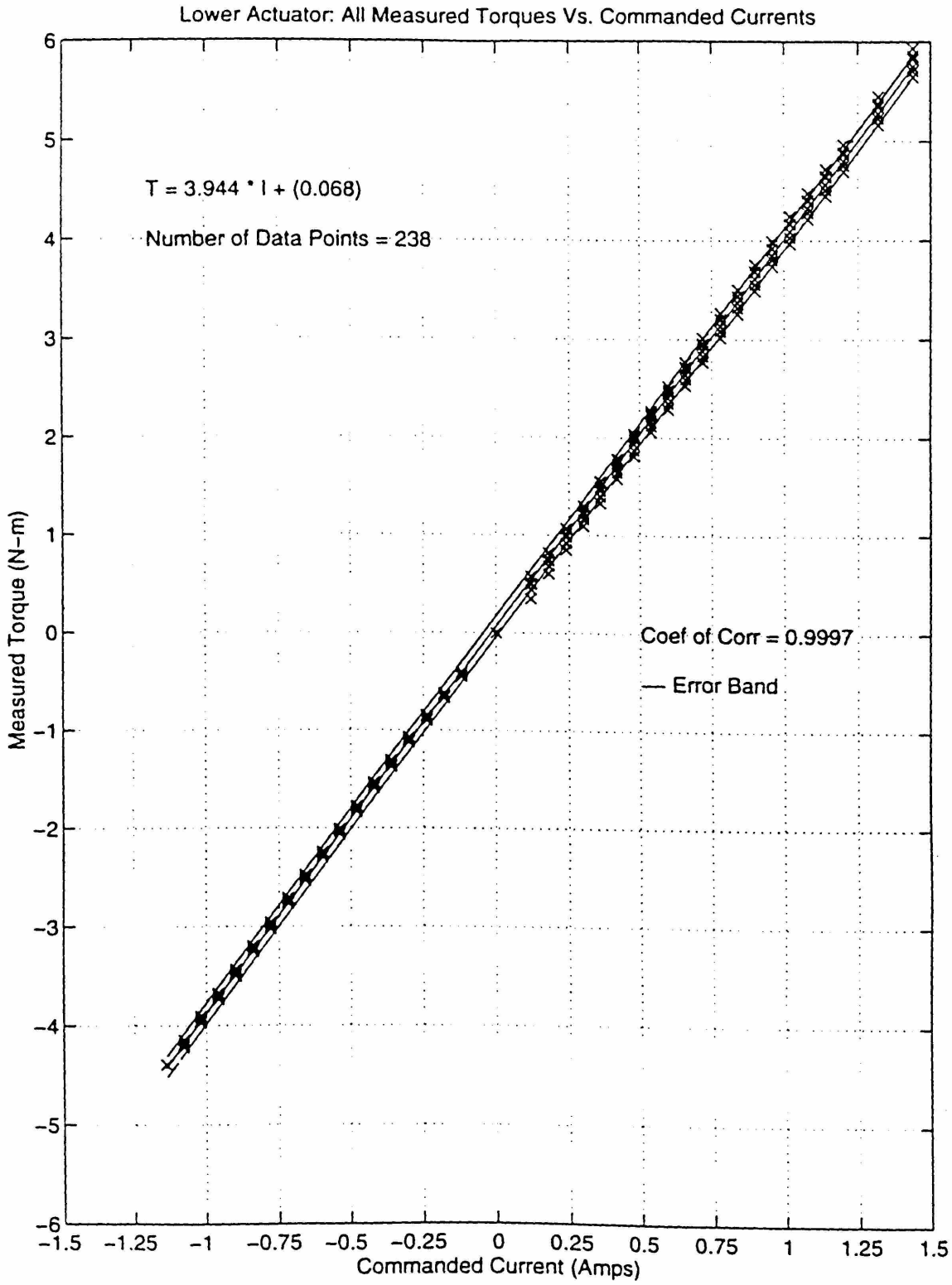

Figure 4.18: Lower Actuator: Combination of Measured Torque Vs. Commanded Current at All Shaft Positions

4.4 Actuator Experiment #3: Sinusoidal Current Command versus Output Torque

The objective of this experiment was to determine the torque bandwidth. The bandwidth indicates how well the output torque follows the commanded input current. This indicates how quickly current can be commanded.

The experimental setup was the same as shown in Figure 4.8. The controller issues a sinusoidal current command to the servo amplifier, and reads the corresponding output torque from the torque sensor. For each setup, the shaft was fixed in one of six positions (at 0° , 60°, 120°, 180°, 240°, and 300°)position. The amplitude of commanded current was 0.18 amps, and the frequency ranged between 0.1 Hz and 45 Hz.

4.4.1 Experimental Results for Upper Actuator Package

A Bode plot of measured torque vs. commanded current is shown in Figure 4.19. The gains at each point are normalized with respect to the dc gain. That is,

$$G = \frac{(T_{meas} / I_{cmd})}{(T_{meas} / I_{cmd})_{dc}}$$

where G is the gain, T_{meas} is the measured sinusoidal torque, and I_{cmd} is the commanded sinusoidal current. The dc gain is equivalent to the torque constant. The gain is fairly constant, and deviates a bit from 0 dB as frequency approaches 45 Hz (gains dropping at about 0.02 dB/decade). There is a slight upward turn in gains at frequencies between 40 Hz and 45 Hz; this is consistent with other experimental data. The output is 90° out of phase at about 20 Hz, and 180 degrees out of phase at about 40 Hz. The graph resembles

a curve of a system with a pure transport delay. This is better seen by making a linear plot of phase versus frequency; the plot is shown in Figure 4.20. The equation relating phase, frequency, and transport delay is

$$\phi = \omega T$$

where w is frequency and T is the transport delay. Using least square approximation, the transport delay is 12 ms (intercept is 0.041 rad).

The transport delay is larger than expected. It is expected that the transport delay should be about 1.2 ms[1]. There are at least two likely sources of the transport delay, the servo amplifier or the torque sensor. The servo amplifier samples the input at 4000 Hz, but has an internal current control loop which we have very little information about. No information is given on how quickly output current is measured in the feedback controller. The current loop might be the largest source of transport delay. Also, according to the Barry Wright Corporation, the torque sensor has a third order low pass filter with cutoff frequency of 120 Hz. It is unknown how precise the third order low pass filter is.

The transport lag in the current loop can be determined by reading the commanded current and the applied current using the servo amplifier. The servo amplifier measures these two parameters and stores them. The measured current is a combination of the phase currents in the three windings, Ia, Ib, and Ic. At certain positions, one of the phase currents is peak and the commanded current, Icmd, is roughly equivalent to this phase current. By examining the Icmd and one of the phase currents in their peak or near peak current position, one might be able to estimate the transport delay in current loop,

[1] Teresa Peterson, Technical Support Representative for Kollmorgen Motion Technologies Group

and also, possibly, get a better understanding of the winding characteristics. Figure 4.21 shows the plot of commanded current versus phase current Ia; Ia is at peak of commanded current (i.e., at dc, 100% of the commanded current flows through winding a). The plot shows a 9° phase lag at 40 Hz, which corresponds to 0.63 msecs delay. This clearly is not the source of the transport delay.

Another possible large contributor to the transport delay is the torque sensor. However, the torque sensor's bandwidth has not been determined. Therefore, for now, the source of the transport delay is unknown. But one important observation is that the phase lag between the output torque and the commanded current at frequencies less than 20 Hz is less than 90°. The frequency range of interest in our application is between 0 Hz and 7 Hz.

4.4.2 Experimental Results for Lower Actuator Package

The experimental result is the same as observed in the upper actuator package. Figure 4.22 shows the plot of measured torque versus sinusoidal commanded current; Figure 4.23 shows the linear plot of phase versus frequency. Again, the transport delay is 12 ms (intercept is 0.043 rad). Figure 4.24 shows the plot of commanded current versus phase current Ic; where current in winding c is at 88% of peak (i.e. at dc, 88% of the commanded current flows through winding c). Again, the lag between the commanded current and the phase current is approximately 9° at 40 Hz.

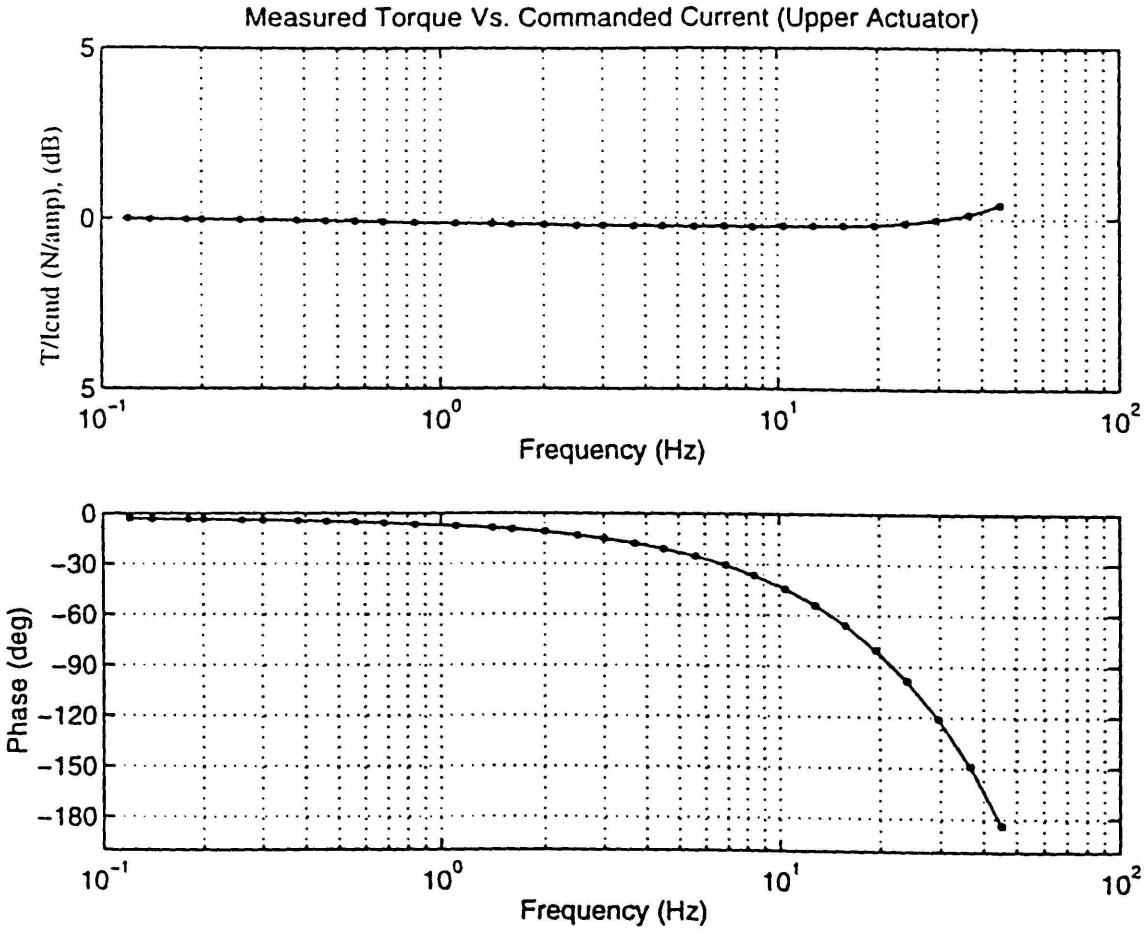

Figure 4.19: Measured Torque Vs. Commanded Current (Upper Actuator @0°)

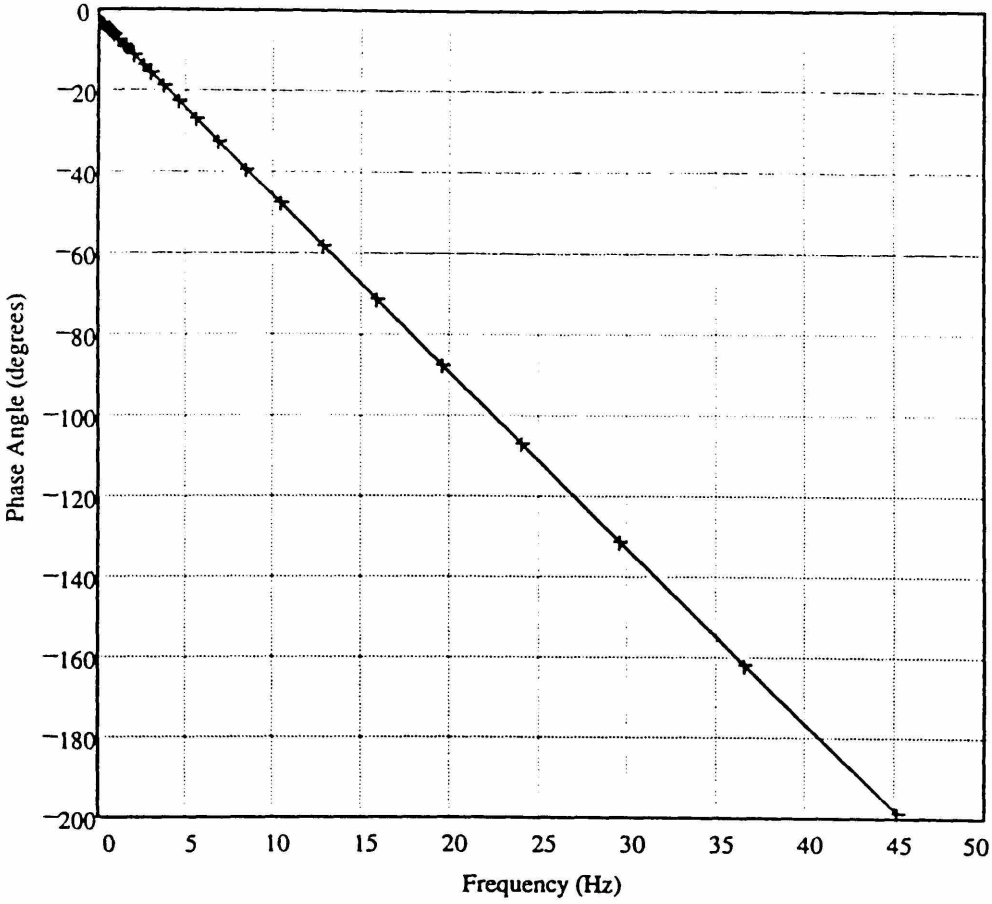

Figure 4.20: Linear Plot of Phase Vs. Frequency (Upper Actuator)

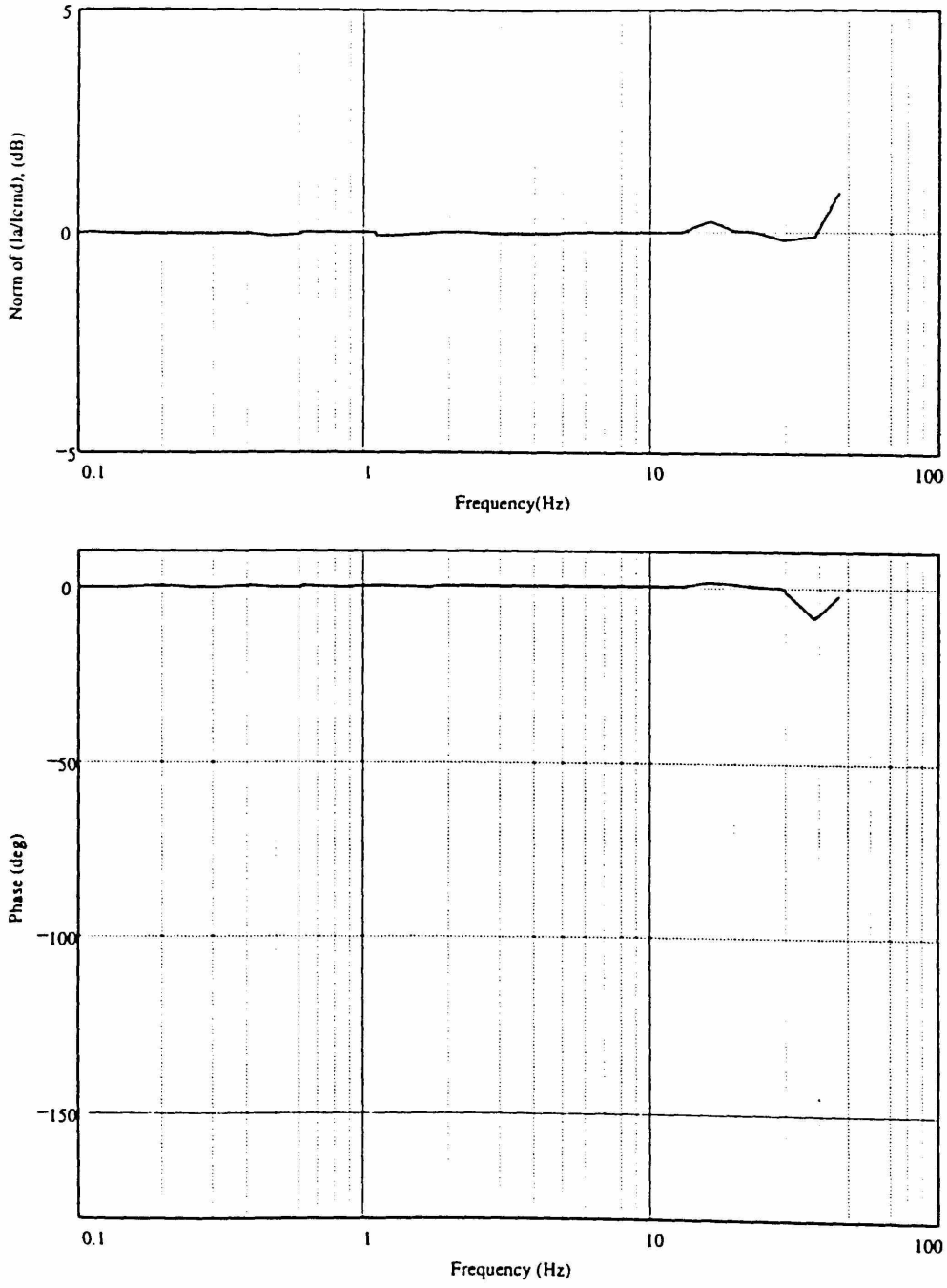

Figure 4.21: Commanded Current Vs. Phase Current Ia (Upper Actuator, at Peak Ia)

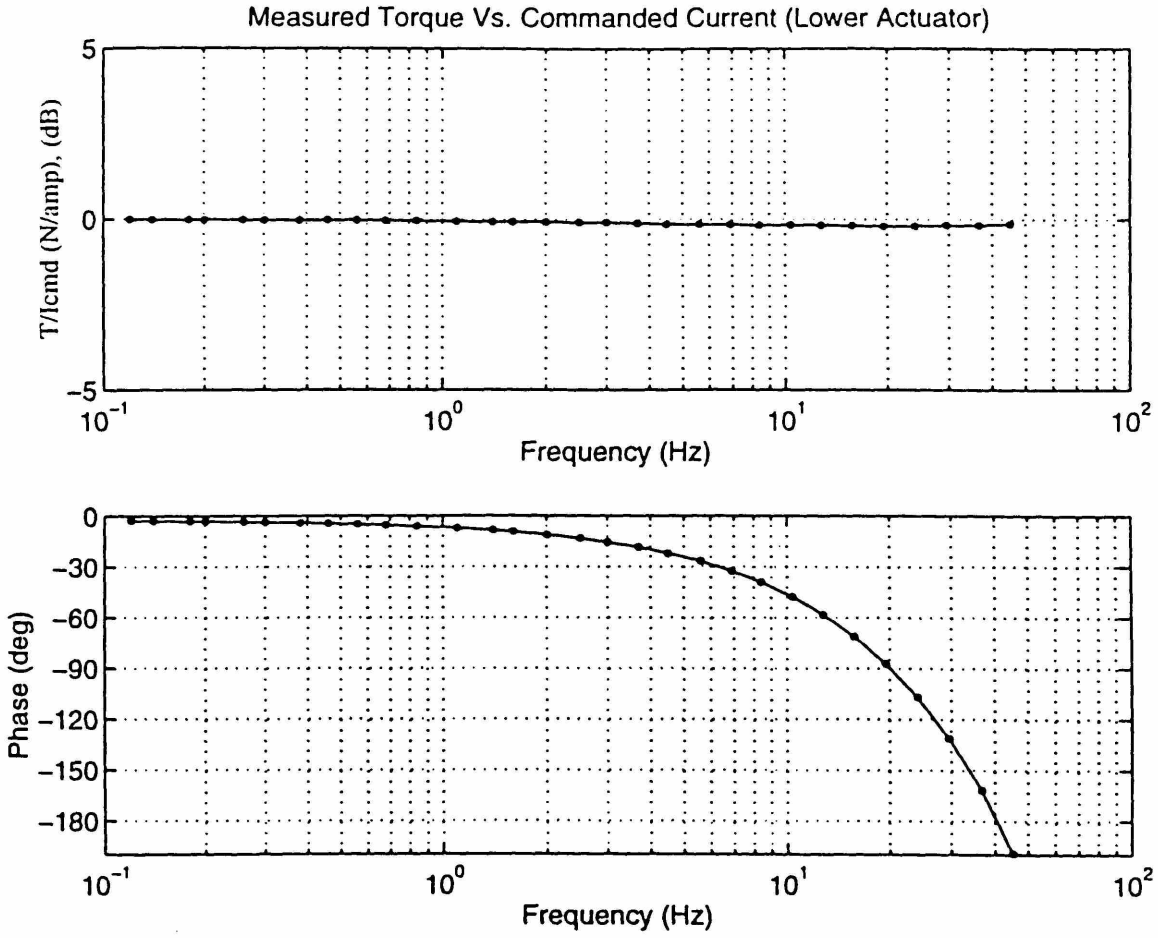

Figure 4.22: Measured Torque Vs. Commanded Current (Lower Actuator)

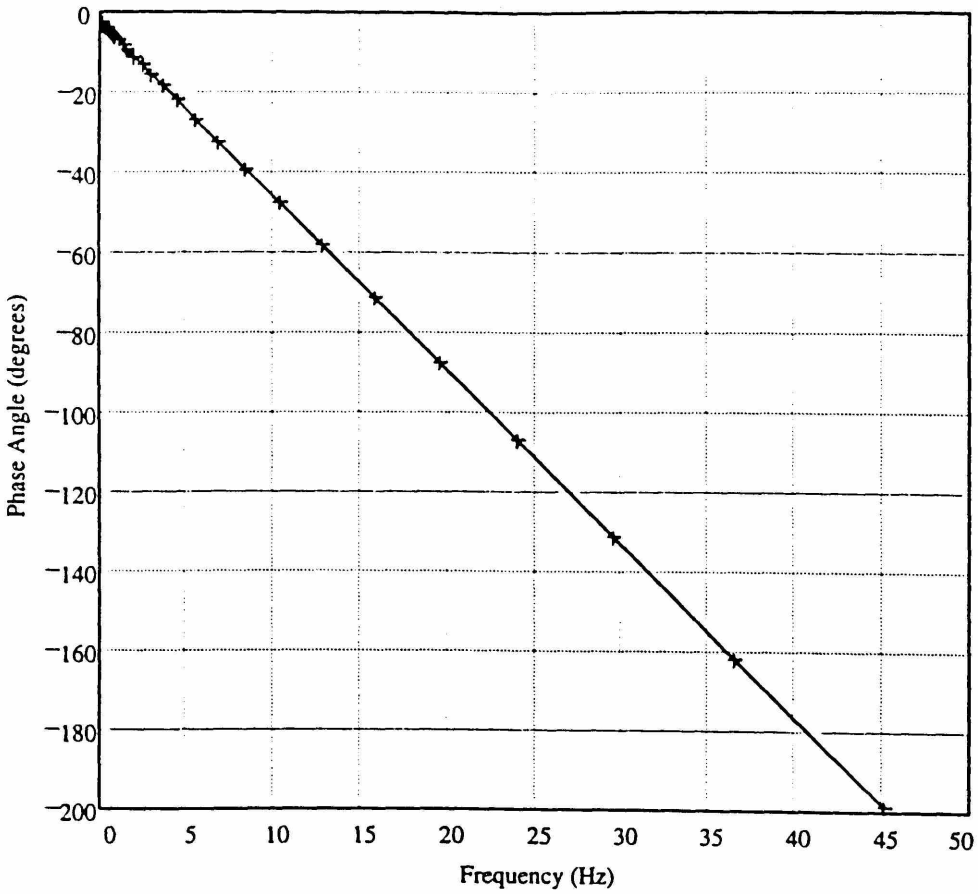

Figure 4.23: Linear Plot of Phase Vs. Frequency (Lower Actuator @ Peak Ic)

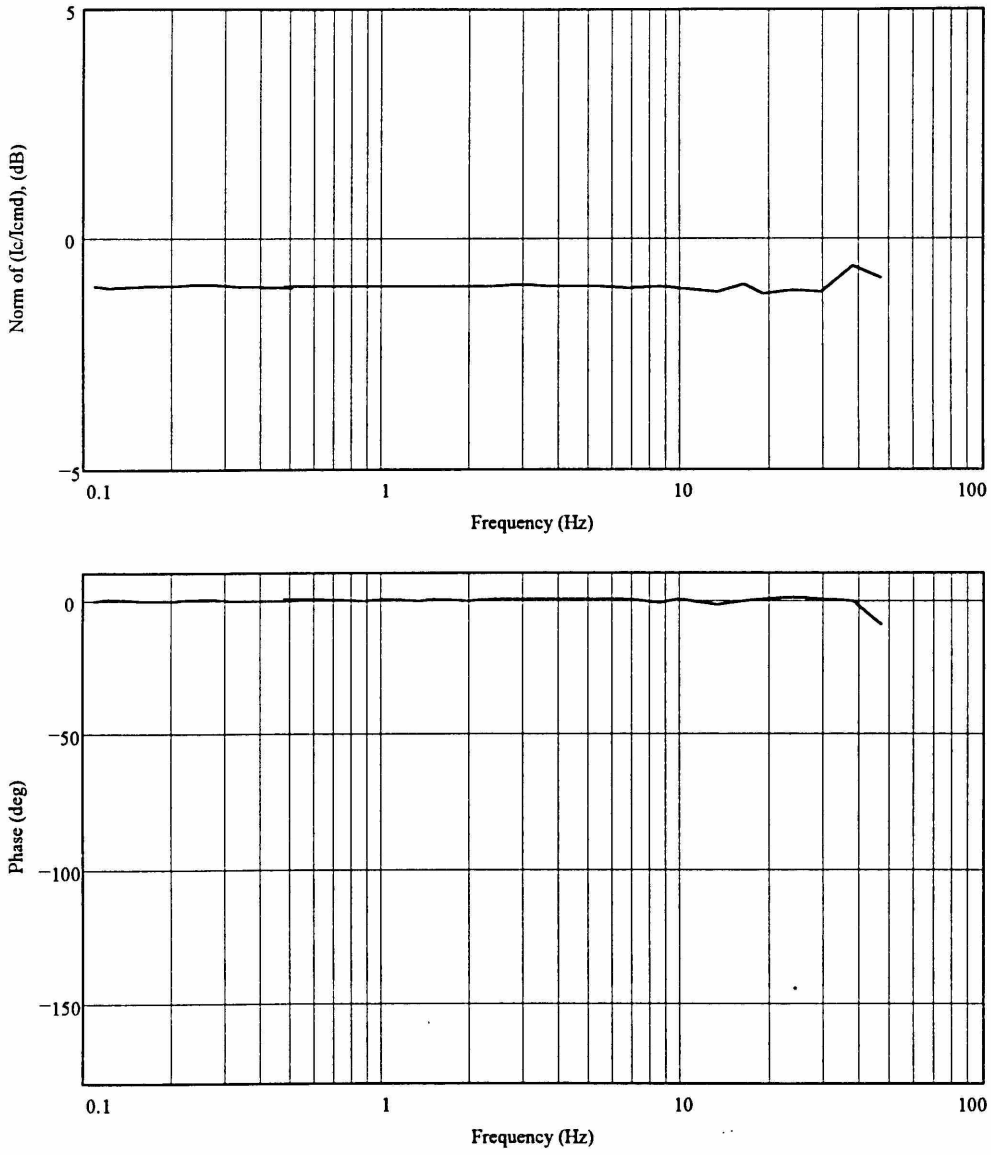

Figure 4.24: Commanded Current Vs. Phase Current Ic (Lower Actuator, at 88% of Peak Ic)

4.5 Summary

In this chapter, the sliding friction in the actuator packages and the torque current relationships were determined from the experimental data. From the results, the average sliding friction in the upper actuator package is about 0.274 N-m in the clockwise direction and 0.286 N-m in the counterclockwise direction. The average sliding friction in the lower actuator package is 0.259 N-m in the clockwise direction and 0.291 N-m in the counterclockwise direction.

The approximate torque current relationship for the upper and lower actuator packages, respectively, are

$T = 3.917\ I + (0.025),\ Nm$

$T = 3.944\ I + (0.068),\ Nm$

with estimated error of +/- 0.107 N-m for both actuator packages.

From the sinusoidal output torque versus commanded current experiment, there is a 12 ms of pure transport delay between commanded current and output torque, but the source of the delay has not been determined. However, it is concluded that the current loop in the servo amplifier is not a major source of the delay.

5. Conclusion

The first objective of this thesis was to build a beta-prototype of the 2-dof module of MIT Manus. The beta-prototype has been built. Chapter 3 discussed some of the design modifications made and why they were made. As was shown, there is room for improving the designs, and thereby, reducing production cost. In particular, some of the supports and the actuator package housings can benefit from redesign. However, real reductions in production costs will be realized only when during the redesigning phase, serious considerations are given to the manufacturing process.

The second objective was to evaluate the performance of the beta-prototype. This objective was not fully achieved, and was limited to the characterization of the actuator packages. This is primarily because there were some problems with getting reliable signals from the 17 bit output of the incremental encoders. However, even with just the characterization of the actuator packages, we have some very meaningful performance information. In chapter 4, one set of experimental results gave an indication of the sliding friction in the actuator packages, a second set gave an estimate of the torque constants, and a third gave an indication of how quickly torque can be commanded. Further characterization is needed, and the characterization might indicate ways to optimize the robot's performance. Also, perhaps, indicate ways to minimize the number of components in the actuator packages.

Bibliography

Bibliography

[1] American Heart Association Heart and Stroke Facts and Statistics. (1993)

[2] Charnnarong, Jain. The Design of an Intelligent Machine. Cambridge, Massachusetts: MIT University Press, 1991.

[3] Coleman, H. W. and Steele, W.G., Experimentation and Uncertainty Analysis for Engineers. John Wiley and Sons, New York, 1989.

[4] Diffrient, Tiley, Harman, Humanscale 1/2/3, MIT press. Cambridge, 1981

[5] Gibbs, David. An Introduction to CNC Machining. Britain: Cassell, 1984.

[6] Hayward, V. and Ashley, O.R. "Performance Measures for Haptic Interfaces" Proceedings of 7th International Symposium on Robotics Research, Munich, Germany. (1995)

[7] Hogan, Neville. "Impedance Control: An Approach to Manipulation Part 1- Theory, Implementation, and Application." Journal of Dynamic Systems, Measurement, and Control 107 (1985)

[8] Hogan, Neville. "Stable Execution of Contact Tasks Using Impedance Control.". Proceedings of IEEE International Conference on Robotics and Automation (1987)

[9] Hogan, N., Krebs, H.I., Sharon, A., Charnnarong J. Interactive Robotic Therapist. U.S. Patent #5,466,213; Massachusetts Institute of Technology, 1995.

[10] Jones, L.A., and Hunter, I.W. "Human Operator Perception of Mechanical Variables and Their Effects on Tracking Performance." ASME Dynamic Systems and Control Division 42: 49-53, (1992)

[11] Khalili, D. and Zomlefer, "An Intelligent Robotic System for Rehabilitation of Joints and Extrimation of Body Segment Parameters." Proceedings of IEEE Trans Biomed Eng 35 (2), (1988)

[12] Lum, P.S., Lehman, S.L., Reinkensmeyer, D.J. "The Bimanual Lifting Rehabilitator: an Adaptive Machine for Therapy of Stroke Patients." IEEE Trans on Rehabilitation Eng 3 (2): 166 - 174. (1995)

[13] Morrel , J.B. and Salisbury, J.K., "In Pursuit of Dynamic Range: Using Parallel Coupled Actuators to Overcome Hardware Limitations." In Experimental Robotics IV, Fourth International Symposium. (1995)

[14] Morrell, J.B. and Salisbury, J.K. "Performance Measurements for Robotic Actuators." Proceedings of the ASME Dynamics Solutions and Control Division 58 (1996): 531-537.

[15] Shigley, Joseph, and Mischke, Charles. Mechanical Engineering Design. New York: McGraw-Hill, 1989.

[16] Reinkensmeyer, D., Rehabilitators, Robots, and Guides: New Tools for Neurological Rehabilitation, 1997.

APPENDICES

APPENDIX A: Beta-Prototype of MIT

Manus: *In-House Fabrication*

Beta-Prototype of MIT-Manus: *In-House Fabrication*

For the alpha-prototype, all the fabrication of parts was done at a professional machine shop. For the beta-prototype the fabrication approach was a little different. As many parts as possible were fabricated in house using Newman Biomechanics Laboratory's computer numerical control (CNC) machine. Using the CNC machine, I was able to fabricate the joint caps, the joint retainers, the joints, the links, the lower column holder, the lower motor holder, the upper mounting plate, the mounting straps, the mounting base plate, and the mounting column holder. The remaining parts, the actuator packages and the mounting column, were fabricated at a local professional machine shop: these parts were fabricated at a professional machine shop due to lack of some tools, lack of needed experience, and time constraints.

By fabricating some of the parts in house we expected to gain a better understanding of the role that manufacturing plays in our robot development, and how to integrate design and manufacturing. "Design and manufacturing must be intimately interrelated. Design and manufacturing should never be viewed as separate disciplines or activities. Each part or component of a product must be designed so that it not only meets design requirements and specifications, but also can be manufactured economically and with relative ease." [Kalpakjain, 1995]. This idea is known as design for manufacturing (DFM). It is quite obvious that by integrating manufacturing and design, we should be able to achieve our design intents while minimizing manufacturing costs.

The objectives are 1) to describe the operation of the CNC machine used in fabrication, and 2) to discuss some of the fabrication difficulties.

Computer Numerical Control (CNC) Machine

Numerical Control (NC) machines are machines having various movements and functions expressed as a series of numbers which are usually initiated through electronic control systems. NC machines are used in a wide range of manufacturing processes such as metal cutting, woodworking, welding, flame cutting, and sheet metal forming [Gibbs, 1984]. NC machines are noted for being capable of high production rates, consistent product quality, require less operator involvement, and ease production of complex shapes.

NC machines have been evolving ever since the Industrial Revolution, but major contributions and break-throughs have only be realized within the past 50 years. In the United States, immediately after World War II, the U.S. Air Force initiated research projects geared towards finding better ways of manufacturing such that production quantity is increased while product quality is maintained. Some of the research grants went towards supporting research efforts for the development of numerical control machines. The objectives were "1) to increase production, 2) to improve the quality and accuracy of manufactured parts, 3) to stabilize manufacturing costs, and 4) to manufacture complex or otherwise impossible jobs." [Gibbs, 1984]

CNC machines are a subset of numerical control machines where the control system utilizes a computer as the controller [Gibbs, 1984]. The computer is allocated to control the movement of the motors which are used to drive each of the axis of the

machine. The controller controls the direction of movement, speed, and length of time each motor rotates. Even though numerical control machines can be used in a wide range of manufacturing processes, the applications we are interested in are restricted to drilling, turning, and milling operations.

Machine and Tool Specifications

Newman Biomechanics Laboratory's CNC machine is the VF-OE model manufactured by Hass Automation, Inc. It operations are commanded using standard CNC machine programming codes known as G-codes and M-codes. The machine has three methods of accepting programs: 1) computer downloaded, 2) manual data input, and 3) direct numerical control. For computer downloading method, the programs can be written using standard text editors and then re-formatted for the CNC machine. Using a RS-232 interface connection between the computer and the CNC machine, the programs are downloaded into the machine's memory. Once in the CNC machine memory, one can proceed to execute the program. For the manual data input, the CNC machine is programmed by manually typing in the commands using the machine's keypad located on the control panel. For the direct numerical control (DNC) method, a computer is connected to the CNC machine, but an entire program is not transferred to the machine's memory. Each time the CNC machine is ready to execute the next line, it calls on the computer to supply the next command line. This is particularly useful when the program is very long and there is not enough memory in the CNC machine to store the program.

For our application, only the computer downloaded method and the manual data input method is used. Before actually machining any part, one can run a simulation of the program on the control panel display to verify that the operations are correct.

The general specification for the machine is documented in Table 1. The actuators of the machine are pneumatic, while the other components, such as axis position sensors, the control panel, and pump for the coolant, are electric. The picture of the machine is shown in Figure 1.

Manufacturer	HAAS Automation Inc.
Model	VF-0E (VF Series VMC)
Travel Range	x-axis: 20 inches; y-axis: 16 inches; z-axis: 20 inches
Smallest Travel Increment	.0001"
Max. Machining Speed	300 in/min
Compressed Air Supply	100 psi @ 4 CFM
Power Requirement	three phase 195-260 V @ 50 or 60 Hz w/ 40 amps ± 5%

Table 1: CNC Machine General Specification

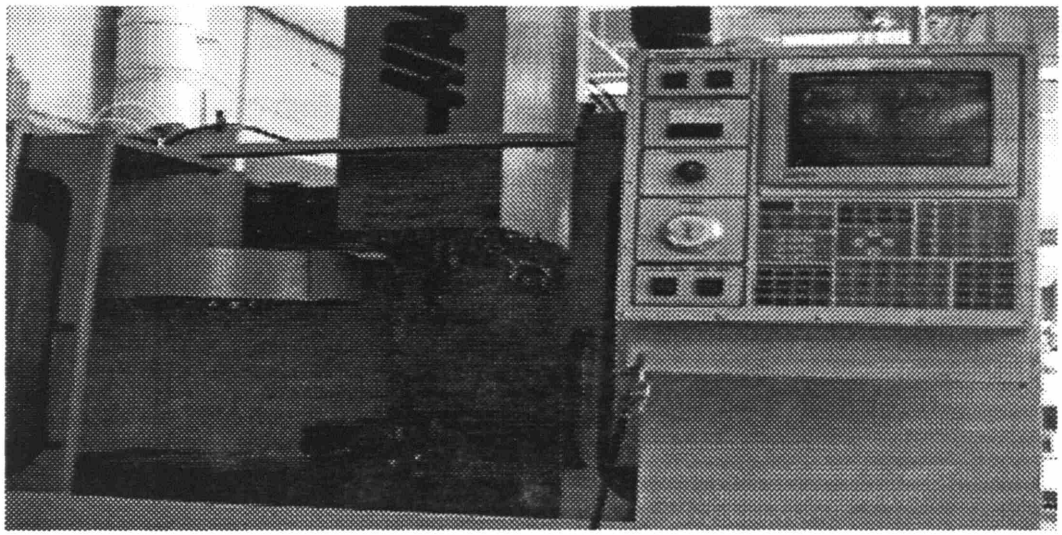

Figure 1: Newman Biomechanics Laboratory's CNC Machine

There are various tools used with the CNC machine, but the ones that pertain to what we are doing are edge finders, dial indicators, end mills and drills. The end mills range in diameter from 1.5 mm (0.061 in) to 2.25 in. They come in various lengths, and the specification of the frequently used end mills are listed below in Table 2.3. We started with multi-flute (more than three flutes) end mills and we had a lot of surface finish problems. When we resorted to using two-flute end mills, we ended up with better finish. The figure below shows the difference between surface of finish using both types of end mills. Unfortunately, the reason for this difference has not been thoroughly researched, but it seems that the reason can be attributed to the two-flute end mills being a bit more rigid in construction.

Type of Tool	Tool Diameter (in)	Length Below Shank	Cutting Length	Typical Feedrates (in/min)	Typical Spindle Speed (RPM)
regular length	1/4"	-	-	-	-
extended shank	3/8"	1 3/4"	3/4"	-	-
regular length	1/2"	-	1"	22	2061
extended shank	1/2"	2 1/4"	1"	22	2061
extended shank	5/8"	2 3/4"	1 3/8"	-	-
extended shank	1"	5"	3"	11	1146
shell	2 1/4"	-	1 1/2"	6	550

Table 2: Frequently Used Tools Specification (End Mills)

Machine Programming Codes

As stated earlier, there are two main standard programming codes for CNC machines: the G-codes and M-codes. "G-codes are preparatory functions, which involve actual tool moves (for example, control of the machine). These include rapid moves, feed moves, radial feed moves, dwells, and roughing and profiling cycles." G-codes commands are preceded by the letter G. "M-codes are miscellaneous functions, which include actions necessary for machining, but not those that are actual tool movement (for example, auxiliary functions). These include spindle on and off, tool changes, coolant on and off, program stops, and other similar related functions." Also, M-code commands are preceded by the letter M [Nanfara, 1995].

CNC Axis and Motion Nomenclature

There are at least two ways to establish coordinate for a CNC machine. One coordinate system can be defined relative to the workpiece, and another, relative to the tool. Also, there are at least two types to CNC machine setup: 1) the tool moves while workpiece is stationary, and 2) the tool is stationary (moves only along the z-axis) while workpiece moves (along the x-axis and y-axis). The CNC machine we used is of the second type.

Despite different machine setups, all CNC machine coordinate system adhere to the same standard coordinate system known as EIA267-C standard. When describing a machine operation, the coordinate system is always defined relative to an assumed stationary workpiece. Note that the machine setup doesn't need to use a stationary workpiece setup, it is just assumed that the workpiece is stationary. The standard was established to allow programmers to describe machine operations without worrying about whether the tool approaches the workpiece or the workpiece approaches the tool [Nanfara, 1995].

The machine coordinate system is governed by the right hand rule. The figure below shows the orientation of the right hand and the corresponding axis labels. The z-axis is along the axis of the main spindle, the x-axis is along the longest travel slide, and the y-axis is along the shortest travel slide. The positive directions is as indicated in the figure. The positive z-axis points into the spindle.

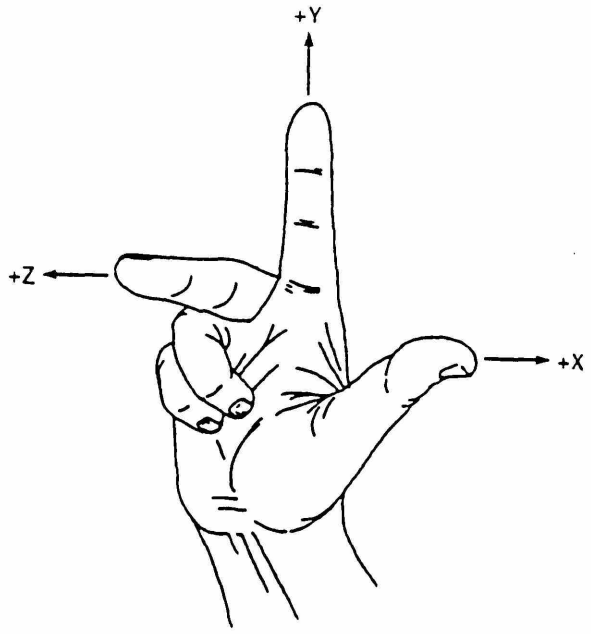

Figure 2: Right Hand Rule for CNC Machine [Nanfara, 1995]

The coordinate description shown in the figure below was used to document and describe the machining programs for the parts fabricated. So, for example, the workpiece shown in the figure it's reference A surface faces the right, and it's reference B surface faces the front, and it's reference C surface faces the top, as suggested by the tail of the arrow.

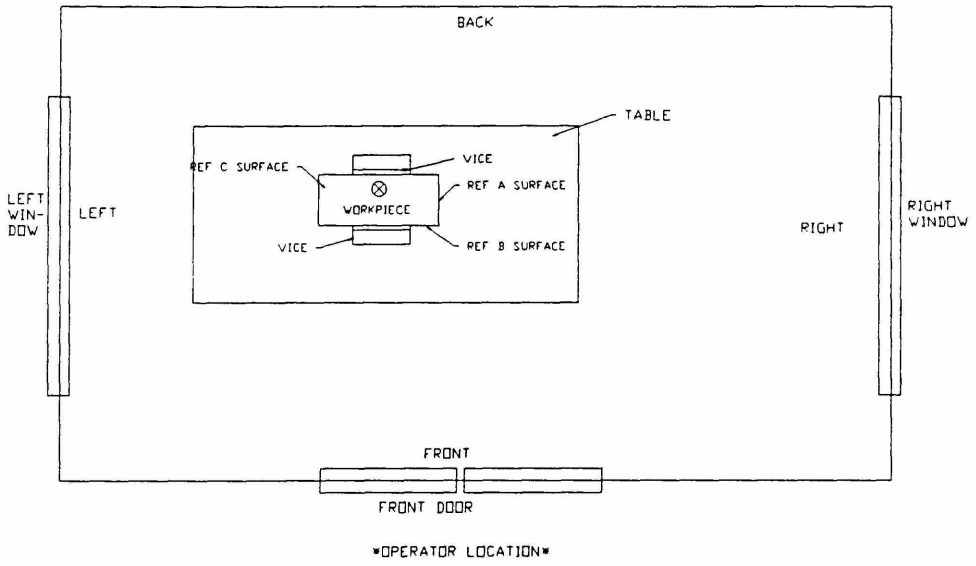

Figure 3: Adopted Coordinate System for this Document

APPENDIX B: Calibration of Torque Sensor

Calibration of Torque Sensor

In all the experiments, the Barry Wright Corporation's 6 axis force/torque sensor, FS6-120A, was used. The force/torque sensor was used only to measure torques, and it is important to establish the accuracy and reliability of these measurements.

To establish the accuracy of the torque sensor, a known set of torques were applied on and measured by the torque sensor. The known torques are applied through a thin beam with precisely drilled and threaded holes spaced 10 in, 11 in, 12 in, and 13 in from the central axis of the torque sensor, a screw is placed in one of these holes, weights are attached to a string, and the string is tied around the screw. The beam sits on the torque sensor horizontally, and so, the hung weights multiplied by the distance of the weights from the central axis of the torque sensor gives the applied torques. The beam is attached to the torque sensor using two dowel pins, and adjustments were made until the beam was horizontal (level indicators used make sure beam is horizontal). The masses were used and their actual mass are shown in Table 1. The masses were measured using self calibrating weight scale.

Mass	Measured Mass	Mass	Measured Mass
20 g	20.0 g	200 g	199.9 g
50 g	50.0 g	500 g	499.8 g
100 g	99.9 g	1000 g	999.6 g

Table 1: Measurement of Masses Used in Experiment

To establish how accurate the torque sensor is, first, it is necessary to establish the accuracy of the applied torques. The accuracy of the applied torques is mainly dependent on the accuracy of the mass measurements and the precision of the location of the threaded holes. The mass measurements are accurate to within +/- 0.1 g, which corresponds to the least significant digit displayed on the weight scale. The precision of the locations of the holes are also assumed to be accurate to within +/- 0.0001 in, which is based on the accuracy of the CNC machine used to drill the holes. Based on uncertainty analysis[1], these errors are known as bias errors, and it is possible to establish how they affect the experimental results. Over the entire range of applied torque, the maximum bias error is +/- 0.0015 N-m and occurs at the peak torques.

Figure 1 shows a plot of measured torque versus applied torque. The first equation shown in the plot (T) is based on least square fit to all the data points, the second equation (T_cw) is based on least square fit to all data points correspond to torques applied in the clockwise direction (positive torques), and the third equation (T_ccw) is based on least square fit to all data points in the counterclockwise direction (negative torques). The "a" denotes applied torque. Ideally, the slopes should be 1, but this is not the case. The slope in the clockwise direction is lower than the slope in the counterclockwise direction, suggesting a slight measurement biases in one of the directions. The slopes are slightly bigger than 1, and there is a slight zero offset. For applied torques greater than 1 N-m, measured torque in the counterclockwise direction is higher. The error (or standard error of estimate[1], SEE) associated with the least square approximation (based on all the data points) is +/- 0.0535 N-m. If bias error is negligible

[1] Steele. Uncertainty Analysis

compared to approximation error, which it is, for 95% level of confidence, according to Steele [1991] states that a +/- 2(SEE) band should be placed around the curvefit. So, for 95% confidence level, instrument error is within +/- 0.107 N-m.

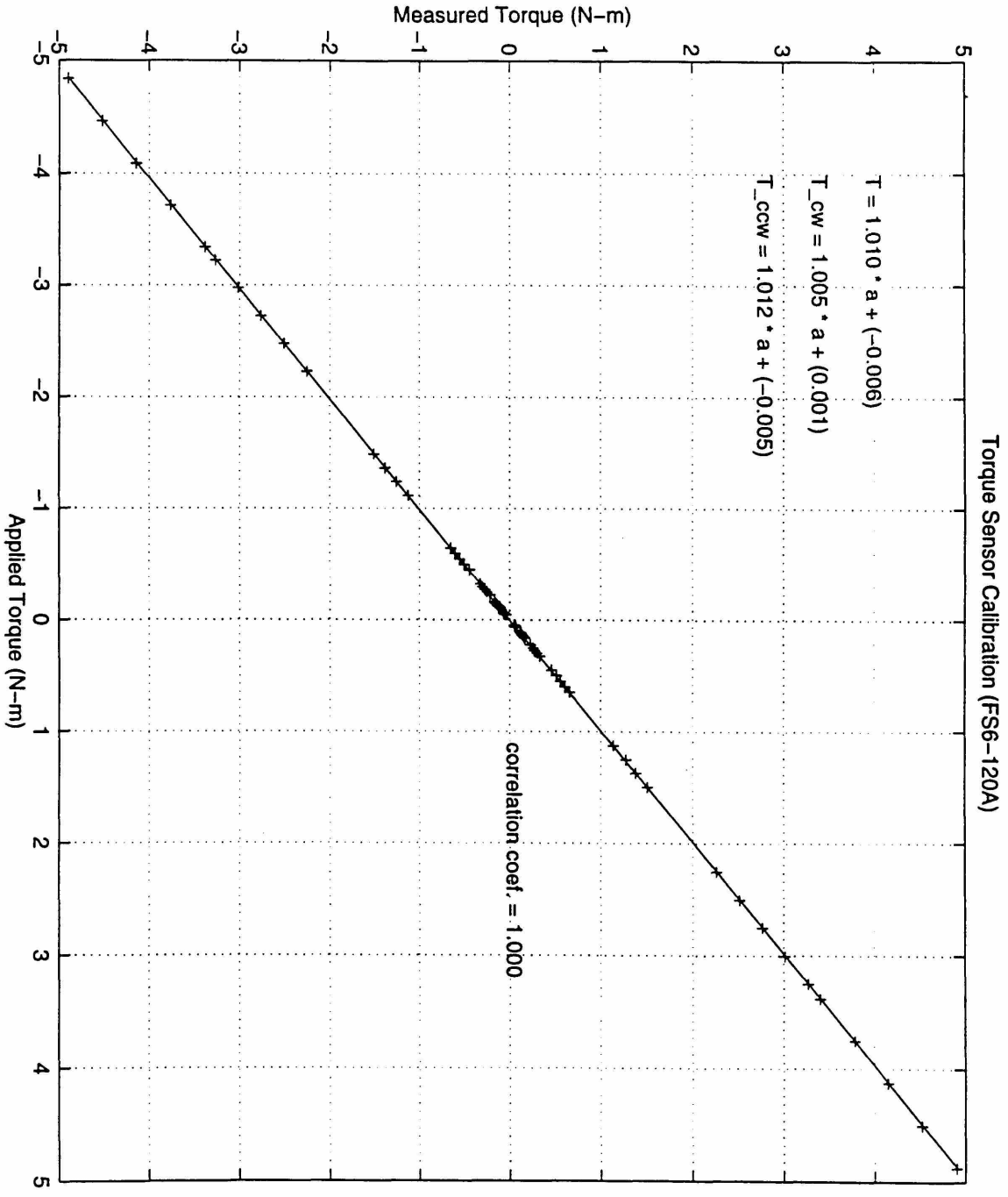

Figure 1: Measured Torque Vs. Applied Torque

APPENDIX C: Actuator and Sensors Details

DIMENSIONS

0301X-00

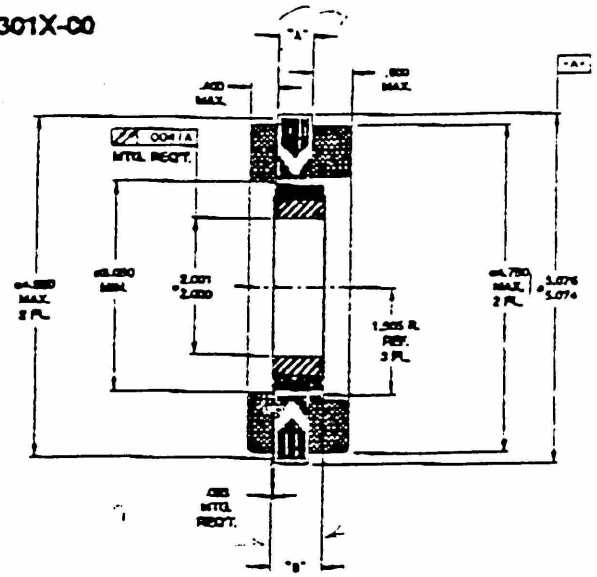

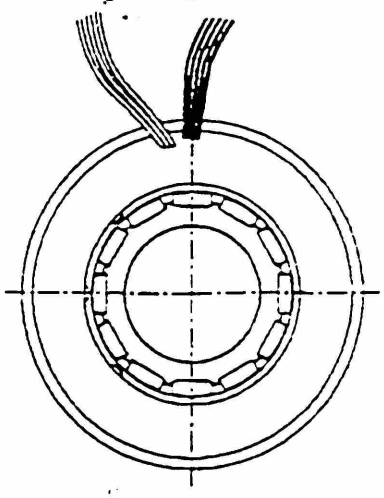

r supplied as two separate components, armature and sensor
mbly and field assembly.
i C.W. rotation, as viewed from lead end, energize per
ation sequence table (located at end of section).
1.5k ohms approx. (customer supplied unless supplied in
G amplifier).
, V-BC and V-CA is back EMF of motor phases AB, BC and
spectively, aligned with sensor output as shown for C.W.
ion only.
ring surface is between Ø4.920 and Ø5.075 on both sides.
ions set for bi-directional rotation.

Dimensions in inches

MODEL NUMBER	RBE-03010	RBE-03011	RBE-03012	RBE-03013	RBE-03014	RBE-03015	RBE-03016
"A" Dimension	0.525	1.300	1.625	2.150	2.625	3.250	3.750
"B" Dimension	0.775	1.550	1.875	2.400	2.875	3.500	4.000

H-0301X-00

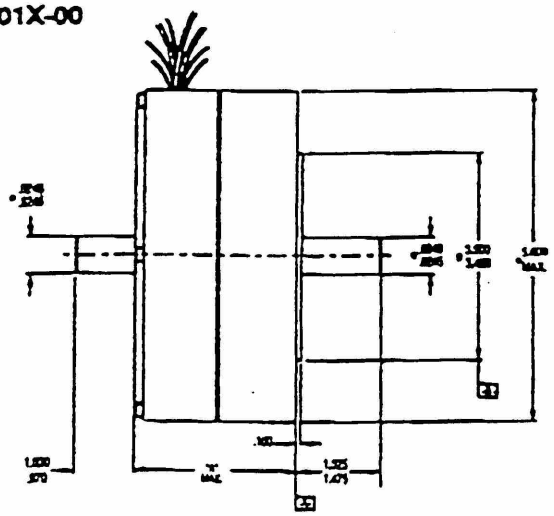

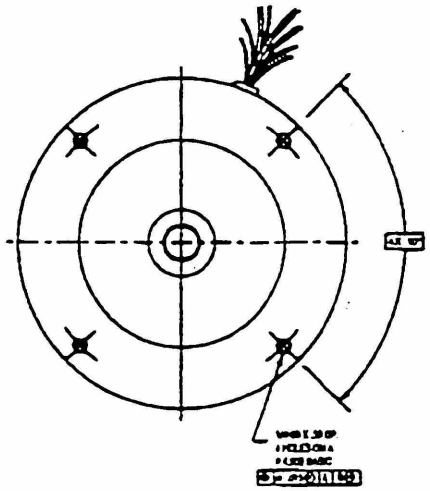

end play: with an 18 lb reversing load, the axial displacement
be .0005-.005.
i C.C.W. rotation, as viewed from pilot end, energize per
tion sequence table (located at end of section).
, V-BC and V-CA is back EMF of motor phases AB, BC and
spectively, aligned with sensor output as shown for C.C.W.
on only.
.5k ohms approx. (customer supplied unless supplied in
3 amplifier).

Dimensions in inches

MODEL NUMBER	RBEH-03010	RBEH-03011	RBEH-03012	RBEH-03013	RBEH-03014	RBEH-03015	RBEH-03016
"A" Dimension	2.820	3.345	3.920	4.445	4.920	5.545	6.045

LEAD CONNECTIONS

IRE
ads: #18 AWG Teflon coated per MIL-W-
1, 3 leads, 6 in min lg. ea. 1-black, 1-red,

Sensor Leads: #26 AWG type "ET" Teflon coated per MIL-W-16878, 5 leads, 6 in min lg. ea. 1-blue, 1-brown, 1-green, 1-orange, 1-yellow.

Motion Type:	Rotary
Mounting:	Hollow-Shaft
Precision:	High
Output Format:	Incremental
Max. Resolution:	
Internal Electronics:	360,000 counts/rev.
External Electronics:	900,000 counts/rev.

Series 835H Hollow-Shaft Encoders

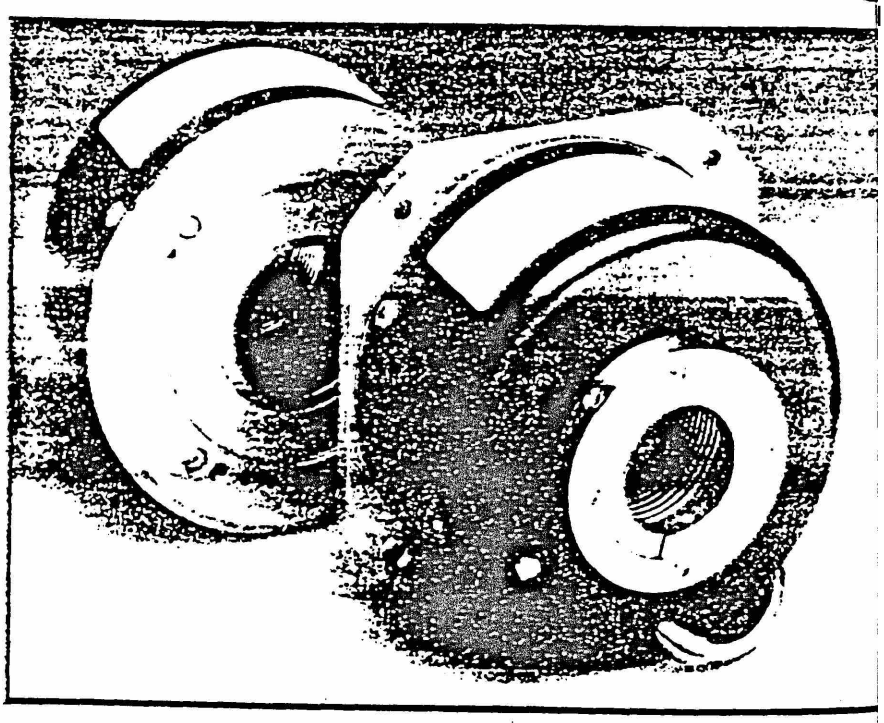

HIGH PERFORMANCE. SIMPLE INSTALLATION. RUGGED.

The Gurley Series 835H Hollow-Shaft Optical Encoders are rugged, high-performance devices designed for use where precise motion sensing is critical.

The Gurley Series 835H models feature discs with up to 11,250 lines per revolution. Internal options provide up to 360,000 counts/rev after 4x quadrature edge detection, while external electronics are available to increase the resolution up to 900,000 counts/rev (1.44 arc sec count). The units may be used with virtually all counter circuits, dedicated encoder interface cards and programmable logic controllers.

Gurley Precision Instruments has designed the encoders so they are especially easy to install and operate. No special shaft design is required, as the Series 835H models fit any size shaft up to 1.25" diameter. An internal flexible coupling simplifies installation, and the units' compact size makes them suitable for use in a wide range of applications.

THREE MODELS AVAILABLE

The Gurley Series 835H Hollow-Shaft Encoders are manufactured in three models, each with line counts up to 11,250 per revolution.

Model 8235H: single reading head; resolution up to 8 times the disc line count.

Model 8335H: two reading heads for higher accuracy, resolution up to 80 times the disc line count.

Model 8435H: four reading heads for the highest accuracy, resolution up to times the disc line count.

Gurley

SPECIFICATIONS

		See Note	Model 8235H	Model 8335H	Model 8435H
Maximum Line Count on Disc			11,250		
Maximum Cycles/Rev. with Internal Electronics			22,500	36,250	90,000
Maximum Counts/Rev. after Quad Edge Detection with Internal Electronics			90,000	225,000	360,000
Maximum Cyles/Rev. with External Electronics		5	NA	225,000	
Maximum Counts/Rev. after Quad Edge Detection with External Electronics		5	NA	900,000	
Instrument Error, ±arcsec		1,2	30	15	5
Quadrature Error, ±electrical degrees		1,3	30	24	15
Interpolation Error, ± quanta		1,4	0.15	0.10	0.05
FREQUENCY RESPONSE, kHz	1x Square Waves	6	100		
	2x Square Waves	6	150		
	5x Square Waves	6	NA	300	
	8x Square Waves	6	NA	1000	
	Up to 20x Square Waves with External Electronics	5, 6	NA	1000	
Maximum Weight, oz (g)			25 (715)		
Starting Torque, in-oz (N-m) [at 20°C]			2.0 (0.014)		
Running Torque, in-oz (N-m) [at 20°C]			1.0 (0.007)		
Moment of Inertia, in-oz-s² (g-cm²)			0.022 (1600)		
Maximum Acceleration, rad/s²			74 x 10		
Operating Temperature Range, °F (°C)			41 to 158 (5 to 70)		
Storage Temperature Range, °F (°C)			0 to 160 (-18 to 71)		
Humidity, % with non-condensing			98		
Shock			15g, 11 ms		
Vibration			50g, 0-2000 Hz		

Notes:

1. *Total Optical Encoder Error* is the algebraic sum of *Instrument Error* + *Quadrature Error* + *Interpolation Error*. In reality, these error sources sum to a value statistically less than the theoretical maximum. Error is typically defined at the signal transitions and therefore does not include quantization error, which is ±1/2 quantum. ("Quantum" is the final resolution of the encoder.)
2. *Instrument Error* is the sum of disc pattern errors, disc eccentricity, bearing runout and other mechanical imperfections within the encoder. This error tends to vary slowly around a revolution.
3. *Quadrature Error* is the combined effect of phasing and duty cycle tolerances and other variables in the basic analog signals. This error applies to data taken at all four transitions within a cycle; if data are extracted from 1x square waves on a 1x basis (i.e. at only one transition per cycle), this error can be ignored.

   Error in arcseconds=(3600) x (error in electrical degrees) / (disc line count)
4. *Interpolation Error* is present only when the resolution has been electronically increased to more than four data points per optical cycle. It is the sum of all the tolerances in the electronic interpolation circuitry.

   Error in arcseconds=(1296000) x (error in quanta) / (counts/rev)
5. With external Model HR2 High Resolution Electronics. Frequency response is as stated for output signals, or 50 kHz at the disc, whichever is limiting.
6. Maximum recommended shaft speed is 4400 rpm on encoders with shaft seals.

As part of our continuing product improvement program, these specifications are subject to change without notice.

8335H High Precision Incremental Optical Encoders offer these features:

- fits any size shaft up to 1.25" (31.75 mm) diameter.
- simplifies shaft design—no threads, no shoulders, no critical length requirements.
- internal flexible coupling speeds installation.
- high resolution, high accuracy, high speed.
- compact size for use in tight spaces.
- long-life LED illumination for reliability
- push-pull phototransistors for signal stability.

The encoders are available with internal signal interpolation for higher resolution. After 4x quadrature edge detection, resolution can be increased to 8 times the disc line count in the 8235H, 20 times in the 8335H and 32 times in the 8435H. With the optional HR2 high resolution electronics, Model 8335H and 8435H encoders achieve a maximum resolution of 80 times the line count, or 1.44 arcsecs. For all models, the optional once-per-revolution index is fully functional to the maximum encoder frequency response.

From The Encoder Leader

At Gurley Precision Instruments, measurement is our business. As a leader in encoders for some 40 years, Gurley has provided units worldwide to the aerospace, defense, machine control, factory automation, process control, instrumentation, medical equipment and other industries.

We continually incorporate the latest technical advances into our encoders, to deliver the best solution at the right price.

If our standard product lines don't resolve your particular application problem, or specifications call for metric units, our engineers will be glad to work with you to come up with a solution specific to your needs.

Gurley Precision Instruments manufactures these encoders to the highest quality standards in Troy, New York. Every encoder is fully tested before shipping.

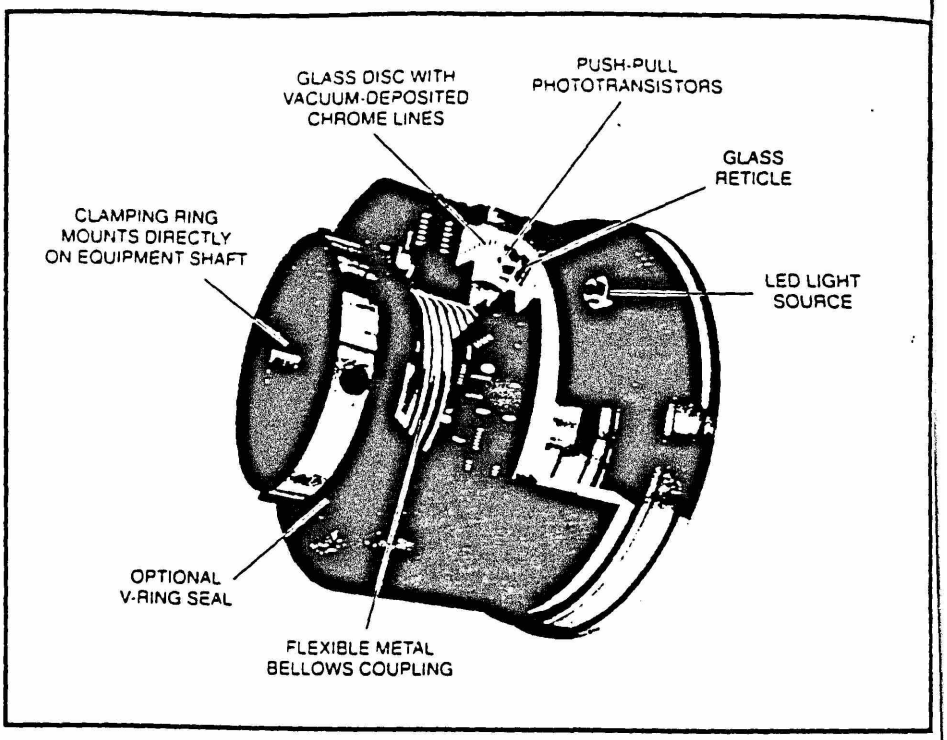

Internal Coupling

A flexible metal bellows and clamping ring form a highly accurate coupling that absorbs normal installation misalignments without affecting encoder accuracy. The design is able to maintain stated accuracy for any combination of misalignments that meet the following constraints:

$100P + 14E + 0.125A \leq 0.5$

Where:

P = Parallel offset, inches (0.005 max)

E = Axial Extension or Compression, inches (0.035 max)

A = Angular Misalignment, degrees (4° max)

Parallel offset, P, is equal to the total offset between the centerline of the encoder and the centerline of the user's shaft, plus half the radial runout of the user's shaft (TIR. 2).

Keeping the misalignments within the above constraints also assures infinite life of the bellows.

Maximum Coupling Deflections

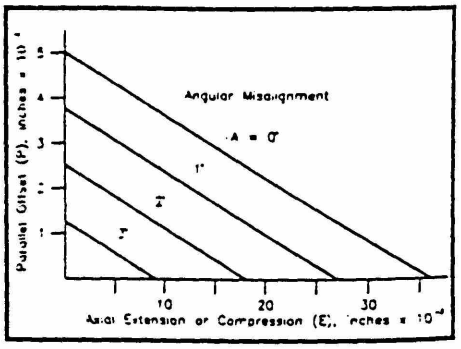

Seals

When ordered with optional shaft seals, the encoder has a magnetic-liquid seal at the base end and a V-seal at the clamp end. The magnetic liquid seal consists of an oil film with suspended magnetic particles. The medium, which is held in place magnetically, forms an effective seal against airborne particulates. The V-ring seal of nitrile rubber comprises a flexible sealing lip attached to the body with an integral resilient "hinge". It rotates with the shaft and seals axially against a stationary surface. The flexible lip and hinge provide effective sealing even with end play or shaft misalignment. With seals, the maximum recommended shaft speed is 4400 rpm.

Sinusoidal Output

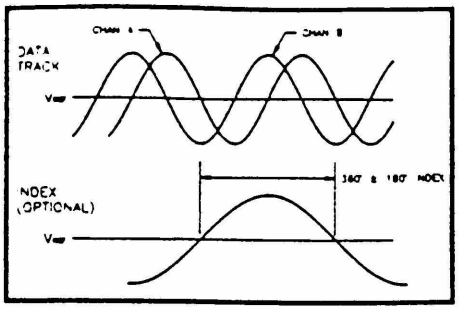

Pulse Output

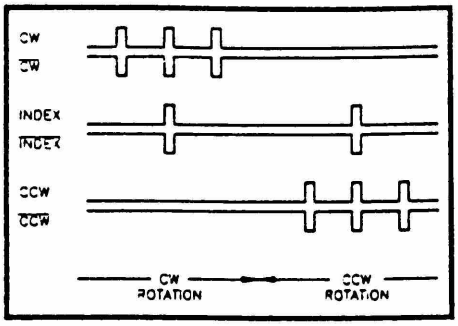

Quadrature Output

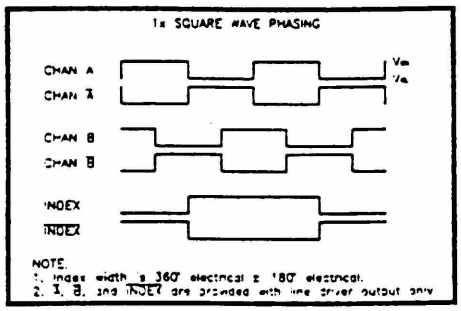

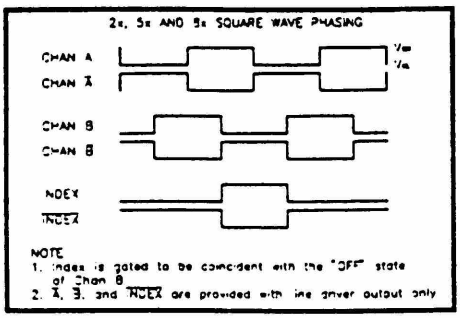

* The output device for these options is protected to survive an extended-duration short circuit across its output.

Power Supply Options

Vcc = +5.0 V DC± 0.25 V @ 225 mA max, or Vcc = 7 to 15 V DC @ 225 mA max (available with Power Buffer or Line Driver options)

Sinusoidal Output Option

This option provides quadrature sinusoids at the same spatial frequency (cycles/rev) as the line count on the disc. At lower line counts, the signals tend to be more trapezoidal than sinusoidal.

Buffered Sinusoids

(Output codes ending in **B**): The output device is an op amp referenced to (50% ± 3%) x V_{CC}. Typical signal roll-off at 100 kHz ≤3dB. Signal values at 1 kHz with 4.7 kΩ load to ground (20°C):

- P-P signal amplitude, data channels: 1.0± 0.1 V
- Amplitude ratio, min chan to max chan: 0.90 to 1.00
- P-P signal amplitude, index channel: 0.7 ±0.3 V

Pulse Output Options

All pulse outputs are direction-sensed (CW pulses and CCW pulses are on different terminals). The output device is an EIA/RS-422 balanced differential line driver. Pulse width is 0.4 ± 0.1 µs. The index pulse is gated so that it always occurs simultaneously with a specific data pulse. The maximum pulse rate is 650 kHz, based on maintaining adequate separation between pulses; however, the frequency response of the square waves from which the pulses are generated is often the limiting factor in determining maximum encoder speed. Available with either 5 V or 7-15 V encoder power input.

1x, 2x, 4x or 8x Pulses*

(Output codes ending in **I, J, K,** or **S**, respectively) are available on all models. Pulses are at 1, 2, 4 or 8 times the line count on the disc.

5x, 10x or 20x Pulses

(Output codes ending in **T, U,** or **V**, respectively) are available on Models 8335H and 8435H only. Pulses are at 5, 10 or 20 times the line count on the disc.

Quadrature Square Wave Output Options

1x or 2x Square Waves: Available on all models. Square waves are at the same or twice the spatial frequency (cycles/rev) as the disc line count.

5x Square Waves: Available on Models 8335H and 8435H only. Square wave spatial frequency is five times the disc line count.

8x Square Waves: Available on Model 8435H only. Square wave spatial frequency is eight times the disc line count.

1x Square Waves, TTL Compatible

(Output codes ending in **C**): Output device is LM339 voltage comparator with internal 2.2kΩ pull-up resistor.

TTL Fanout = 5 $V_{OH} \geq V_{CC}$ - 0.25 V
I_{SINK} = -8 mA $V_{OL} \leq$ 0.8 V

2x or 5x Square Waves, TTL-Compatible

(Output codes ending in **L** or **N**, respectively): Output device is high-speed CMOS logic gate. Max rating:
I_O = ± 25mA (V_O = 0 to V_{CC})

1x Square Waves with Open Collector

(Output codes ending in **E**): Output device is LM339 voltage comparator with open collector output transistor. Outputs are pulled up to +5 V DC with internal 10kΩ resistor. Customer may provide external pull-up as desired, within rating of LM339.

$V_{COH} \leq$ +36V $I_{COL} \leq$ 16 mA

1x*, 2x*, 5x or 8x* Square Waves with Line Drivers

(Output codes ending in **D, Q, O** or **F**, respectively): The output device is an EIA, RS-422 balanced differential line driver. Available with either 5 V or 7-15 V encoder power input.

1x, 2x or 5x Square Waves with Power Buffer

(For 5 V input, output codes ending in **G, R** or **P**; for 7-15 V input, output codes ending in **H, M** or **W**): Output device is 2N3725 driver transistor. Outputs are pulled up to supply voltage with an internal 10kΩ resistor. Customer may provide external pull-up as desired, within rating of output device.

$V_{COH} \leq$ +40 V $I_{COL} \leq$ 200 mA

DIMENSIONS

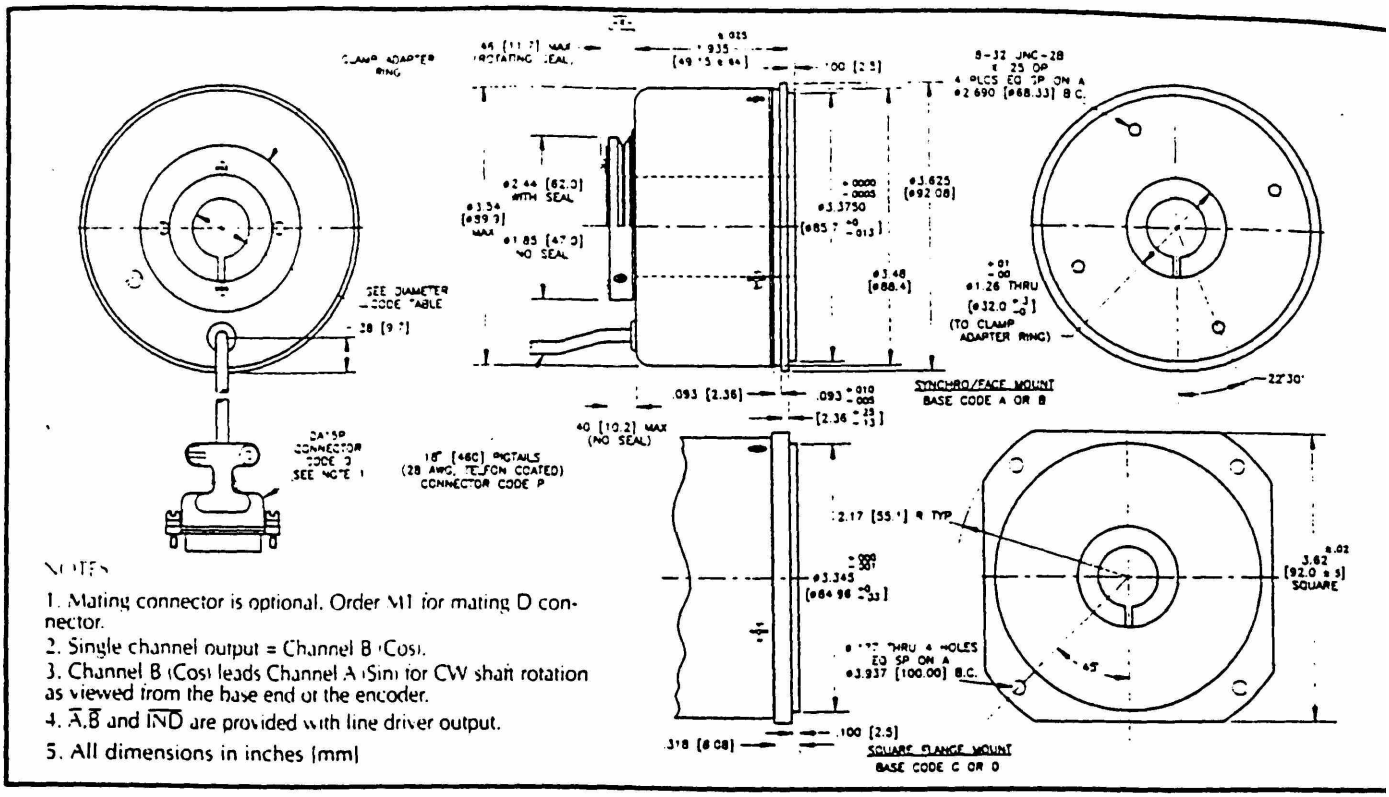

NOTES

1. Mating connector is optional. Order M1 for mating D connector.
2. Single channel output = Channel B (Cos).
3. Channel B (Cos) leads Channel A (Sin) for CW shaft rotation as viewed from the base end of the encoder.
4. $\overline{A}$,$\overline{B}$ and $\overline{IND}$ are provided with line driver output.
5. All dimensions in inches [mm]

EXTENDED RESOLUTION

With internal electronics, the Series 835H offers resolution up to 360,000 counts/rev (3.6 arcsec/count) after 4X quadrature-edge detection. If finer resolution is required (up to 900,000 counts/rev, or 1.44 arcsec/count), the HR2 external electronics package provides a wide range of options that ensures compatibility with virtually all commercially available counter circuits, dedicated encoder interface cards and programmable logic controllers:

- Any number of quadrature square waves from 1 to 20 times the line count on the disc.
- Fixed-duration pulses at 1, 2 or 4 times any integer from 1 to 20.
- A choice of CW, CCW or PULSE DIRECTION output pulse format.
- A zero-index (reference) signal in either gated 1/2 cycle, gated 1/4 cycle, or fixed-duration pulse format.
- EIA/RS-422 or open-collector line drivers.
- On-board low-dropout voltage regulator.

Please refer to the HR2 data sheet for full details.

OUTPUT PIN CONNECTIONS

See Notes 2, 3, 4

	Termination	Phototransistor or Buffered Sine Wave Output	Square Wave Output	Pulse Output
WIRE COLOR (CODE P)	Yellow	Sin	A	CW
	Brown		$\overline{A}$	$\overline{CW}$
	Green	Cos	B	CW
	Orange		$\overline{B}$	$\overline{CCW}$
	Blue	Index	IND	IND
	White		$\overline{IND}$	$\overline{IND}$
	Gray	Case Ground	Case Ground	Case Ground
	Red	+V	+V	+V
	Black	Common	Common	Common
PIN # DA-15P (CODE Q)	1		$\overline{IND}$	$\overline{IND}$
	2		IND	IND
	4	+V	$\overline{B}$	$\overline{CW}$
	5	Index	B	CW
	7		$\overline{A}$	$\overline{CCW}$
	8	Shield	A	CCW
	9	Sin	Case Ground	Case Ground
	10		+V	+V
	11	Cos		
	13		Common	Common
	14		Shield	Shield
	15	Common		

BASE CODE

Without Shaft Seals	With Shaft Seals	Description
A	B	Combination synchro/face mount
C	D	Square flange mount

DIAMETER CODE

User's Shaft Outside Dia.*	Diameter Code	Adapter Ring Inside Diameter
+0.000/-0.001 in		
1.250"	**1250E**	1.250" NOM
1.125"	**1125E**	1.125" NOM
1.000"	**1000E**	1.000" NOM
0.875"	**0875E**	0.875" NOM
0.750"	**0750E**	0.750" NOM
0.500	**0500E**	0.500"NOM
+0.000/-0.028 mm		
30.000 mm	**3000M**	30.00 mm NOM
25.000 mm	**25000M**	25.00 mm NOM
20.000 mm	**2000M**	20.00 mm NOM
10.000 mm	**1000M**	10.00 mm NOM

*Consult Gurley Precision Instruments for other sizes.

ORDERING INFORMATION

To construct a model number, fill in the boxes with a code from the appropriate table below.

8235H	- 8192	- CB	Q	C	- 1000 E	- —
MODEL NO.	LINE COUNT	OUTPUT CODE	CONNECTOR	BASE CODE	DIAMETER	SPECIAL CODE

MODEL NO.

8235H	8335H	8435H

LINE COUNT

360	500	512	900	1000	1024
1575	1800	2000	2048	2500	2540
2700	3600	3175	3300	3600	4000
4050	4096	4200	4310	4500	5000
5400	6000	6400	6480	7200	8000
8192	9000	9900	10000	10800	11250

CONNECTOR

P 18" Pigtails
Q 18" Pigtails with DA15P connector

BASE CODE

Without Shaft Seals	With Shaft Seals	Description
A	B	Combination synchro/face mount
C	D	Square flange mount

DIAMETER

1250E	for 1.250" diameter shaft
1125E	for 1.125" diameter shaft
1000E	for 1.000" diameter shaft
0875E	for 0.875" diameter shaft
0750E	for 0.750" diameter shaft
0500E	for 0.500" diameter shaft
3000M	for 30.00 mm diameter shaft
2500M	for 25.00 mm diameter shaft
2000M	for 20.00 mm diameter shaft
1000M	for 10.0 mm diameter shaft

SPECIAL CODE

A two-letter code to define specific non-standard features. Consult factory for details.

OUTPUT CODE

Output Waveform	5 V Input				7-15 V Input			
	Single Channel		Two Channels		Single Channel		Two Channels	
	With Index	No Index	With Index	No Index	With Index	No Index	With Index	No Index
Buffered Sinusoids	AB	BB	CB	DB				
1x Sq. Waves– TTL Compatible	AC	BC	CC	DC				
1x Sq. Waves– Open Collector	AE	BE	CE	DE				
1x Sq. Waves– Line Driver	AD	BD	CD	DD	ED	FD	GD	HD
1x Sq. Waves– Power Buffer	AG	BG	CG	DG	AH	BH	CH	DH
2x Sq. Waves– TTL Compatible			CL	DL				
2x Sq. Waves– Line Driver			CQ	DQ			GQ	HQ
2x Sq. Waves– Power Buffer			CR	DR			CM	DM
5x Sq. Waves– TTL Compatible*			CN	DN				
5x Sq. Waves– Line Driver*			CO	DO			GO	HO
5x Sq. Waves– Power Buffer*			CP	DP			CW	DW
8x Sq. Waves– Line Driver**			CF	DF			GF	HF
1x Pulses			CI	DI			GI	HI
2x Pulses			CJ	DJ			GJ	HJ
4x Pulses			CK	DK			GK	HK
5x Pulses*			CT	DT			GT	HT
8x Pulses			CS	DS			GS	HS
10x Pulses*			CU	DU			GU	HU
20x Pulses*			CV	DV			GV	HV

* Available with Models 8335H and 8435H only.
** Available with Model 8435H only.

SPECIAL CAPABILITIES FOR UNIQUE SITUATIONS

In addition to our line of standard rotary and linear encoders, we regularly design and manufacture special encoders for custom applications. These range from military, aerospace and similar high reliability requirements, to high volume, low cost, limited performance commercial requirements. They include both incremental and absolute encoders.

Gurley Precision Instruments
514 Fulton St., PO Box 88 • Troy, NY 12181-0088
Phone (518)272-6300 • 1(800)759-1844
Fax (518)274-0336 • Twx (710)443-8156

1094-5M Printed in U.S.A.
©Gurley Precision Instruments

Gurley
Precision Instruments

CHANGES TO SERIES 835H DATA SHEET DATED 1094

- The maximum output frequency for 8X square waves should be 500 kHz. Up to 1 MHz is possible in special situations; please consult factory.
- At the bottom of the SPECIFICATIONS table, the shock specification should be 50g, 11 ms and the vibration specification should be 15g, 0-2000 Hz.
- In the OUTPUT PIN CONNECTIONS table, the pulse output on the green wire should be CCW.
- In the QUADRATURE OUTPUT phasing diagram, the index signal with 8X square waves is 1/4 cycle wide, gated with A and B high.
- In the LINE COUNT box on the back page, add 4302, 7000, 7640 and 9550.
- The maximum allowable shaft diameter is reduced from 1.25" to 1.20". (1.25" may be acceptable under very limited conditions; consult factory.)
- The specification sheet parameters for shaft misalignment are based on bellows load-vs.-life considerations. There are additional interference considerations that limit the allowable angular misalignment:

Shaft dia. inches	Max angular misalignment, degrees
1.20	0.7
1.10	1.9
1.00	3.2

H106 - 23

Corrections835H.doc
05/23/96

514 FULTON STREET • TROY, NEW YORK 12181 • PHONE (518) 272-6300 • TWX 710-443-8156 • FAX (518) 274-0336